Characterization of panglial gap junction networks in the thalamus and hippocampus reveals glial heterogeneity

Dissertation

zur

Erlangung des Doktorgrades (Dr. rer. nat.)

der

Mathematisch-Naturwissenschaftlichen Fakultät

der

Rheinischen Friedrich-Wilhelms-Universität Bonn

vorgelegt von

Stephanie Griemsmann

aus

Wiesbaden

Bonn 2014

Angefertigt mit Genehmigung der Mathematisch-Naturwissenschaftlichen Fakultät der Rheinischen Friedrich-Wilhelms-Universität Bonn

1. Gutachter	**Prof. Dr. Christian Steinhäuser**
	Institut für Zelluläre Neurowissenschaften
	Universität Bonn
2. Gutachter	**Prof. Dr. Walter Witke**
	Institut für Genetik
	Universität Bonn
Tag der Promotion:	16.04.2015
Erscheinungsjahr:	2015

Do not go where the path may lead, go instead where there is no path and leave a trail.
-Ralph Waldo Emerson

Acknowledgements

First of all, I would like to thank my supervisor Prof. Dr. Christian Steinhäuser, who gave me the opportunity to work on this great project and for the scientific guidance, fruitful discussions and support.

I would like to thank Prof. Dr. Walter Witke, Prof. Dr. Klaus Willecke and Prof. Dr. Klaus Mohr for accepting my request to be part of the examination committee and for their time and efforts in reviewing this work.

Especially, I would like to thank Prof. Dr. Martin Theis for valuable scientific advice on connexins and mouse lines.
I would like to thank PD Dr. Gerald Seifert for the introduction to the field of astrocyte electrophysiology, support in the AMPA/$GABA_A$ receptor study and the single-cell RT-PCRs.
I also would like to thank PD. Dr. Ronald Jabs for excellent support in the field potential analysis and valuable methodical and technical support in all kind of questions and programming Igor-tools.
In addition, I sincerely want to thank Prof. Dr. Christian Henneberger for fruitful discussions on network analysis, and the great advances in network analysis employing Matlab tools.
My sincere thanks go to Dr. Peter Bedner for useful input on gap junctions, Cre recombinases and of course CPEBs.
My special thanks go to Simon Höft for endless hours of cell counting, sharing experience, scientific discussion and final successful publication. The thalamus rules! I also want to thank Lena Claus, Anna Beinhauer and Camille Philippot for their commitment and enthusiasm for thalamic glia.
I also would like to express the appreciation to my colleague Jiong Zhang for the support in analysing connexin expression in the thalamus.
Of course, I want to thank the entire lab for the great time, soccer betting, movie-nights and support: Alex, Aline, Annika, Daniel, Dilaware, Ines, Ivana, Johannes, Julia, Kerstin, Kirsten, Magda, Michel, Roland, Semi, Siggi, Stefan, Steffi A., Susan, Tushar und Verena. My special thanks for excellent technical support go to Ina Fiedler, Anja Matijevic and Thomas Erdmann.

Finally, I want to thank my family who always supported me and encouraged me throughout my life. My deepest thanks go to my boyfriend Dirk for his love and moral support.

Contents

Abbreviations

2-NBDG	2-(N-(7-nitrobenz-2-oxa-1,3-diazol-4-yl)amino)-2-deoxyglucose
4-AP	4-aminopyridine
AC	astrocyte
ACSF	artificial cerebrospinal fluid
Aldh1L1	aldehyde dehydrogenase 1 family, member L1
AMPA	α-amino-3-hydroxy-5-methyl-4-isoxazolepropionic acid
ANLS	astrocyte-neuron lactate shuttle
APS	ammonium persulfate
as	antisense
ATP	adenosine triphosphate
BAPTA	1,2-bis(o-aminophenoxy)ethane-N,N,N',N'-tetraacetic acid
BCA	bicinchonic acid assay
β-Gal	β-galactosidase
Biocytin	N-biotinyl-L-lysine
BSA	bovine serum albumine
bp	base pairs
CA	Cornu Ammonis
CCD	charge-coupled device
$[Ca^{2+}]_i$	intracellular Ca^{2+} concentration
$[Cl^-]_o$	extracellular Cl^- concentration
C_m	membrane capacitance
CNS	central nervous system
CNPase	2',3'-cyclic nucleotide 3'-phosphodiesterase
CSF	cerebrospinal fluid
CSPG	chondroitin sulfate proteoglycan
CT	cortico-thalamic
Cx	Connexin
D-AP5	DL-2-amino-5-phosphonovaleric acid
DEPC	diethyl pyrocarbonate
DG	dentate gyrus
dH_2O	double distilled water
DIC	differential interference contrast
DKO	double knockout
DNA	deoxyribonucleic acid

dNTP	deoxynucleotide triphosphate
DTT	dithiothreitol
e	embryonal
e.g.	for example
ECFP	enhanced cyan fluorescent protein
ECL	enhanced chemiluminescence
EDTA	ethylene diaminetetraacetic acid
EGFP	enhanced green fluorescent protein
EGTA	ethylene glycol tetraacetic acid
FDH	10-formyltetrahydrofolate dehydrogenase
Fig.	figure
FITC	Fluorescein isothiocyanate
fl	floxed flanked by loxP sites
GABA	γ-aminobutyric acid
$GABA_A$ receptor	ionotropic $GABA_A$ receptor
GCL	granule cell layer
GD	glucose deprivation
GFAP	glial fibrillary acidic protein
GFP	green fluorescent protein
GJ	gap junction
GJC	gap junction channel
GJN	gap junction network
GLAST	glutamate/aspartate transporter
GLT1	glutamate transporter 1
GluA	AMPA receptor subunit
GluT	glucose transporter
GS	glutamine synthetase
HEPES	4-(2-hydroxyethyl)-1-piperazineethanesulfonic acid
HC	hippocampus
hGFAP	human glial fibrillary acidic protein
HRC	horse radish peroxidase
I	current
IHC	immunohistochemistry
IRES	internal ribosome entry site
KCC2	K^+-Cl^- cotransporter 2
kDa	kilo Dalton
Kir	inwardly-rectifying K^+
ko	knock-out
LSM	laser scanning microscope
LTD	long term depression
LTP	long-term potentiation
MAPK	mitogen-acitvated protein kinase

MBP	myelin basic protein
MCT	monocarboxylate transporter
MP	membrane potential
mRNA	messenger ribonucleic acid
n	number of samples
NBQX	2,3-dihydroxy-6-nitro-7-sulfamoyl-benzo[f]quinoxaline-2,3-dione
NeuN	neuronal nuclei antigen
NG2	nerve/glia antigen 2
NGS	normal goat serum
NMDA	N-methyl-D-aspartic acid
NP40	nonidet P-40
ODDD	oculodentodigitale dysplasia
OL	oligodendrocyte
OPC	oligodendrocyte precursor cell
p	postnatal day
PBS	phosphate buffered saline
PCR	polymerase chain reaction
PDGF	platelet-derived growth factor
PDGFαR	platelet-derived growth factor α receptor
PFA	paraformaldehyde
PKC	protein kinase C
PLP	phospholipoprotein
PNS	peripheral nervous system
pyr.	pyramidale
rad.	radiatum
RG-like cell	radial glia-like cell
R_m	membrane resistance
RNA	ribonucleic acid
R_s	series resistance
RT	reverse transcription
RTN	reticular thalamic nucleus
S100β	S100 calcium binding protein β
SD	standard deviation
SDS	sodium dodecyl sulfate
SDS-PAGE	sodium dodecyl sulfate-polyacrylamide gel electrophoresis
se	sense
SEM	standard error of the mean
SGZ	subgranular zone
SR101	sulforhodamine 101
st.	stratum
Tab.	table
TBS	Tris-buffered saline

TC	thalamo-cortical
TEMED	N,N,N,N-tetramethyl-ethylene-diamine
TH	thalamus
TRITC	tetramethylrhodamine
TTX	tetrodotoxin
U	enzyme units
V	voltage
VB	ventrobasal thalamus
VPL	ventral posterior lateral nucleus
VPM	ventral posterior medial nucleus
wt	wild type
w/v	weight per volume
ZO-1	zonula occludens-1

1 Introduction

1.1 Nervous System

The vertebrate nervous system consists of two parts, the central nervous system (CNS) and the peripheral nervous system (PNS). The CNS is formed by the brain and spinal cord, while the PNS consists of the remaining neuronal tissue in the body. The brain is located in the head and protected by meninges covering its entire surface. The brain is subdivided into five parts: telencephalon, diencephalon, mesencephalon, metencephalon and myelencephalon. It contains cavities, the ventricles, filled with cerebrospinal fluid (CSF). These ventricles are connected with each other and the spinal cord (Bear et al., 2006).
The brain tissue consists of different cell-types, e.g. neurons, glial cells, endothelial cells and ependymal cells. Murine brains contain around $71x10^6$ neurons which form a complex network with around 10^{11} synapses between cells (Herculano-Houzel et al., 2006). Glia make up 65% of the mouse brain (Allen and Barres, 2009). Optically two different nerve tissues can be distinguished. White matter is highly myelinated and grey matter is less myelinated and also consists of unmyelinated neurons.
The different parts of the brain can be further subdivided into distinct regions which fulfil specific functions. This study focused on the thalamus and hippocampus, which will be explained in further detail below.

1.1.1 Thalamus

The thalamus is part of the diencephalon, each hemisphere contains a thalamus. They are located subcortically in the centre of the brain, close to the third ventricle (Bear et al., 2006). The thalamus relays all information to the cortex and is therefore also called the gate to consciousness (Crick and Koch, 2003). Still, the thalamus is also involved in information processing and not only a relay station (Sherman and Guillery, 2002).
The thalamus is subdivided into several nuclei. First order nuclei fulfil different functions in somatosensory information transduction to the cortex, while higher order nuclei relate information between different cortical areas. First order nuclei receive information from different inputs, e.g. visual, auditive and sensory information (Grant et al., 2012).
In this study, glial cells in the ventrobasal thalamus (VB) were studied. This region is subdivided into the ventral posterior lateral (VPL) and the ventral posterior medial (VPM) nuclei. It is a first order nucleus and receives input from the whiskers. These

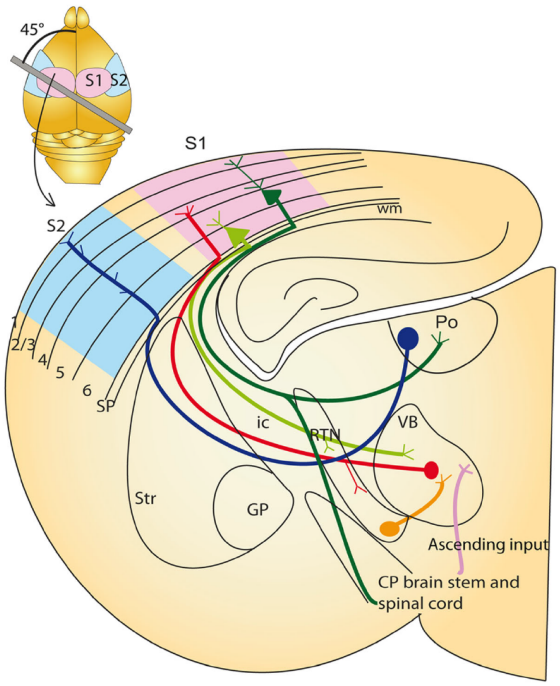

Figure 1.1 Thalamocortical circuits in the adult mouse brain. The line in the inset (brain outline on top) indicates the slice orientation of the large section containing thalamocortical projections. The coronal schematic slice depicts the signalling pathways between the ventrobasal thalamus (VB) and somatosensory cortex. The VB receives synaptic input from the brain stem via the ascending pathway. Thalamic neurons (red) relay information to layer 4 of the primary somatosensory cortex S1 (light pink) and the cortex signals back from layer 6 to the VB (light green). The axons pass through the internal commissure (ic). Both thalamo-cortical (TC) and cortico-thalamic (CT) neurons have synaptic connections with GABAergic neurons in the reticular thalamic nucleus (RTN), establishing inhibitory feedback and feedforward circuits to the VB (orange). Additionally, signals from layer 5 of the somatosensory cortex signal (dark green) to the posterior thalamic nucleus (Po), a higher order nucleus, which in turn projects (dark blue) to another cortical area, e.g. S2 (light blue). Str, striatum; GP, globus pallidus. From Grant et al., 2012.

signals arrive in distinct areas termed barreloids, corresponding to barrels in the cortex (Van Der Loos, 1976; Haidarliu and Ahissar, 2001; López-Bendito and Molnár, 2003). The VB is therefore integrated in the trigeminal pathway, sending sensory information via the brain stem to the thalamus and finally to the cortex (Bosman et al., 2011).

The VB receives synaptic input from the ascending pathway, also called lemniscal pathway (Fig. 1.1). This pathway terminates on the dendritic arbor of VB neurons which have excitatory glutamatergic synapses (Ralston, 1969). The VB nuclei contain relay neurons projecting to the somatosensory cortex, mainly to layer 4 via the thalamocortical (TC) pathway (Agmon and Connors, 1991). The VB contains a somatotopic map of the whisker field as observed in the cortex (Erzurumlu et al., 2010). The relay neurons reside completely in one barreloid with their dendrites during early development, but starting around postnatal (p) day p18 they extend dendritic processes into

neighbouring barreloids (Zantua et al., 1996). The axons extend through the reticular thalamic nucleus (RTN) and the internal capsule to reach the cortex. TC neurons make synapses on RTN neurons. GABAergic neurons in the RTN have an inhibitory effect on VB neurons by closing an inhibitory feedback loop. Cortical neurons from layer 6 send information back to the VB via cortico-thalamic (CT) projections which also make synapses on RTN neurons (Bourassa et al., 1995; Pinault, 2011; Grant et al., 2012), thereby providing an inhibitory feedforward circuit. In the VB they make synapses on distal dendrites of relay neurons (Grant et al., 2012).
The thalamus does not only contain excitatory glutamatergic synapses and inhibitory GABAergic synapses, but also electrical synapses in the RTN nucleus throughout life (Landisman and Connors, 2005; Niculescu and Lohmann, 2013; Lee et al., 2014). Electrical synapses were never observed in VB neurons after p12 (Lee et al., 2010).
The thalamus is highly interconnected with other brain regions and its normal function is crucial for somatosensory information processing in the brain. Thalamic dysfunctions have been associated with schizophrenia and absence epilepsies (Cope et al., 2009; Pinault, 2011).

1.1.2 Hippocampus

The hippocampus is part of the cortex and located in the medial temporal lobe. The name is derived from the Greek word for seahorse, because of its structure resembling a seahorse. Similar to the thalamus, the hippocampus is a paired structure with a hippocampus in each hemisphere. The hippocampus is subdivided in several regions: Cornu Ammonis (CA) 1 to CA3 and the dentate gyrus (DG). The CA regions are further subdivided in several layers. The stratum (st.) pyramidale (pyr.) contains the somata of pyramidal neurons, stretching their axons in the st. oriens. On the other side of st. pyr. the dendrites extend into the st. radiatum (rad.). The next layer is the st. lacunosum moleculare. While excitatory pyramidal neurons reside with their somata in the st. pyr., the other layers contain inhibitory interneurons and several types of glial cells. The dentate gyrus has a typical V-shape and contains the neuronal granular cell layer, the inside is called the hilus and the outer layer is the st. moleculare (Fig. 1.2; Amaral and Witter, 1989). The innermost layer of the granule cell layer, the subgranular zone (SGZ), is one of the neurogenic niches in the adult brain, containing neural stem cells which continuously form new neurons (Seri et al., 2001).
The hippocampus has a well characterized neuronal signalling circuit, the trisynaptic excitatory pathway, shown in Figure 1.2. Synaptic input from the entorhinal cortex arrives in the dentate gyrus and is propagated by mossy fibres to CA3 pyramidal neurons. Schaffer collaterals from CA3 neurons project on dendrites of CA1 pryamidal neurons in st. radiatum. The axons of CA1 neurons signal back to the entorhinal cortex (Deng et al., 2010).
The hippocampus is involved in learning and memory such as episodic and spatial memory. On a cellular level long lasting changes in synaptic transmission, called synaptic

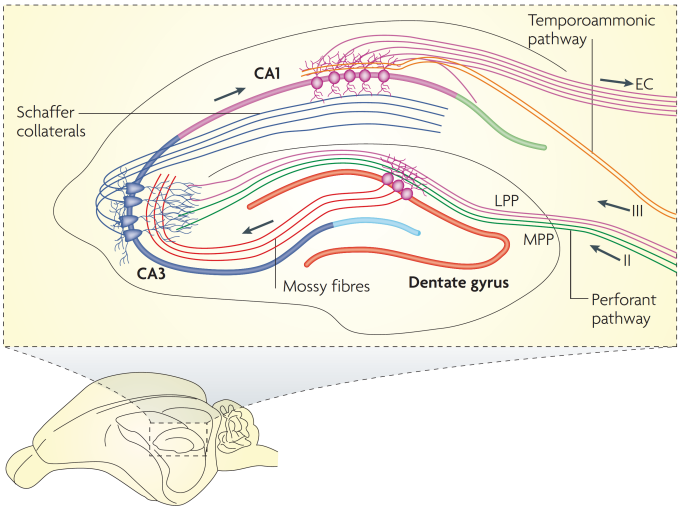

Figure 1.2 Anatomy and neuronal circuit of the hippocampus. The small inset depicts the localization of the hippocampus in the murine brain. The hippocampus receives synaptic input from the entorhinal cortex (EC) via the dentate gyrus (DG). Mossy fibres from the DG signal on CA3 neurons which in turn send information via the Schaffer collaterals to CA1 pyramidal neurons. Their axons stretch into st. oriens in direction to the EC. The small image illustrates the localization of the hippocampus in the rodent brain. LPP, lateral perforant pathway; MPP, medial perforant pathway. From Deng et al., 2010.

plasticity, were correlated with memory formation. Rodents exposed to hippocampus-related learning tasks displayed long lasting changes of synaptic strength (Martin and Morris, 2002). The hippocampus is also involved in emotional behaviour. The emotional status influences adult neurogenesis in the SGZ (Deng et al., 2010). Furthermore, reduced adult neurogenesis impaired learning, the integration of newly formed neurons is therefore essential for memory formation (Martin and Morris, 2002).

1.2 Glial cells in the brain

The brain consists of different cell-types. In addition to neurons, glia are important for normal brain functions. These cells were discovered by Rudolf Virchow in the mid-1800s and first administered a supportive role in the brain. Their name is derived from the Greek word for glue (Virchow, 1846; Barres, 2008). Today the importance of glia in the brain is widely recognized (Nedergaard et al., 2003; Barres, 2008; Lee et al., 2012; Herculano-Houzel, 2014). Glial cells are divided into two subgroups, microglia and macroglia. The latter group is further subdivided into astrocytes, oligodendrocytes, NG2 cells and ependymal cells.

1.2.1 Microglia

Microglia are the immune cells of the CNS resembling macrophages found in other tissues. They have a small cell soma and several processes to continuously scan their surroundings. They are present in all brain regions and are activated by inflammation or lesions (Rock et al., 2004). Activation leads to morphological changes including a more ramified structure. Furthermore, microglia migrate to the lesion site, proliferate and remove toxic substances and debris by phagocytosis (Amat et al., 1996; Sierra et al., 2013). Activated microglia *in vitro* display functional gap junction channels formed by connexin43, in the brain activated microglia contain increased connexin43 protein levels (Eugenín et al., 2001). The presence of functional gap junction channels could not be confirmed *in situ*: Microglia never displayed tracer coupling to other cells irrespective of their activation status (Richter et al., 2014; Wasseff and Scherer, 2014).

1.2.2 Ependymal cells

Ependymal cells have a cuboidal shape and line the walls of the ventricles. They evolve from radial glia cells and have motile cilia for propulsion of the cerebrospinal fluid (CSF). Furthermore, they play a role in brain homoeostasis by exchange of molecules with the CSF (Spassky et al., 2005). A special subgroup of ependymal cells are the tanycytes which line the floor of the third ventricle. These cells extend long processes to the hypothalamus possibly propagating signals from the CSF to CNS neurons and another process to blood vessels (Langlet, 2014). They are chemosensitive and modulate neuronal activity to regulate brain energy balance, and are involved in energy homoeostasis by regulating metabolic signalling to the hypothalamus (Langlet, 2014).

1.2.3 Astrocytes

Astrocytes are abundantly present throughout the brain. The name is derived from their star-like morphology. They have a ramified structure with fine processes, their morphology becomes increasingly complex with brain architecture. Furthermore, with increasing brain complexity the ratio of astrocytes per neuron increases (Nedergaard et al., 2003; Allaman et al., 2011).
Astrocytes are close interaction partners at the blood-brain-barrier and play a role in the gliovascular network. Endothelial cells line the walls of the vasculature which are enwrapped by astrocytic endfeet to take up water, ions and metabolites from the blood and release toxic substances, excess water and ions into the blood (Nedergaard et al., 2003; Strohschein et al., 2011). Additionally, they control the blood flow in the brain and are involved in angiogenesis, the formation of new blood vessels (Haydon and Carmignoto, 2006; Wang and Bordey, 2008). Astrocytes are therefore important for brain homoeostasis, and express a variety of transporters and channels in their endfeet like aquaporins, K^+ channels, glucose transporters (GluT) and connexins (Wang and Bordey, 2008).

Anatomical studies revealed that astrocytes reside in the brain in a non-overlapping manner contacting each other with their processes (Bushong et al., 2002). Neighbouring cells are connected with each other via gap junction channels (GJC) and thereby form a network. In the hippocampus this network is established during early postnatal development (Schools et al., 2006). Gap junction channel mediated networks will be further described in section 1.4.
Electrophysiological analysis revealed a passive current pattern in whole-cell recordings. Interestingly, astrocytes lacking GJC have a passive current pattern like pap junction (GJ)-coupled astrocytes (Wallraff et al., 2006). The current pattern reflects the high density of K^+ channels, inward-rectifying K^+ (Kir) and two-pore domain K^+ (K_{2P}) channels (Kang et al., 1998; Wallraff et al., 2004; Seifert et al., 2009). In addition, their membrane potential is close to the K^+ equilibrium in the brain, around -80 to -90 mV (Nedergaard et al., 2003; Wang and Bordey, 2008). A role in spatial K^+ buffering was already postulated in the 1960s for astrocytes and confirmed by several studies indicating K^+ diffusion in the astroglial network and cell swellings in case of non-functional networks (Orkand et al., 1966; Wallraff et al., 2006; Pannasch et al., 2011).
Astrocytes closely interact with neurons at synapses which led to the concept of the tripartite synapse (Araque et al., 1999; Agulhon et al., 2008; Pannasch and Rouach, 2013). They enwrap synapses with their processes and take up neurotransmitters like glutamate and GABA from the synaptic cleft and express glutamate transporters (Matthias et al., 2003). Astrocytes respond to glutamate with increased $[Ca^{2+}]_i$ levels mediated by G-protein coupled receptors like mGluR5 in VB astrocytes (Nedergaard et al., 2003; Parri et al., 2010). Furthermore, they express the enzyme glutamine synthetase (GS) to transform glutamate into glutamine (Norenberg, 1979; Nedergaard et al., 2003). Astrocytes also release gliotransmitters like D-serine, ATP and glutamate and are active partners in neuronal activity in addition to uptake of neurotransmitters (Henneberger et al., 2010; Sahlender et al., 2014).
Glutamine synthetase is one of the widely used astrocyte markers (Coulter and Eid, 2012). Further examples for classical astrocyte markers are glial fibrillary acidic protein (GFAP), the calcium binding protein S100β and aldehyde dehydrogenase 1 family, member L1 (Aldh1L1) also known as 10-formyltetrahydrofolate dehydrogenase (FDH) (Cahoy et al., 2008; Wang and Bordey, 2008). GFAP is expressed by hippocampal astrocytes, but not in the thalamus, while S100β was described in both thalamic and hippocampal astrocytes (Frassoni et al., 2000; Matthias et al., 2003; Muneoka et al., 2012). Aldh1L1 was found to be enriched in astrocytes in a transcriptome analysis, and suggested to be a universal astrocyte marker throughout the brain (Cahoy et al., 2008).
In summary, astrocytes fulfil a variety of functions which are essential for brain homoeostasis and thus for normal brain function.

1.2.4 Oligodendrocytes and NG2 cells

Oligodendrocytes are the third macroglial cell-type in the brain. They have few 'oligo' branches extending from the cell soma and are the myelinating cells of the CNS. Schwann cells fulfil the same function in the PNS. In contrast to astrocytes they do not contact blood vessels.
Interfascicular oligodendrocytes enwrap neuronal axons with their processes and thereby insulate the axon. Myelination starts during postnatal development in a region dependent manner with a peak expression of myelin proteins during the third postnatal week (Verity and Campagnoni, 1988; Fuss et al., 2000). The myelin sheath is an extension of the cell membrane and consists of several membrane layers. The cell membrane is a lipid bilayer and in the myelin sheath additionally contains glycosphingolipids, sulphatides like O4 and galactolipids. The cytoplasm is extruded from these layers. Additionally, it contains proteins like myelin basic protein (MBP), phospholipoprotein (PLP), 2',3'-cyclic nucleotide 3'-phosphodiesterase (CNPase) and also connexins. The axon is not entirely enwrapped, but in between consecutive myelinated parts it has direct contact to the extracellular space at the nodes of Ranvier.
Another class of oligodendrocytes are non-myelinating perineuronal oligodendrocytes. These cells are located in apposition to neuronal cell bodies in grey matter like cortex. They express CNPase and GS, but no glutamate transporters like GLAST or GLT1 and might play a role in metabolic support (Takasaki et al., 2010).
Mature myelinating oligodendrocytes are typically identified by their expression of myelin proteins CNPase, MBP and PLP (Cahoy et al., 2008; Jahn et al., 2009). The development of oligodendrocytes has been widely studied and differentiation stages are distinguished by changes in morphology and marker expression.
During early development precursors express several transcription factors like Olig1, Olig2, and Sox10 which regulate cell proliferation and development. Oligodendrocyte precursors express NG2 and platelet derived growth factor receptor α (PDGFαR) and later differentiate into myelinating cells in the juvenile brain (Karram et al., 2008; Nishiyama et al., 2009; Trotter et al., 2010). NG2 (nerve-glia antigen 2) cells were discovered in the 1980s by Stallcup using antibodies against the chondroitin sulphate proteoglycan 4 (CSPG4; Stallcup, 1981. Still, some of these NG2 expressing cells reside in the mature brain and are synaptically innervated by neurons (Bergles et al., 2000; Jabs et al., 2005). The expression of Ca^{2+} permeable (α-amino-3-hydroxy-5-methyl-4-isoxazolepropionic acid) (AMPA) receptors was confirmed in hippocampus and thalamus (Seifert and Steinhäuser, 1995; Parri et al., 2010). In the adult brain in white matter Olig2 expressing precursors differentiate into myelinating oligodendrocytes, while in grey matter these cells persist as NG2 cells (Dimou et al., 2008). The role of these cells in the mature brain remains elusive. Interestingly, NG2 cells seem to scan their environment with their highly motile processes and respond to synaptic input with local Ca^{2+} elevations (Haberlandt et al., 2011). The NG2 protein is a transmembrane protein which might play a role in stabilizing Neuron-NG2 synapses. However, employing NG2 knock-

out mice this effect could not be confirmed, even though an earlier study showed that NG2 and AMPA receptors are clustered intracellularly by glutamate receptor interaction protein (GRIP; Stegmüller et al., 2003; Passlick et al., 2014). NG2 cells are sometimes referred to as the fourth macroglial cell-type, as not all of these cells differentiate into oligodendrocytes.
Oligodendrocytes express a set of connexins which is different from astrocyte connexins. As mentioned before, oligodendrocytes comprise connexin channels in their myelin sheath (see above). Additionally, oligodendrocytes form a gap junction network in white matter which also contain NG2 cells (Maglione et al., 2010; Tress et al., 2012) and will be further described in section 1.4.

1.2.5 RG-like cells

Radial-glia like cells (RG-like cells) are neural stem cells in the adult brain. These cells reside in neurogenic niches in the subventricular zone of the lateral ventricle and the SGZ of the DG (Doetsch et al., 1999; Seri et al., 2001). RG-like cells have a characteristic morphology with their cell soma located in the SGZ and a long process stretching through the granule cell layer (Filippov et al., 2003b). These cells proliferate and thereby generate new neural precursor cells which differentiate into neurons (Seri et al., 2001; Doetsch, 2003). RG-like cells have astrocyte-like properties, e.g. they express GFAP and gap junction proteins and are coupled to neighbouring cells (Seri et al., 2001; Kunze et al., 2009). Functional analysis revealed a localization dependent presence of AMPA receptors on their processes, glutamate transporters on the soma and gamma-aminobutyric acid ($GABA_A$) receptors on the entire cell surface (Renzel et al., 2013). This is in contrast to hippocampal astrocytes which do not express AMPA receptors but comprise glutamate transporters (Matthias et al., 2003).
Like radial glia in the embryonic brain, RG-like cells serve as a scaffold for migrating neural precursors during differentiation (Frassoni et al., 2000; Elias et al., 2007). Radial glia trans-differentiate into astrocytes when migration is completed in contrast to RG-like cells (Schmechel and Rakic, 1979; Doetsch, 2003; Kimelberg, 2004). Recent results indicate a role in memory and learning for newly generated neurons (Deng et al., 2010).

1.3 AMPA and $GABA_A$ receptors in glial cells

For a long time astrocytes were thought to be passive cells located between neurons. They display a passive current pattern in response to de- and hyperpolarizing voltage steps. Today we know that astrocytes express a variety of channels despite their passive current pattern. These channels are either ionotropic receptors leading to ion flux over the membrane or metabotropic receptors that activate second messengers and thereby induce a signalling cascade in the cell.
VB astrocytes express a variety of receptors like histamine receptors, AMPA (GluA1),

NMDA (NR2B), $GABA_A$, group I mGluRs and group II mGluA2+3 receptors (Parri et al., 2001; Parri and Crunelli, 2002). Neuronal synaptic activity leads to $[Ca^{2+}]_i$ increases in thalamic astrocytes by activating mGluAs on astrocytes (Pirttimaki and Parri, 2012). Additionally, VB astrocytes display spontaneous Ca^{2+} oscillations in young mice at p4, which decrease until p14. Interestingly, these oscillations have pacemaker properties at a frequency of 0.019Hz (Parri and Crunelli, 2001).
AMPA receptors are ionotropic receptors activated by glutamate. They are transmembrane channels expressed by neurons and glial cells (Burnashev et al., 1992). There are four different AMPA receptor subunits GluA1, GluA2, GluA3 and GluA4. The presence of the GluA2 subunit and its RNA-editing at the Q/R-site is responsible for the Ca^{2+} impermeability. The subunits exist in two splice isoforms known as "flip" and "flop" which differ in a small sequence of the extracellular loop prior to the fourth transmembrane region. Splice isoforms along with a second RNA-editing site, the R/G-site, influence channel gating kinetics. Four of these subunits form an ion channel (Burnashev et al., 1992; Bear et al., 2006; Guzman and Jonas, 2010). In response to neurotransmitter activation the channel opens and permits the influx of the cations Na^+, K^+ and Ca^{2+}, the latter only in the absence of the GluA2 subunit.
Astrocytes respond to glutamate application with inward currents (Steinhäuser et al., 1994). In cerebellar Bergmann glia functional AMPA receptors display high Ca^{2+} permeabilities and do not express the GluA2 subunit (Burnashev et al., 1992; Müller et al., 1992). Loss of AMPA receptors induce retraction of processes from synapses and have severe consequences on a behavioural level by impaired motor performance (Saab et al., 2012). In the supraoptic nucleus of the hypothalamus two distinct types of astrocytes were observed. One type lacks AMPA receptors and glutamate uptake and the second type expresses glutamate transporters (Matyash and Kettenmann, 2010).
In the murine hippocampus distinct cell-types were observed according to their glutamate currents. Cells displaying a complex current pattern, known as NG2 cells, express AMPA receptors, while passive astrocytes express glutamate transporters (Matthias et al., 2003; Seifert et al., 2003). These observations were confirmed by a study in the rat hippocampus analysing astrocytes termed variable-rectifying astrocytes and NG2 cells termed outward-rectifying astrocytes (Zhou and Kimelberg, 2001).
The group of glutamate receptors includes NMDA and kainate receptors in addition to AMPA receptors. Astrocytes lack NMDA receptors in most brain regions. Only in cortical astrocytes and Bergmann glia functional NMDA receptors were reported which display a weaker Mg^{2+} block compared to neuronal NMDA receptors (Wang and Bordey, 2008; Matyash and Kettenmann, 2010). Kainate receptors are not expressed by astrocytes (Porter and McCarthy, 1997).
$GABA_A$ receptor channels are composed of 5 subunits, usually 2 α-, 2 β- and 1 γ- or δ-subunit. Every subunit is encoded by related genes. There are 6 different α-, 3 β-, 3 γ- and 1 δ- genes (Kandel et al., 2012). These gene transcripts are differentially expressed in a region dependent manner and are developmentally regulated. The α3 mRNA was found to be highly expressed in the RTN, while in the ventral posterior nucleus α1, α4,

β2 and δ were the predominating mRNAs. In hippocampal pyramidal cells and granule cells in the dentate gyrus express high levels of many $GABA_A$ mRNAs, but completely lack α4 expression (Wisden et al., 1992). During embryonal and early postnatal development the expression pattern in the cortex and thalamus differs from adult brain. In young animals the α2, α3, α5 and β3 were prominently expressed and then downregulated before being replaced by other gene transcripts (Laurie et al., 1992). The presence of the γ2 subunit is a characteristic feature of synaptic $GABA_A$ receptors in neurons as well as in NG2 cells (Passlick et al., 2013). Activation of these channels allows influx of the anions Cl^- and HCO_3^-. This induces a depolarization in young neurons and a hyperpolarization in mature neurons due to the increasing expression of the KCl cotransporter KCC2 (Stein et al., 2004), thereby providing an inhibitory effect in neurons. Astrocytes do not make synapses with other cells and lack this subunit. Furthermore, they lack the neuron-specific KCC2 and respond to GABA with a depolarization (Stein et al., 2004; Matyash and Kettenmann, 2010).
In contrast to glutamate receptor currents all astrocytes express $GABA_A$ receptor currents. Bergmann glia cells display developmentally regulated $GABA_A$ receptor expression with a peak at p7-10 (Matyash and Kettenmann, 2010). Also astrocytes in the hippocampus and supraoptic nucleus always display $GABA_A$ receptors as well as RG-like cells. Furthermore, both in mouse and rat, NG2 cells and astrocytes express these receptors (Steinhäuser et al., 1994; Zhou and Kimelberg, 2001; Passlick et al., 2013; Renzel et al., 2013).

1.4 Connexin gap junction channels

Vertebrates express connexin (Cx) gap junction proteins which are a class of transmembrane proteins. There are different types of connexins which are distinguished by their molecular weight, e.g. Cx30 has a molecular weight of 30 kDaltons (kDa; Beyer et al., 1989). Another nomenclature involves gene names which are grouped in families (α, β, γ, etc.) defined by sequence homology of the different connexins and length of the cytoplasmic C-terminus (Söhl et al., 2001). There are 21 known connexins in humans and 20 connexins in mouse with a molecular weight between 23 to 62 kDa and 23 to 57 kDa respectively. 11 connexins were found in nervous tissue (Willecke et al., 2002; Söhl and Willecke, 2003; Giaume et al., 2010).
Six connexin subunits form a hemichannel in the cell membrane, known as connexon. By rearrangement of the connexin proteins the channel can be closed (Willecke et al., 2002). Two adjacent hemichannels form a gap junction channel (GJC) to connect the cytoplasm of two cells. Several GJC assemble and thereby form a GJ plaque (Fig.1.3A). The GJC can be formed by two connexons of the same connexin type, termed homotypic channels, or by connexons of two different connexins forming a heterotypic channel. Additionally, one hemichannel can be formed by one or several types of connexin proteins. Homomeric hemichannels are formed by one type of connexin

and heteromeric channels contain different connexin proteins (Willecke et al., 2002; Goldberg et al., 2004). Connexins have four transmembrane domains, two extracellular loops, one intracellular loop and the N- and C-terminal tails located in the cytoplasm. Sequences are partially highly conserved, like the cysteine residues required for extracellular disulfide bonds, or variable, like the length of the C-terminus or the length of the extracellular loops (Fig. 1.3B; Rozental et al., 2000; Willecke et al., 2002). A crystal structure analysis by Maeda et al. (2009) of the Cx26 GJC revealed the ultrastructure of the channel. All transmembrane domains are helices. The N-terminal helices form the channel wall and are therefore responsible for channel permeability for small molecules, e.g. the Cx26 GJC has a diameter of 14 Å at its smallest site (Maeda et al., 2009).
GJC are selectively permeable regarding molecular weight, shape, net charge and the resulting interactions with the connexins forming the channel (Goldberg et al., 2004; Giaume et al., 2010). The pore domain connects the cytoplasm of two adjacent cells and allows the diffusion of small molecules below 1-1.2 kDa in size (Laird, 2006; Giaume et al., 2010). Extensive *in vitro* studies have been performed using different tracers to analyse connexon and GJC permeability for these molecules (Elfgang et al., 1995; Yum et al., 2007; Ahn et al., 2008; Orthmann-Murphy et al., 2007b; Magnotti et al., 2011b). In the brain GJC are important for exchange of second messengers (cAMP, IP_3), ions (K^+, Na^+, Ca^{2+}), water and metabolites (glucose, lactate) among others (Holthoff and Witte, 2000; Niermann et al., 2001; Rouach et al., 2002; Bedner et al., 2006; Wallraff et al., 2006; Rouach et al., 2008; Giaume et al., 2010).
The length of the C-terminus is highly variable between connexins (see above) and contains several phosphorylation sites and binding sites for cytoplasmic matrix proteins, e.g. Zona occludens (ZO)-1, ZO-2, α- and β-tubulin (Laird, 2006). The phosphorylation of serine or tyrosine amino acids by mitogen-acitvated protein kinase (MAPK), protein kinase A (PKA), protein kinase C (PKC), v- and c-src kinases modulates the life cycle of connexins and gating properties of GJC (Lampe and Lau, 2000; Laird, 2006; Solan and Lampe, 2014). Interestingly, the lifetime of connexins is very short and highly regulated in an activity dependent manner by phosphorylation and binding to tight-junction associated proteins ZO-1 and ZO-2. The latter are involved in GJ assembly and stabilization in the membrane (Duffy et al., 2002; Laird, 2006).
Connexins are expressed in different organs, among others in heart, liver and brain. Furthermore, their expression is developmentally regulated, region dependent and cell-type specific (Dermietzel et al., 1989; Willecke et al., 2002; Nagy et al., 2004; Theis et al., 2005). Most cell-types express several connexins, e.g. astrocytes express Cx26, Cx30 and Cx43, while oligodendrocytes express a different set of connexins: Cx29, Cx32 and Cx47 (Nagy et al., 2003; Bedner et al., 2012). A specific connexin is expressed by several cell-types, e.g. in the brain Cx43 is expressed by astrocytes, leptomeningeal cells and ependymal cells (Laird, 2006).
Connexin hemichannels, which connect the cytoplasm with the extracellular space, were observed in many cells (Willecke et al., 2002; Goodenough and Paul, 2003). Under physiological conditions these hemichannels are mostly closed. Additionally, cells

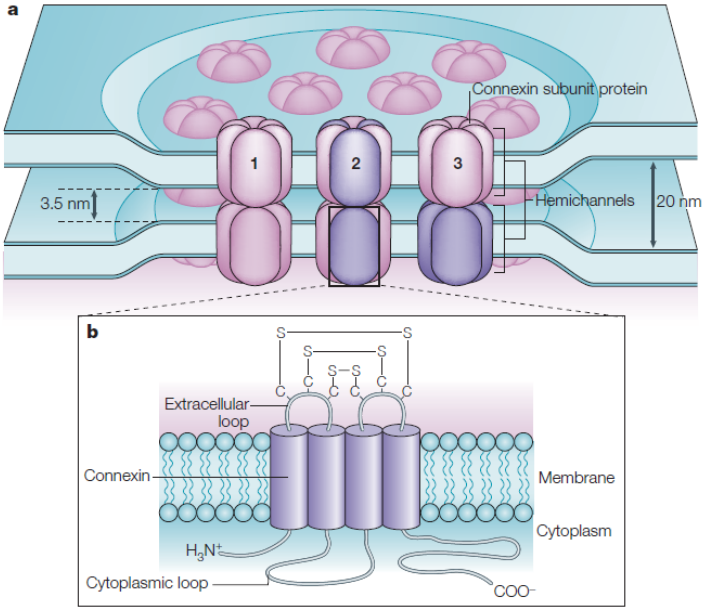

Figure 1.3 Gap junction plaque topology and connexin structure. (A) Gap junction plaques consist of several gap junction channels between two adjacent cells which are formed by connected hemichannels. Six connexins form a hemichannel. Gap junction channels consisting of one connexin type are homomeric/homotypic (1), when composed of different connexins they are termed heteromeric (2), and in case of two connected hemichannels of different connexins heterotypic (3). (B) Connexins have 4 transmembrane domains, two extracellular loops, one intracellular loop and the N- and C-terminal tails on the cytoplasmic side. Extracellular disulphide bonds are highly conserved, in addition, several connexins contain phosphorylation sites on their C-terminal tail. From Söhl et al., 2005.

also contain another channel protein in mammals, termed pannexins, which show substantial homology to innexins found in invertebrates (Goodenough and Paul, 2003; Giaume et al., 2010). They might be involved in gliotransmitter release and open in response to physiological and pathophysiological stimuli (Bennett et al., 2012; Orellana and Stehberg, 2014).

Several human diseases are associated with connexin mutations and mouse models have been generated to study modifications or complete loss of connexin (Willecke et al., 2002; Laird, 2006; Giaume et al., 2010). Loss of Cx26 leads to non-syndromic deafness and in some cases to alterations in the skin (Cohen-Salmon et al., 2002; Laird, 2006). Several Cx32 mutations lead to X-linked Charcot-Marie-Tooth disease, a neuropathy affecting the PNS by demyelination (Willecke et al., 2002; Menichella et al., 2003). Oculodentodigital dysplasia (ODDD) is a disease caused by mutations in the human *Gja1* gene, coding for Cx43, and includes abnormalities of the fingers, toes, eyes, face and teeth (Laird, 2006; Dobrowolski et al., 2008). Recessive mutations of Cx47 lead to Pelizaeus-Merzbacher-like disease, a progressive leukodystrophy involving hypomyelination and spasticity by loss-of-function mutations (Orthmann-Murphy et al., 2007a; Tress et al., 2011). Connexin expression and proper GJ formation is therefore crucial for normal brain function.

1.4.1 Astrocyte connexins

Astrocytes express three connexins: Cx26, Cx30, and Cx43, which are not expressed by oligodendrocytes or neurons in the CNS (Rash et al., 2001; Nagy and Rash, 2003). Glial cells have >100x more GJC than neurons. Considering the spatial anatomical domains of astrocytes and assuming a uniform distribution of these GJC on the cell surface, most interastrocytic (A/A) junctions must be autologous (Rash et al., 1998; Bushong et al., 2002; Nagy and Rash, 2003). Most likely these reflexive GJC facilitate homoeostasis between different cellular compartments (Grosche et al., 1999; Rouach et al., 2002). GJC with neighbouring cells are mostly located at the endfeet of astrocytes enwrapping blood vessels and at their fine processes (Giaume et al., 2010). Functional studies in several brain regions revealed that astrocyte networks selectively overlap with neuronal functional entities (Houades et al., 2006; Houades et al., 2008; Roux et al., 2011). Furthermore, these networks adapt to changes in neuronal activity and are required for normal brain function (Rouach et al., 2008; Pannasch et al., 2012). Cx26 is expressed in astrocytes and leptomeninges in the CNS and in the inner ear. It has been widely studied due to its mutations causing a non-syndromic deafness (Rash et al., 2001; Willecke et al., 2002). Cx26-deficient mice die early in embryogenesis due to impaired transplacental glucose uptake (Gabriel et al., 1998). In the brain Cx26 was detected around blood vessels, in leptomeninges and in astrocytes and has a perivascular, sub-pial and subependymal localization (Mercier and Hatton, 2001). Cx26 shows subcellular colocalization with Cx30 and Cx43. GJCs between astrocytes containing Cx26 and Cx30 are often found near neuronal processes (Nagy et al., 2001; Rash et al., 2001). Furthermore, Cx26 was detected in GJ plaques together with Cx32 (Nagy et al., 2001; Rash et al., 2001). Cx26 is differentially expressed with highest levels during embryonal development and early postnatal life and decreasing thereafter in the brain (Dermietzel et al., 1989; Nagy et al., 2001). In the adult brain high levels of Cx26 were observed in the thalamus, while in the hippocampus only low levels and in the cortex no Cx26 was detected apart from leptomeninges (Nagy et al., 2001; Nagy et al., 2011). A study employing $Cx26^{+/LacZ}$ mice did not confirm astrocytic Cx26 expression, though the reporter was found in leptomeninges in the brain and in other organs (Filippov et al., 2003a). Cx26 is highly homologous to Cx30 and in some studies antibodies cross-reacting with Cx30 were applied, overestimating Cx26 expression in the brain (Orthmann-Murphy et al., 2008). The *Gjb2* locus is located near the *Gjb6* (Cx30) locus on chromosome 14 (Willecke et al., 2002; Boulay et al., 2013).
Cx30 is also found in astrocytes, but in contrast to Cx26, it is only expressed during postnatal development starting from the second postnatal week (Dahl et al., 1996; Kunzelmann et al., 1999). It is located near blood vessels and expressed by ependymal cells and leptomeningeal cells in addition to astrocytes (Kunzelmann et al., 1999). Mutations of Cx30 were thought to induce deafness due to observations in a Cx30 knock-out mouse line. These mice were affected by the additional loss of Cx26 due to the proximity of the genes on one chromosome (Teubner et al., 2003; Lynn et al., 2011). A

recently generated new knock-out mouse was healthy and hearing was normal (Boulay et al., 2013). The expression level of Cx30 is lower in the hippocampus compared to Cx43, the third connexin expressed by astrocytes (Gosejacob et al., 2011). Functional analysis employing the tracer biocytin revealed a differential impact on network formation of 22% or around 50% reduction in network size (Gosejacob et al., 2011; Pannasch et al., 2014). Furthermore, Cx30 is not expressed by white matter astrocytes and is selectively higher permeable for cations over anions (Nagy et al., 1999; Nagy et al., 2004; Yum et al., 2007). Expression levels of Cx30 in the cerebellum and thalamus are higher compared to hippocampus (Nagy et al., 1999; Gosejacob et al., 2011). Cx30 plays a role in astrocytic glutamate transport and thereby influences synaptic transmission (Pannasch et al., 2014). Immunohistochemical analysis revealed colocalization with Cx43 (Kunzelmann et al., 1999; Nagy et al., 1999).
Cx43 is widely expressed throughout the body, and because of its crucial role in heart function many studies were performed on expression and regulation of Cx43 (Yamamoto et al., 1990; Lampe and Lau, 2000; Laird, 2006). Cx43 expression in the brain is upregulated during embryonal development and remains high through adulthood (Dermietzel et al., 1989). The *Gja1* gene is located on chromosome 10 and is also expressed by leptomeningeal cells and ependymocytes in the brain (Rash et al., 2001; Willecke et al., 2002). Loss of Cx43 in hippocampal astrocytes leads to a 50% decrease in network size, spreading depression in neurons and to an increase in Cx30 protein levels (Theis et al., 2003; Degen et al., 2012). Loss of both Cx30 and Cx43 leads to complete uncoupling of astrocytes in the hippocampus, dysmyelination and vacuolizations (Wallraff et al., 2006; Lutz et al., 2009; Pannasch et al., 2011). Furthermore, spatial K^+ buffering, metabolite transport and neurotransmitter clearance are impaired leading to increased synaptic transmission and spontaneous epileptiform activity amongst others. Hippocampal astroglial networks modulate extracellular homoeostasis and thereby influence synaptic strength (Wallraff et al., 2006; Rouach et al., 2008; Pannasch et al., 2011).
Radial glia-like cells are neuronal precursors which reside in neurogenic niches in the adult brain. These cells have astrocyte like properties and express Cx30 and Cx43, deletion of both connexins resulted in uncoupled RG-like cells in the subgranular zone of the dentate gyrus (Kunze et al., 2009; Liebmann et al., 2013). Recently, it was shown that Cx30 expression is not required for adult neurogenesis, but Cx43 is important (Liebmann et al., 2013). In addition, connexins have a non-channel function influencing migration of neuronal precursors (Elias et al., 2007).
In conclusion, astrocytes express Cx26, Cx30 and Cx43 *in vivo* to form gap junctions and establish a glial network whose function is closely linked to neuronal activity.

1.4.2 Oligodendrocyte connexins

Oligodendrocytes express a specific set of connexins that differs from astrocytes: Cx29, Cx32 and Cx47 (Dermietzel et al., 1989; Rash et al., 2001; Altevogt et al., 2002;

Nagy and Rash, 2003). Interestingly, in freeze-fracture replica immunogold labelling analysis interoligodendrocytic (O/O) junctions were rarely or not at all observed (Massa and Mugnaini, 1982; Rash et al., 2001; Kamasawa et al., 2005). Gap junction plaques on oligodendrocytes were connected to astrocytes or established autologous junctions between cell membrane layers (Rash et al., 2001; Nagy and Rash, 2003; Nagy et al., 2004; Kamasawa et al., 2005).
Cx29 was never located in gap junction plaques between cells, but rather in autologous junctions between different layers of the myelin sheath close to nodes of Ranvier in the adult brain, but also at the cell soma (Li et al., 2002; Nagy and Rash, 2003; Nagy et al., 2003; Nagy et al., 2004; Kamasawa et al., 2005; Ahn et al., 2008). The *Gje1* gene on chromosome 5 is expressed from the first postnatal week and is gradually upregulated until adulthood (Söhl et al., 2001; Willecke et al., 2002; Nagy et al., 2003). The expression is restricted to neural tissue in PNS Schwann cells and CNS oligodendrocytes (Altevogt et al., 2002; Nagy et al., 2004). Functional analysis of gap junction networks in white matter revealed no decrease in network size upon loss of Cx29 which confirms the non-intercellular gap junction localization of Cx29 (Maglione et al., 2010). Western blot analysis revealed high expression levels in the thalamus and lower expression in the hippocampus and cortex, probably accounting for the differences in myelination in these brain regions (Nagy et al., 2003). In the myelin sheath Cx29 was found to colocalize with Cx32, the second oligodendrocytic connexin (Nagy et al., 2004).
Several studies located Cx32 on oligodendrocyte somata, initial processes and in the myelin sheath (Nagy et al., 2003; Nagy et al., 2004; Kamasawa et al., 2005). It is especially located at Schmidt-Lantermann incisures, between paranodal loops close to nodes of Ranvier and in the outermost layer of myelin, but not in compact myelin and rarely at A-O junctions (Scherer et al., 1995; Nagy et al., 2004; Kamasawa et al., 2005). In contrast, in the PNS Cx32 was only observed between myelin layers of Schwann cells (Scherer et al., 1995; Menichella et al., 2006). Expression of the *Gjb1*-encoded Cx32 is only detected during postnatal development starting from the second postnatal week and is not restricted to neural tissue (Dermietzel et al., 1989; Nelles et al., 1996). Loss of Cx32 in mice did not induce any neurological disorders (Nelles et al., 1996; Scherer et al., 1998). Functional studies in white matter areas revealed no impact of Cx32 on glial network size (Maglione et al., 2010). *In vitro* studies revealed restricted passage of anions through Cx32 GJC (Goldberg et al., 2004). In the outer myelin layers Cx32 was found together with Cx47 (Kamasawa et al., 2005).
Initial studies revealed Cx47 expression mainly in neural tissue, especially in neurons (Teubner et al., 2001). Cx47 is encoded by the *Gja12* gene on chromosome 11. Further analysis detected Cx47 only in oligodendrocytes, but not in neurons, and confirmed the mainly neural tissue expression (Menichella et al., 2003; Odermatt et al., 2003; Kamasawa et al., 2005). Cx47 was mainly localized on the soma of oligodendrocytes and on the outer surface of the myelin sheath, most likely at A-O junctions (Menichella et al., 2003; Nagy et al., 2003). In functional studies employing tracer diffusion, loss of Cx47 had a strong impact on network size. Additional loss of Cx32 led to un-

coupled oligodendrocytes (Maglione et al., 2010). Furthermore, loss of Cx47 induced morphological alterations in the CNS including vacuolizations between the axon fibre and the myelin sheath (Menichella et al., 2003; Odermatt et al., 2003). Cx47 is therefore highly important for myelination. It is upregulated together with myelinating proteins, first detected around p10 and highly expressed until p30, while in adult mice expression levels are lower (Menichella et al., 2003). Additionally, loss of Cx47 is accompanied by loss or relocation of other glial connexins in the brain, but not by upregulation of other oligodendrocyte connexins (Odermatt et al., 2003; Li et al., 2008). In conclusion, connexin expression in oligodendrocytes is important for normal myelination and homoeostasis in the brain (Kamasawa et al., 2005; Maglione et al., 2010).

1.4.3 Neuronal connexins

Neurons communicate with each other via chemical or electrical synapses. Gap junction channels in neurons form electrical synapses which play an important role during the prenatal phase of neurogenesis (Kunze et al., 2009; Niculescu and Lohmann, 2013). At this early stage of development a simple communication method is required to coordinate proliferation, migration and positioning of the neurons in the neocortex (Montoro and Yuste, 2004). Chemical synapses mainly develop during postnatal development, when neuronal circuits are established, and might be better suited for neuronal communication in adulthood (Montoro and Yuste, 2004; Niculescu and Lohmann, 2013; Pereda, 2014). Brain maturation involves synaptic pruning, unnecessary chemical synapses are eliminated during this process. Electrical synapses aid in this process and also microglia are involved in synaptic pruning (Paolicelli et al., 2011; Pereda, 2014).
Even though most electrical synapses disappear during postnatal development, some electrical synapses persist throughout life in several brain regions (Connors and Long, 2004). For formation of these synapses neurons express mainly Cx36 and Cx45 which are differentially regulated (Belluardo et al., 2000; Krüger et al., 2000). Cx36 expression starts during late embryogenesis and increases within the first postnatal week, before it slightly declines, but is still expressed throughout life (Bittman et al., 2002; Maxeiner et al., 2003). The Cx36 gene *Gja9* is located on chromosome 2 (Söhl and Willecke, 2003).
In contrast, Cx45 is embryonally expressed with a peak expression in the second postnatal week and is downregulated afterwards in most brain regions. In adulthood, Cx45 expression has been observed only in the thalamus, CA3 region of the hippocampus, the molecular layer of the cerebellum and layers II and VI in the parieto-occipital and entorhinal cortex (Krüger et al., 2000; Maxeiner et al., 2003). The *Gja7* gene is located on chromosome 11 and its expression parallels the astrocytic Cx26 expression pattern during development (Maxeiner et al., 2003; Söhl and Willecke, 2003).
Though chemical synapses replace electrical synapses in most brain regions, interneurons

in the cortex and RTN neurons in the thalamus remain highly connected in the adult brain, while in the VB electrical synapses were only found before the end of the second postnatal week (Niculescu and Lohmann, 2013). Starting in the second postnatal week these electrical synapses are replaced and a disynaptic circuit including RTN neurons is established (Lee et al., 2010).
These gap junctions are not exclusively found between neurons, but also between neurons and astrocytes in the juvenile cortex and locus ceruleus (Alvarez-Maubecin et al., 2000; Bittman et al., 2002). In the cortex these gap junctions were asymmetric, therefore dye transfer was observed only from astrocytes to neurons at p7 and developmentally reduced already at p14 (Bittman et al., 2002).
Connexin expression is abundant in neurons and their precursors and developmentally downregulated during maturation of the brain.

1.4.4 Heterotypic gap junction channels between glial cells

Gap junction channels were first thought to be exclusively formed between cells of the same type. Freeze fracture studies in the early 1980s revealed that GJC also occur between astrocytes and oligodendrocytes in the white matter of the cat brain (Massa and Mugnaini, 1982). These gap junctions were mainly observed on oligodendrocyte somata, initial processes and the uncompacted outermost myelinating processes (Massa and Mugnaini, 1982; Nagy and Rash, 2003). These channels were expected to be heterotypic as astrocytes and oligodendrocytes express a different set of connexins (Orthmann-Murphy et al., 2008).
In vitro studies in HeLa and N2A cells confirmed the function of GJC between astrocytic and oligodendrocytic connexons, though not all combinations are permeable. The following combinations produced functional channels in HeLa cells: 26/26, 30/30, 43/43, 32/32, 47/47, 26/30, 26/32, 30/32, 30/47 and 43/47 (Elfgang et al., 1995; Yum et al., 2007; Magnotti et al., 2011b). Connexins 32/47, 26/47 and 32/43 do not form heterotypic channels and Cx29 does not form intercellular channels (Altevogt and Paul, 2004; Ahn et al., 2008; Magnotti et al., 2011b). The *in vitro* study employing N2A cells confirmed most of these data, but opposite to the above mentioned results no functional heterotypic channels were observed for connexins 30/43 and 30/47, the latter is in contrast to findings in HeLa cells (Orthmann-Murphy et al., 2007b). In conclusion, the cell culture studies suggested that functional channels between astrocytes and oligodendrocytes are formed by connexins 30/32 and 43/47 (Nagy et al., 2003; Orthmann-Murphy et al., 2007b). An immunohistochemical study in the spinal cord proposed functional channels formed by 26/32, 30/47 and 43/47 (Altevogt and Paul, 2004).
Heterotypic channels were intensively studied as it was thought that oligodendrocytes do not form GJC with each other and are connected via astrocytes (Massa and Mugnaini, 1982; Nagy et al., 2004). Even though in cell culture oligodendrocyte connexins proofed to form functional channels (see above). Functional analysis in the corpus callosum

confirmed the presence of direct GJC between oligodendrocytes (Maglione et al., 2010; Wasseff and Scherer, 2011), while in the cortex these GJC did not exist (Wasseff and Scherer, 2011). Furthermore, the *in vivo* studies suggested Cx47 to be the most important connexin in white matter for astrocyte-oligodendrocyte GJCs as loss of Cx47 abolished panglial networks as revealed by biocytin diffusion (Maglione et al., 2010). The study by Wasseff and Scherer (2011) employed Sulforhodamine-B and found Cx32 to be more important for network size. These discrepancies most likely reflect the GJC selectivity for different dyes.
Several studies demonstrated the subcellular relocation of connexins, when one connexin is deleted in cells. Loss of Cx32 reduced Cx30 and Cx26 on oligodendrocyte somata in several brain regions, while Cx43 and Cx47 were not affected (Nagy et al., 2003). Likewise loss of Cx30 leads to relocation of Cx32 (Lynn et al., 2011).
Loss of one connexin usually leads to a mild phenotype with only minor morphological changes in the brain (Dere et al., 2003; Menichella et al., 2003; Odermatt et al., 2003; Theis et al., 2003; Sargiannidou et al., 2009). In contrast, double knock-out (DKO) of two connexins usually leads to severe phenotypes and partial mortality. Several DKO lines were generated of which the 30/43 and 43/47 DKO were reported to be viable with modest changes in brain morphology (Wallraff et al., 2006; Lutz et al., 2009; Kunze et al., 2009; Magnotti et al., 2011a). Three other DKOs, one lacking oligodendrocyte connexins 32/47, and two combinations impairing panglial coupling by lack of 30/47 and 32/43 displayed severe changes in brain morphology, especially in myelinated areas, but also grey matter areas (Menichella et al., 2003; Odermatt et al., 2003; Menichella et al., 2006; Magnotti et al., 2011a; Tress et al., 2012). Morphological changes involved alterations in myelin structure including vacuolizations, astrogliosis and microglia activation. These alterations lead to severe phenotypes. The 32/43 DKO displayed absence-like seizure activity and sensorimotor impairments (Magnotti et al., 2011a). Interestingly, not all 30/47 DKOs were affected by early mortality and surviving animals displayed intact oligodendrocyte networks and elevated Cx32 levels, although astrocyte-oligodendrocyte connections were lost.
A recent study demonstrated that ablation of Cx43 destabilizes Cx47 in the oligodendrocyte membrane by alterations in Cx47 phosphorylation (May et al., 2013), which explains the similarities of the phenotype in Cx32/43 compared to Cx32/47 DKOs. Loss of oligodendrocyte connexins led to myelin vacuolizations, axon loss, reduced oligodendrocyte numbers and as a consequence to action tremors (Menichella et al., 2003; Odermatt et al., 2003; Menichella et al., 2006). In these mice, oligodendrocyte coupling to neighbouring astrocytes and oligodendrocytes is abolished (Maglione et al., 2010; Wasseff and Scherer, 2011).
The described alteration in mice lacking two connexins indicate that the cells are not able to compensate for the lack of more than one connexin. Along with the observed severe phenotypes, there is strong evidence that glial networks are required for normal brain function.

1.5 Neuron-Glia Network Interaction

Glial cells were regarded as the glue between neurons for a long time. This view has changed dramatically with the advances in neuroscience over the past years. Normal brain function relies on several functions fulfilled by glia, like neurotransmitter uptake, metabolite supply, ion homoeostasis and gliotransmitter release (Giaume and Theis, 2010; Allaman et al., 2011). Recent publications demonstrated the importance of glial networks for metabolite transport and K^+ buffering which are impaired in mice lacking glial networks leading to neuronal dysfunctions (Wallraff et al., 2006; Rouach et al., 2008; Fünfschilling et al., 2012; Lee et al., 2012; Tress et al., 2012).
The role of glia in K^+ buffering was first described in amphibia by Orkand et al. (1966). The localization of astrocytes contacting blood vessels with their endfeet and extending their processes to nodes of Ranvier and into the synaptic cleft makes them ideal partners in ion homoeostasis. On their endfeet they have Kir4.1 and aquaporin4 channels to expel K^+ ions and water into the capillaries (Rash, 2010; Strohschein et al., 2011). The extracellular K^+ concentration is tightly regulated ($[K^+]_e$ 2-3 mM) and low compared to the intracellular K^+ concentration ($[K^+]_i$ 135 mM). Already slight increases in extracellular K^+ concentrations lead to neuronal epileptic discharges (Wallraff et al., 2006). Impaired K^+ buffering was observed in the hippocampus of mice with a disrupted astroglial network and led to cell swellings (Wallraff et al., 2006; Pannasch et al., 2011). The mechanism of K^+ buffering is still under debate. As the first studies were performed on unmyelinated axons of amphibians, the postulated Orkand model cannot be easily transferred to myelinated axons. In this model astrocytes take up K^+ from the extracellullar space which is released by neurons. In contrast, in the CNS of higher order vertebrates it was observed that K^+ is released at nodes of Ranvier and in addition in the internodal space, the latter is not accessible for astrocytes (Rash, 2010). In the myelin Cx29 hemichannels and voltage gated K_v1 channels are located closely together in the adaxaonal membrane, especially at juxtaparanodal sites (Altevogt et al., 2002; Nave, 2010). K^+ siphoning involves oligodendrocytes in addition to astrocytes which directly contact the outermost myelin sheath (see above). The myelin swellings and vacuolizations observed in X-linked Charcot-Marie-Tooth disease, Pelizaeus-Merzbacher-like disease and Cx32/47 DKO mice further support a role of oligodendrocytes in K^+ buffering (Orthmann-Murphy et al., 2008; Rash, 2010).
Interestingly, there is not only an effect of glial cells on neuron function, but neuronal activity shapes glial networks. Elevated extracellular K^+ and glutamate levels increas astroglial GJ communication in the cortex (Enkvist and McCarthy, 1994). Furthermore, neuronal activity reinforced the diffusion of bioactive molecules in the astroglial network, like glucose, but not biocytin (Rouach et al., 2008). Interestingly, this effect involves neuronal AMPA receptors, but not astrocytic glutamate transporters. Furthermore, hippocampal astrocytes are devoid of AMPA receptors (Matthias et al., 2003; Wallraff et al., 2004; Giaume and Theis, 2010). Blocking neuronal activity reduced net-

work size by influencing Cx30 GJC (Roux et al., 2011). This observation was further confirmed by elevated Cx30 levels in the brain of animals living in enriched environments (Rampon et al., 2000).
Increasing neuronal activity requires higher energy supply to the brain. Compared to body weight the brain is just a small organ, but it is responsible for 20% of the oxygen and energy consumption (Giaume et al., 2010). Interestingly, during high neuronal activity glucose uptake is not increased in neurons, but in astrocytes in the mouse barrel cortex (Chuquet et al., 2010). Moreover, astrocytic endfeet cover 99.7% of the capillaries and metabolites can be easily transported in the glial network to sites of neuronal energy demand (Barros, 2013). Astrocytic localization between neurons and blood vessels favours a role in metabolite transport as it was shown for ion homoeostasis. In complex nervous systems astrocytes are more abundant and obtained a more complex morphology (Nedergaard et al., 2003; Barros, 2013). The GJ network can supply energy to neurons also over long distances and might therefore be crucial for neuronal survival during hypoglycaemia or ischaemia (Giaume et al., 2010). The model of energy supply to neurons was first described by Pellerin and Magistretti (1994) as the astrocyte-neuron lactate shuttle (ANLS; Fig. 1.4). According to this model astrocytes produce lactate in response to neuronal activity at glutamatergic synapses. Glutamate is taken up by astrocytes and activates the Na^+/K^+-ATPase which requires ATP. For this purpose glucose is taken up by astrocytes from the blood vessels and metabolised to lactate by glycolysis and ATP production is increased. Lactate is then transported into the synaptic bouton and serves as an energy source in the neuron to sustain its function (Pellerin and Magistretti, 1994; Pellerin and Magistretti, 2012). Several studies summarized in Pellerin and Magistretti (2012) support the ANLS model.
In addition to the use of lactate by neurons, other molecules are under debate as possible nutrients, like pyruvate and ketone bodies like β-hydroxybutyrate which can also be transported to neurons (Morrison et al., 2013). A study in the optic nerve indeed confirmed that neuronal activity can be maintained for a long time by adding glucose, lactate or pyruvate, partially glutamine, but not β-hydroxybutyrate to the extracellular solution (Brown et al., 2001).
Studies on metabolic pathways in the brain confirmed that neurons outsourced glycolysis to astrocytes which is most likely a protection against oxidative stress for neurons. Furthermore, glycogen storage is fulfilled by astrocytes which produce lactate in case of energy demands which protects neurons during hypoglycemia (Brown and Ransom, 2007; Barros, 2013). Disruption of this energy supply chain via the ANLS pathway from astrocytes to neurons leads to severe brain dysfunction and amnesia (Suzuki et al., 2011). The astrocytic network plays an important role in metabolite transport. Impaired diffusion leads to neuronal synaptic depression during exogenous glucose deprivation in the hippocampus (Rouach et al., 2008; Escartin and Rouach, 2013).
Different cell-types in the CNS express distinct transporters for glucose and lactate uptake. Neurons express glucose transporter 3 (GluT3) and monocarboxylate transporter 2 (MCT2), while astrocytes express GluT1 and MCT4, and oligodendrocytes

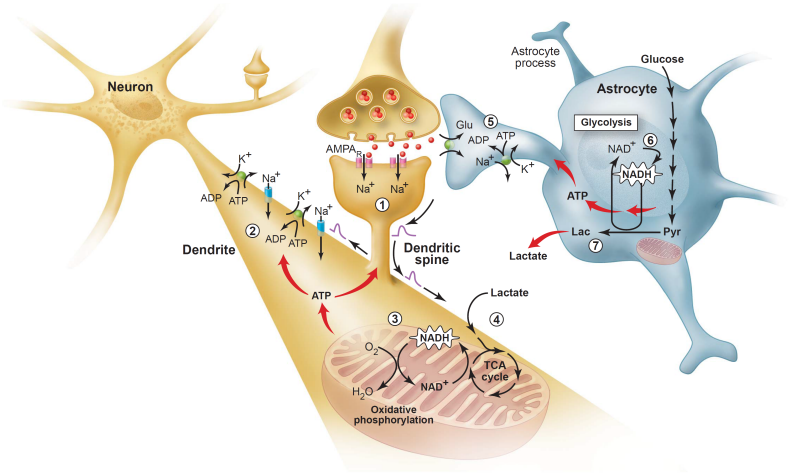

Figure 1.4 Astrocyte-Neuron Lactate Shuttle. The ANLS model was introduced in the middle of the 1990s. It depicts the influence of glutamatergic neuronal signalling at synapses (1) and axonal action potential propagation (2) on astrocyte glycolysis in grey matter. Glutamate clearance by astrocytes from the synaptic cleft activates glial Na^+/K^+-ATPase (5). The increased ATP demand induces glycolysis (6) and lactate production (7) in astrocytes which is released into the extracellular space and taken up by neurons for energy supply (4) and metabolised in neuronal mitochondria (3). From Pellerin and Magistretti, 2012.

were found to express GluT1 and MCT1 (Tekkök et al., 2005; Barros and Deitmer, 2010; Lee et al., 2012). During neuronal activity GluTs are activated in astrocytes, but not in neurons (Barros and Deitmer, 2010; Chuquet et al., 2010). In contrast, lactate transport by neuronal MCT2 is favoured over other MCTs (Barros and Deitmer, 2010). Several studies focusing on lactate transport in the brain identified oligodendrocytes as important partners in energy supply. The direct contact of axons with the myelin of Schwann cells in the PNS and oligodendrocytes in the CNS is required for nutrient transport. MCTs are located directly at these contact sites in the adjacent membranes. The observed differences compared to the ANLS model most likely reflect the distinct functional organization. The ANLS model focuses on energy supply to synapses, while the above stated studies focused on energy supply to myelinated axons. Astrocyte contact to axons is limited by myelination. In the brain 99% of the axon surface is covered by myelin (Morrison et al., 2013). In addition, this also limits the axonal contact to the extracellular space for metabolite uptake. The study by Fünfschilling et al. (2012) identified oligodendrocytes as a source of lactate for white matter axons which is provided by aerobic glycolysis. The role of astrocytes remained elusive, but oligodendrocytes do not have direct contacts to blood vessels. It is unclear whether the glucose is taken up from the extracellular space via GluT1 or received via gap junctions from astrocytes. Interestingly, MCT1 expression in oligodendrocytes was crucial for energy supply to axons: lack of MCT1 caused severe axonopathies and was motorneuron toxic (Lee et al., 2012). Overall energy demands are higher in grey matter compared to white

matter (Amaral et al., 2013). It is therefore likely that astrocytes are a prime source of lactate at glutamatergic synpases in grey matter, while myelinated axons receive nutrients from oligodendrocytes (Pellerin and Magistretti, 1994; Suzuki et al., 2011; Fünfschilling et al., 2012; Lee et al., 2012). Summarizing, the ANLS model and the oligodendrocyte-axon interactions in brain metabolism indicate that normal brain function requires a functional panglial rather than only an astrocytic network (Amaral et al., 2013; Morrison et al., 2013).
Neuronal synapses are enwrapped by astrocytic processes which led to the concept of the tripartite synapse (Araque et al., 1999; Perea et al., 2009). Astrocytes regulate neuronal excitability and synaptic transmission, thereby modulating synaptic plasticity (Perea et al., 2009). They release vesicles and gliotransmitter like D-serine, ATP and glutamate at synapses (Mothet et al., 2005; Bezzi et al., 2004; Perea et al., 2009; Henneberger et al., 2010; Sahlender et al., 2014). Furthermore, astrocytes respond to neuronal signalling with Ca^{2+} waves in their syncytium, though the propagation mechanism via GJ or extracellular signalling pathways is still under debate (Nedergaard et al., 2003; Haydon and Carmignoto, 2006; Pirttimaki and Parri, 2012). Also the already mentioned glutamate uptake from the synaptic cleft is an important function. Astrocytes express GS to convert glutamate to glutamine. The glutamine is then transported to neurons for synaptic transmitter production (Allaman et al., 2011; Amaral et al., 2013). Indeed the amino acid neurotransmitters glutamate, GABA and aspartate are made from astrocytic glutamine (McKenna, 2011; Amaral et al., 2013). The glutamate shuttle was discovered over 40 years ago (van den Berg and Garfinkel, 1971) and GS expression in glia was revealed by several studies shortly after (Martinez-Hernandez et al., 1977). GS expression is not confined to astrocytes, but we know for more than 25 years that also oligodendrocytes express GS (D'Amelio et al., 1987; Cammer, 1990; Miyake and Kitamura, 1992). Indeed, in the presence of unmyelinated axons oligodendrocytes take up glutamate by glutamate transporter 1 (GLT1; DeSilva et al. (2009)).
The astroglial interactions at the synapse also involve connexins. In a recent study it was shown that Cx30 has a non-GJ function for process extension into synapses. In Cx30 knock-out mice astrocytes displayed increased glutamate uptake by extending their processes into the synaptic cleft, thereby decreasing excitatory synaptic transmission and impairing synaptic plasticity due to glutamate clearance (Pannasch et al., 2014). Interestingly, mice lacking astroglial connexins Cx30 and Cx43 displayed increased synaptic transmission and impaired long term plasticity by reduced glutamate and K^+ clearance (Pannasch et al., 2011).
In summary, neurons and glial cells form a functional entity in the brain.

2 Aim of the Study

Over the past decades glial cells have been extensively studied in several brain regions. Increasing evidence supports the active role of glia in brain function and the view of glial heterogeneity. The thalamus is known as the "gate to conciousness" and many studies focused on its neuronal functions. The present study aimed at increasing our knowledge about thalamic glia and their physiological role in brain function in comparison to hippocampal glial cells. This gave the rationale in my thesis to focus on the following four questions:

(i) Analysis of glial network properties in the ventrobasal thalamus.
Astrocytes are connected with each other via gap junction channels and thereby form an extensive network. Unexpectedly, thalamic astrocytes seemed to be devoid of gap junction channels (Parri et al., 2001). Employing transgenic and connexin knock-out mice, the first part of the study aimed at characterizing glial networks during development and identifying the connexins involved in network formation and their cell-type composition in the ventrobasal thalamus.

(ii) Characterization of glial cells in the thalamus and hippocampus.
In the mature ventrobasal thalamus only low expression of GFAP, a classical astrocyte marker in the hippocampus, was observed.(Frassoni et al., 2000). This study aimed at characterizing protein expression in thalamic glial cells in comparison to hippocampal glia by immunohistochemical analysis.

(iii) What is the functional role of glial networks in the thalamus?
Gap junction channels are permeable for many molecules like metabolites, second messengers and ions (Giaume et al., 2010). The thalamus relays all sensory information to the cortex and neuronal activity requires sufficient energy supply. It was a goal of this study to establish a method to analyse the influence of glial networks and potential glial energy supply on corticothalamic signalling employing field potential recordings.

(iiii) Analysis of ionotropic receptor expression in thalamic astrocytes.
Astrocytes express several receptors for neurotransmitters and respond to neuronal activity (Matyash and Kettenmann, 2010). The present study aimed at characterizing the expression pattern of ionotropic AMPA and $GABA_A$ receptor subunits in thalamic astrocytes using single-cell RT-PCR analysis.

3 Materials

3.1 Chemicals

Chemicals were purchased from Abcam (Cambridge, UK), Abbott (Illinois, USA), Applichem (Darmstadt, Germany), BelaPharm Medistar (Ascheberg, Germany), Biorad (München, Germany), Biostatus (Shepshed, UK), Carl Roth (Karlsruhe, Germany), cp pharma (Burgdorf, Germany), Dianova (Hamburg, Germany), Invitrogen (Darmstadt, Germany), Linde (Pullach, Germany), Merck (Darmstadt, Germany), Millipore (Darmstadt, Germany), Polysciences (Warrington, USA), New England Biolabs (Frankfurt, Germany), Promega (Madison, USA), Qiagen (Hilden, Germany), Roche (Mannheim, Germany), Sigma-Aldrich (München, Germany), Thermo Fisher Scientific (Waltham, USA) and Tocris (Bristol, UK). PCR Primers were ordered from Eurofins MWG (Ebersberg, Germany).

Chemicals

2-Mercaptoethanol
2-NBDG
50 bp ladder
100 bp DNA ladder
Agarose 1000
Aqua polymount
Acetic acid
Acrylamide solution (Rotiphorese Gel30)
APS
BAPTA
Biocytin
BSA
Boric acid
Bromophenol blue
$CaCl_2$
Carbogen
CepetorKH
DEPC-water

Draq5
D-AP5
dNTPs
EDTA
EGTA
Ethanol
Ethidium bromide
First strand buffer
Glucose
Glutaraldehyde
Glycine
Glycerol
HEPES
Hoechst 33258
Isoflurane
Isopropanol
KCl
Ketamine
K-Gluconate
L.A.B. Solution
Low Molecular Weight DNA ladder
Methanol
$MgCl_2$
$MgSO_4$
Milk powder
Na_2-ATP
Na-Azide
NaCl
Na-deoxycholate
$NaHCO_3$
NaH_2PO_4
NaOH
NBQX
Nonidet-P40
NGS
Novex Sharp Protein Standard
Paraformaldehyde
Picrotoxin
Protease and phosphatase single use inhibitor
Proteinase K
Random hexanucleotide primer
Restore Western Blot stripping buffer

Restriction enzymes
RNase inhibitor
Roti-Load buffer (4x)
SR101
Sterile water
Streptavidin-Cy2
Streptavidin-Cy3
Streptavidin-Cy5
Streptavidin-A647
Sucrose
Tris
Tris-Base
Tris-Cl
TritonX-100
TTX
Tween-20
TEMED
Xylariem

Kits

GoScript reverse transcriptase (Promega)
Go*Taq* flexi DNA polymerase (Promega)
MinElute PCR Purification Kit (Qiagen)
Platinum *Taq* polymerase (Invitrogen)
Pierce BCA protein assay Kit (Thermo Fisher Scientific)
SuperSignal West Dura extended duration substrate (Thermo Fisher Scientific)
Taq polymerase (Invitrogen)

3.2 General materials

Borosilicate Glass	Science Products, Hofheim, Germany
Coverslips, Object slides	Engelbrecht, Edermünde, Germany
Disposable pipettes	Roth, Karlsruhe, Germany
Glass pipettes	Brand, Wertheim, Germany
Gloves	Ansell, Staffordshire, UK
Instant adhesive	Uhu, Bühl, Germany
Kimtech	Kimberley Clark
Needles and Syringes	BD, Franklin Lakes, USA
Parafilm	Pechiney Plastic Packaging, Chicago, USA
Plastic pasteur pipettes	Roth, Karlsruhe, Germany
Pipettman	Gilson, Middleton, USA
PVDF membrane	Millipore, Schwalbach, Germany
Razor blade	Wilkinson, Bucks, UK
Reaction tubes, Well plates	Sarstedt, Nümbrecht, Germany
Surgical instruments	Fine Science Tools, Heidelberg, Germany
Syringe filters 4 mm	Thermo Fisher Scientific, Waltham, USA
Tape	Leukoplast, Hamburg, Germany
Tips, Tubes	Greiner Bio-One, Frickenhausen, Germany
Venofix	Braun, Melsungen, Germany
Whatman paper	Whatman International, Maidstone, UK

3.3 Software

GeneTools	Synoptics, Cambridge, UK
Igor Pro	Wave Metrics, Portland, USA
ImageJ	NIH, Maryland, USA
Inkscape	The Inkscape Team
LAS AF	Leica Microsystems, Wetzlar, Germany
MC Stimulus II	Multi Channel Systems, Reutlingen, Germany
MetaVue	Molecular Devices, Sunnyvale, USA
Tida	Heka, Lambrecht, Germany

3.4 Equipment

Amplifier DPA-2F	npi, Tamm, Germany
Amplifier DPA-2FS	npi, Tamm, Germany
Axiophot	Carl Zeiss, Gttingen, Germany
Centrifuges	Eppendorf, Wesseling, Germany
Eclipse E600FN microscope	Nikon, Tokyo, Japan
DIC camera	Cohu, Poway, USA
EPC-7	Heka, Lambrecht, Germany
EPC-800	Heka, Lambrecht, Germany
Fluorescence lamp	Nikon, Tokyo, Japan
GeneGnome XRQ	Synoptics, Cambridge, UK
Heat block	VWR, Darmstadt, Germany
HERAEUS Fresco17 centrifuge	Thermo Fischer Scientific, Bonn, Germany
IPC pump	Ismatec, Wertheim, Germany
ITC-16 computer interface	Heka, Lambrecht, Germany
Leica SP5 LSM	Leica Microsystems, Wetzlar, Germany
Leica SP8 LSM	Leica Microsystems, Wetzlar, Germany
Leica TCS NT confocal	Leica Microsystems, Wetzlar, Germany
LIH 1600	Heka, Lambrecht, Germany
Micromanipulator, electric	Luigs und Neumann, Ratingen, Germany
Micromanipulator MHW-3, hydraulic	Narishige, Japan
MC Stimulus II	Multi Channel Systems, Reutlingen, Germany
Microwave	Severin, Germany
Mini-Protean 3 Cell	Biorad München, Germany
Mini-Trans blot Cell	Biorad München, Germany
MyCycler, Thermal cycler	Biorad, München, Germany
Oscilloscope HM 507	Hameg, Mainhausen, Germany
pH meter	Mettler Toledo, Giessen, Germany
Pipette puller P-2000	Sutter Instruments, Hofheim, Germany
Pipette puller PP-830	Narishige, Japan
Shaking water bath	Memmert GmbH, Schwabach, Germany
Table top small centrifuge	VWR, Darmstadt, Germany
SEC-05LX	npi, Tamm, Germany
SM1, SM5 control box	Luigs und Neumann, Ratingen, Germany
STG-2004	Multi Channel Systems, Reutlingen, Germany
STG-4004	Multi Channel Systems, Reutlingen, Germany
Vibration isolation platform LW 3036B-OPT	Newport, Irvine, USA
Vibratome VT1200S	Leica, Nussloch, Germany
Vortexer	VWR, Darmstadt, Germany
Weight balance	Sartorius group, Göttingen, Germany

3.5 Antibodies

Primary Antibodies

Epitope	Species	Type	Dilution	Company
Aldh1L1	mouse	mc	1:25	Abcam
β-Gal	rabbit	pc	1:400	Molecular Probes
Cx30	rabbit	pc	1:250	Zymed-Invitrogen
Cx43	rabbit	pc	1:5,000	Sigma
GFAP	rabbit	pc	1:750	Dako
GFP	mouse	mc	1:500	Invitrogen
GFP	chicken	pc	1:600	Abcam
GS	mouse	mc	1:200	Millipore
GS	mouse	mc	1:1,000	Transduction Laboratories
Iba1	mouse	mc	1:400	WAKO
Olig2	rabbit	pc	1:1,000	Millipore
NeuN	mouse	mc	1:200	Chemicon
NG2	rabbit	pc	1:100	Millipore
S100β	mouse	mc	1:250	Abcam
α-Tubulin	mouse	mc	1:20,000	Sigma

Secondary Antibodies

Antibody	Species	Dilution	Company
anti-mouse-A488	goat	1:500-600	Molecular Probes
anti-rabbit-A488	goat	1:500	Molecular Probes
anti-chicken-A488	goat	1:500	Molecular Probes
anti-mouse-A594	goat	1:500	Molecular Probes
anti-rabbit-A594	goat	1:500	Molecular Probes
anti-mouse-A647	goat	1:500	Molecular Probes
anti-rabbit-A647	goat	1:500	Molecular Probes
anti-mouse-HRP	goat	1:10,000	GE healthcare
anti-rabbit-HRP	goat	1:10,000	GE healthcare

Streptavidine Conjugates

Streptavidin-Cy2	1:100
Streptavidin-Cy3	1:300
Streptavidin-Cy5	1:200
Streptavidin-A647	1:600

3.6 PCR primers

Cx26-E3
5'-ACAGGATTGGGAGTCTAGAAG-3'

Cx26-E5
5'-TTTGTCTACTCTGTAGCTGTG-3'

Cx26-A5
5'-ACAGAAATGTGTTGGTGATGG-3'

Nestin-Cre us
5'-TCCCTTCTCTAGTGCTCCACGTCC-3'

Nestin-Cre ds
5'-TCCATGAGTGAACGAACCTGGTCG-3'

3.7 RT-PCR primers

Gene	**Sequence**	**Product length/ GeneBank Acc.#**
Alpha se	5'-AACATGACMAYGCCMAAYAAGCT-3'	554 bp
Alpha as	5'-GCATARCAGACAGCWATRAACCA-3'	
α1 nested se	5'-CCAGCCCGTTCAGTGGTTGTA-3'	180 bp
α1 nested as	5'-GCACGGCAGATATGTTTGAAT-3'	NM_010250
α2 nested se	5'-TTACAATGCTTCTGACTCCGTTCA-3'	306 bp
α2 nested as	5'-CGRGCACTGATRCRWARGGT-3'	NM_008066
α3 nested se	5'-CTTGGGAAGAACAAATCTGTGGA-3'	305 bp
α3 nested as	5'-CGRGCACTGATRCRWARGGT-3'	NM_008067
α4 nested se	5'-ACCAAAGGCCCTGAGAAGTCA-3'	308 bp
α4 nested as	5'-CGRGCACTGATRCRWARGGT-3'	NM_010251
α5 nested se	5'-GCTGGAGGATGATGGCACACTTCT-3'	208 bp
α5 nested as	5'-GTTGAGCCTGGAGCCATCTTCTG-3'	NM_176942
Beta se	5'-CTGGATGARCAAAACTGYAC-3'	443 bp
Beta as	5'-ACAAAGACAAARCAWCCCAT-3'	

Gene	**Sequence**	**Product length/ GeneBank Acc.#**
β1 nested se	5'-ATGGAGGAGAGGGAGCAGTAACT-3'	358 bp
β1 nested as	5'-CAGCCCATGAGATAGATGTCAATC-3'	NM_008069
β2/3 nested se	5'-GGCGYGGCGRTGACAAKGC-3'	307 bp
β2/3 nested as	5'-TCCCGRAGGTGRGTGTTGAT-3'	NM_008070, NM_008071
Gamma se	5'-ATTTGGATTCCAGACACYWTCTT-3'	392 bp
Gamma as	5'-AAGTAGCCCATTCTTCKRCTCAG-3'	
γ1 nested se	5'-CGCCTGCTGCGGATTTG-3'	180 bp
γ1 nested as	5'-CACAGAGGGCTTTTTCCACTTGT-3'	NM_010252
γ2 nested se	5'-AAAAMRGCTGAGGCTCACTGGAT-3'	211 bp
γ2 nested as	5'-AACTGCGCTTCCATTGATAAACA-3'	NM_177408
γ3 nested se	5'-AAAAMRGCTGAGGCTCACTGGAT-3'	272 bp
γ3 nested as	5'-CTGAGGCCCATGAAGTCAAACTGA-3'	NM_008074
Delta se	5'-ATGGCGCCAGGGCAATGAATG-3'	424 bp
Delta as	5'-GTGGAGGTGATGCGGATGCTGTAT-3'	
δ1 nested se	5'-TATGCCCGAAACTTCCGACCAG-3'	308 bp
δ1 nested se	5'-AAAATCACCCCATCAGGCTGTAGG-3'	NM_008072
AMPA-R se	5'-GGATCMACWAAAGARTTYTTCA-3'	412 bp
AMPA-R as	5'-TCAGGCTSAGRGCACTSGTCT-3'	
GluA1 se	5'-GTGTTTGTTCGGACCACAGAG-3'	275 bp NM_001113325
GluA2 se	5'-GTGAGGACTACGGCAGAAGGAGTA-3	260 bp
GluA2 as	5'-TCGTACCACCATTTGTTTTTCA-3'	NM_001083806
GluA3 se	5'-AGCTGATGGGGTAGCCCGAGTTC-3'	258 bp NM_016886
GluA4 se	5'-AGAGCCATCTGTGTTCACTA-3'	285 bp NM_019691
GluA1, 3, 4 as	5'-TCMCCTTTATCGTACCACCATTT-3'	

Gene	Sequence	Product length/ GeneBank Acc.#
S100β se	5'-AGGCCATGGTTGCCCTCATTGAT-3'	246 bp
S100β se	5'-ACTCATGGCAGGCCGTGGTCA-3'	
S100β nested se	5'-TACTCCGGGCGAGAGGGTGACAA-3'	186 bp
S100β nested as	5'-GGCGACGAAGGCCATGAACTCC-3'	NM_009115

3.8 Restriction enzymes

Enzyme	Restriction site	Incubation	Company
BsaHI	5'- GRCGYC -3'	37°C	NEB
TspRI	5'- NNCASTGNN -3'	37°C	NEB
MseI	5'- TTAA -3'	37°C	NEB
HpaI	5'- GTTAAC -3'	37°C	NEB

3.9 Solutions and buffers

3.9.1 Solutions for electrophysiology

Preparation solution

NaCl	87 mM
KCl	2.5 mM
NaH_2PO_4	1.25 mM
$NaHCO_3$	25 mM
$MgCl_2$	7 mM
$CaCl_2$	0.5 mM
Glucose	25 mM
Sucrose	75 mM

and pH 7.4 adjusted with carbogen (95% O_2/5% CO_2)

Artificial cerebrospinal fluid (ACSF)

NaCl	126 mM
KCl	3 mM
$MgSO_4$	2 mM
$CaCl_2$	2 mM
Glucose	10 mM
NaH_2PO_4	1.25 mM
$NaHCO_3$	26 mM

and pH 7.4 adjusted with carbogen (95% O_2/5% CO_2)

Intracellular standard solution

KCl	130 mM
$MgCl_2$	2 mM
$CaCl_2$	0.5 mM
BAPTA	5 mM
HEPES	10 mM
Na_2-ATP	3 mM
pH 7.28	

Intracellular K-gluconate solution

K-gluconate	130 mM
$MgCl_2$	1 mM
Na_2-ATP	3 mM
HEPES	20 mM
EGTA	10 mM
pH 7.2	
supplemented with the tracer	
0.5% biocytin or	
14.6 mM 2-NBDG	

3.9.2 Solutions and buffers for immunohistochemistry

Phosphate buffered saline (10x)

NaCl	1.5 mM
KCl	2.7 mM
Na_2HPO_4	8.3 mM
NaH_2PO_4	1.7 mM
dissolved in dH_2O	
pH 7.4	

PBS with sodium azide

NaN_3	0.01% (w/v)
dissolved in 1x PBS	

PFA solution

Paraformaldehyde	4% (w/v)
dissolved in 1x PBS	

Blocking solution

NGS	10% (v/v)
TritonX-100	2-0.5% (v/v)
diluted in 1x PBS	

Antibody solution

NGS	2% (v/v)
TritonX-100	0.1% (v/v)
diluted in 1x PBS	

Blocking solution for biocytin

NGS	10% (v/v)
BSA	5% (v/v)
TritonX-100	2% (v/v)
diluted in 1x PBS	

Antibody solution for biocytin visualization

NGS	2% (v/v)
BSA	2% (v/v)
TritonX-100	0.1-0.5% (v/v)
diluted in 1x PBS	

Hoechst nuclei staining solution

Hoechst	1% (v/v)
diluted in dH_2O	

Draq5 nuclei staining solution

Draq5	0.1% (v/v)
diluted in 1x PBS	

3.9.3 Buffers for SDS-PAGE gel

Contents	**Stacking gel**	**Resolving gel**	
2 x gels à 1.5 mm	**(4%)**	**(10%)**	**(12%)**
Rotiphorese gel 30	1.3 ml	10.5 ml	12 ml
Stacking gel (pH 6.8)	2.5 ml	-	-
Resolving gel (pH 8.8)	-	7.5 ml	7.5 ml
dH_2O	6.2 ml	12 ml	10.5 ml
TEMED	6 µl	18 µl	18 µl
APS (10%)	60 µl	180 µl	180 µl

3.9.4 Solutions and buffers for Western blotting

Phosphatase inhibitor

Thermo Fisher phosphatase inhibitor cocktail 100x
dissolved in protein lysis buffer

Protein lysis buffer (modified RIPA buffer)

Tris-base	50 mM
NaCl	150 mM
Nonidet P-40 (NP40)	0.5% (v/v)
Na-deoxycholate	0.5% (w/v)
TritonX-100	1% (v/v)
sterile-filtered, pH 7.5	

APS stock buffer

Ammonium persulfate	10% (w/v)
dissolved in dH_2O	

SDS stock buffer

Sodium dodecyl sulfate	10% (w/v)
dissolved in dH_2O	

Stacking gel buffer

Tris-base	0.5 M
SDS stock buffer	0.4% (v/v)
sterile-filtered, pH 6.8	

Resolving gel buffer

Tris-base	1.5 M
SDS stock buffer	0.4% (v/v)
sterile-filtered, pH 8.8	

Laemmli sample buffer (4x)

Tris-HCl	62.5 mM
SDS stock buffer	3% (v/v)
Glycerol	10% (v/v)
Bromophenol blue	0.01% (w/v)
2-Mercaptoethanol	5% (v/v)
dissolved in dH_2O, pH 6.8	

SDS running buffer (1x)

Tris-base	0.25 M
Glycine	1.92 M
SDS stock buffer	1% (v/v)
dissolved in 5 l dH_2O, pH 8.3	

Transfer buffer (5x)

Tris-HCl	50 mM
Tris-Base	0.1 M
Glycine	0.8 M
dissolved in 2 l dH_2O, pH 8.3	

Transfer buffer (1x)

Transfer buffer (5x)	20% (v/v)
Methanol	20% (v/v)
diluted in dH_2O	

Washing blot buffer

Tris-HCl	8.5 mM
Tris-Base	1.7 mM
NaCl	50 mM
Tween 20	0.05%(v/v)
dissolved in 2 l dH_2O, pH 6.3	

Blocking buffer

Milk powder	5% (w/v)
dissolved in washing blot buffer	

3.9.5 Solutions and buffers for molecular analysis

Laird-Lysis-Buffer

Tris-HCl	100 mM
NaCl	200 mM
EDTA	5 mM
SDS	0.2% (w/v)
diluted in dH_2O, pH 8.5	

Proteinase K

Proteinase K	4 µl of 20 mg/ml stock
dissolved in 500 µl Laird-Lysis -Buffer	

TBE (10x)

Tris-Base	1 M
Boric acid	0.83 M
EDTA	10 mM

Ethidium bromide

Ethidium bromide	10% (10 mg/ml)
diluted in 1x TBE	

3.10 Animals

Maintenance and handling of animals used in this study was according to local government regulations. Mice were kept under standard housing conditions with 12 h/12 h dark-light cycle, food and water *ad libitum*. All measures were taken to minimize the number of animals used.

3.10.1 Cx26fl/fl:Nestin-Cre mice

Since Cx26 is essential for embryonal development, mice with brain-specific deletion of Cx26 were generated using a conditional knock-out strategy (Cohen-Salmon et al., 2002). A constitutive deletion of Cx26 is lethal at embryonal day E11 due to decreased transplacental glucose uptake (Gabriel et al., 1998). Deletion of Cx26 in the mouse brain was achieved by taking advantage of the Cre/loxP system. The coding region of exon 1 of the *Gjb2* gene is flanked by two loxP sites in Cx26fl mice. A Cre recombinase under the control of the rat Nestin promoter was used to delete the floxed (fl) deoxyribonucleic acid (DNA) sequence resulting in the deletion of Cx26 in Nestin-Cre expressing cells (Tronche et al., 1999; Nagy et al., 2011). Nestin is a type VI intermediate filament mainly expressed in neural progenitor cells (Zimmerman et al., 1994).

3.10.2 Cx30LacZ/LacZ mice

Cx30-deficient mice were generated by Teubner et al. (2003). In these mice the Cx30 (*Gjb6*) coding region has been replaced by a LacZ reporter sequence which is therefore expressed under control of Cx30 gene regulatory elements. The LacZ-encoded β-galactosidase contains a nuclear localization signal and can be visualized by immunohistochemistry. Due to the gene targeting strategy these mice were reported to be deaf, most likely due to decreased expression of Cx26, whose gene is located in close proximity to the *Gjb6* locus (Lynn et al., 2011). Analysis of reporter expression in mouse brain revealed region-dependent reporter expression (Gosejacob et al., 2011).

3.10.3 Cx43ECFP knock-in mice

The Cx43ECFP mouse line expresses the reporter enhanced cyan fluorescent protein (ECFP) under the control of the Cx43 (*Gja1*) promoter (Degen et al., 2012). A global knock-out of *Gja1* is lethal due to morphological disturbances of the right ventricular outflow tract (Reaume et al., 1995). Therefore the Cx43ECFP knock-in mouse line was generated by breeding Cx43fl(ECFP) mice, with PGK-cre mice (Lallemand et al., 1998). Mice are always heterozygous, due to lethality of homozygous animals and the reporter is expressed in all Cx43-expressing cells of the body. Immunohistochemical analysis confirmed astrocyte-specific ECFP expression in the mouse brain (Degen et al., 2012).

3.10.4 Cx30LacZ/LacZ;Cx43fl/fl:hGFAP-Cre mice

Cx30/43 double knock-out (DKO) animals were obtained by breeding Cx30LacZ mice with Cx43fl(LacZ) and hGFAP-Cre mice (Theis et al., 2001; Theis et al., 2003; Zhuo et al., 2001). These mice express LacZ instead of Cx30 in all cells of the body. Additionally, Cx43 is deleted in all GFAP-expressing cells (e.g. astrocytes and radial glia-like cells) in the CNS and express LacZ under the control of the *Gja1* promoter. Loss of these two connexins in the mouse brain leads to a complete disruption of astrocyte gap junction-mediated coupling and, as a consequence to impaired spatial K^+ buffering and spontaneous epileptic activity (Wallraff et al., 2006).

3.10.5 Cx30LacZ/LacZ;Cx43flG138R/flG138R:Nestin-Cre mice

This mouse line was generated by breeding Cx30LacZ mice with Cx43G138R mice and additionally Nestin-Cre mice to study effects of Cx43 variants on radial glia-like cell networks. The Cx43G138R line is a mouse model for Oculodentodigital dysplasia (ODDD), a disease caused by mutations in the human *Gja1* gene, coding for Cx43 protein. The clinical manifestations include abnormalities of the fingers, toes, eyes, face and teeth (Dobrowolski et al., 2008). The human Cx43G138R point mutation was inserted into the wild-type (wt) mouse *Gja1* gene and the resulting $Cx43^{G138R/+}$ mice showed all phenotypes known for ODDD in human patients. The conditional knock-out using a Nestin-Cre mouse line allowed for the neurally restricted expression of the point mutation (Tronche et al., 1999). The Cre recombinase activity led to deletion of the loxP-flanked Cx43-wt region and at the same time to the expression of a Cx43G138R-internal ribosomal entry site (IRES)- enhanced green fluorescent protein (EGFP) cassette under the control of the *Gja1* regulatory elements (Dobrowolski et al., 2008).

3.10.6 Cx30LacZ/LacZ;Cx43fl/K258stop:hGFAP-Cre mice

This mouse line is the result of cross-breeding four mouse lines, the Cx30LacZ, the Cx43fl(LacZ), the hGFAP-Cre and the Cx43K258stop (Theis et al., 2001; Zhuo et al., 2001; Teubner et al., 2003; Maass et al., 2004) mouse line. The Cx43K258stop mice express a C-terminally truncated Cx43 protein in place of the full-length protein, in which Cx43 is lacking the last 125 amino acid residues of the cytoplasmic C-terminal domain. Due to a defect of the epidermal barrier more than 97% of the homozygous Cx43K258stop mice die shortly after birth (Maass et al., 2004). Surprisingly, former studies showed that decreasing the Cx43K258stop gene dosage rescued the lethal epidermal phenotype (Maass et al., 2007), hence Cx43K258stop mice were crossed with mice heterozygous for a conditional *Gja1* knock-out allele. Therefore, we raised $Cx43^{fl/K258stop}$:hGFAP-Cre heterozygous mice carrying one Cx43K258stop allele and a Cx43fl(LacZ) allele which is deleted in the CNS by virtue of the hGFAP-Cre transgene to investigate the effect of truncated Cx43 in adult neurogenesis.

3.10.7 Cx30LacZ/LacZ;Cx47EGFP/EGFP mice

This double knock-out mouse line is the result of breeding the Cx30LacZ mouse line with Cx47EGFP mice (Teubner et al., 2003; Odermatt et al., 2003). Both the deletion of Cx30 and Cx47 *Gjc2* occurs in all cells of the body. The Cx47 single knock-out is viable, fertile and shows no behavioural abnormalities. Closer morphological analysis of the brains confirmed oligodendrocyte-specific Cx47-EGFP expression and revealed vacuolizations in the myelin (Odermatt et al., 2003). Combining the two mouse lines lacking an astroglial connexin and an oligodendroglial connexin should disrupt panglial networks (Tress et al., 2012). Indeed, this could be confirmed in white matter, where no tracer spread from oligodendrocytes to astrocytes was detected in biocytin-labelled networks. Further analysis of these double knock-outs revealed that 40% of the mice die between p42 and p90. They display extensive astrogliosis, microglia activation and myelin malformations with vacuolizations (Tress et al., 2012).

3.10.8 hGFAP-EGFP mice

The transgenic mouse line hGFAP-EGFP expresses the reporter EGFP under the control of the human GFAP promoter (Nolte et al., 2001). Transgenic mice were generated in a FVB/N background, an inbred mouse strain with good reproductive performance and therefore well suited to generate transgenic mice by micro-injection into oocytes. An additional advantage of this mouse line are the consistently large litters (Taketo et al., 1991). GFAP is the major intermediate filament in mature astrocytes, but is also expressed by other cells, e.g. in the PNS by Schwann cells (Jessen and Mirsky, 1985). In the CNS of these mice GFAP-expressing cells are EGFP labelled. In many brain regions good overlap of EGFP and GFAP immunostaining was observed and the cells had a typical astrocyte morphology. In the thalamus strong EGFP expression was observed, despite the absence of GFAP-labelling (Nolte et al., 2001; Frassoni et al., 2000). Analysis of membrane currents in acute brain slices revealed EGFP expression in two cell-types, astrocytes and NG2 cells (Wallraff et al., 2004).

3.10.9 PLP-GFP mice

The PLP-GFP mouse line is a transgenic line generated to identify mature myelinating oligodendrocytes in living tissue. This mouse line has a C57/Bl6 background and expresses the green fluorescent protein under the control of a PLP promoter (Fuss et al., 2000). The protein PLP is a myelin protein and is specifically expressed in myelinating oligodendrocytes, although there is a known splice variant (DM-20) expressed in pre-myelinating oligodendrocytes (Trapp et al., 1997). Analysis of GFP expression confirmed that reporter expression in this mouse line is confined to terminally differentiated oligodendrocytes. Furthermore GFP is located in the cytoplasm and not in the myelin sheets, due to deletion of the localization signal (Fuss et al., 2000).

4 Methods

4.1 Electrophysiology

4.1.1 Preparation of acute brain slices

For preparation of acute brain slices, animals were anaesthetized with Isoflurane, killed by decapitation and the brains were quickly removed. Horizontal slices for whole cell patch clamp experiments were obtained by cutting off the cerebellum and a small part of the dorsal cortex. The brain was then glued dorsally on a specimen holder. Slice thickness was 200 µm for whole-cell patch clamp experiments. Field potentials (FP) were recorded in 300 µm thick slices with a 30° angle with the horizontal plane. Therefore the cerebellum was cut off and the brain was split along the midline. The hemisphere was laid on a plastic block with an angle of 30° onto its midline cutting edge and a small piece of the dorsal brain was cut off, afterwards the hemispheres were glued dorsally on a specimen holder.
The brains were placed in ice cold preparation solution bubbled with carbogen (95% O_2/5% CO_2). Using a vibratome, horizontal slices containing the ventrobasal nuclei of the thalamus and the hippocampus were obtained. Slices were stored at 35°C for 20 min, cooled down to room temperature and transferred into ACSF bubbled with carbogen. For some experiments slices were incubated in ACSF supplemented with 1 µM SR101 at 35°C for 20 min and subsequently transferred to ACSF at room temperature. The composition of the solutions is described in section 3.9.1.

4.1.2 Electrophysiology setup

The electrophysiological experiments employing tracer diffusion were performed in a recording chamber of a patch clamp setup. A slice was placed in the chamber and held in place with nylon threads glued onto a U-shaped platinum wire. The recording chamber was mounted on a holder that could be manually moved in x- and y-directions. Tissue visualization was achieved with an upright microscope E600FN (Nikon) equipped with an infrared DIC at 4x magnification (Nikon). The microscope was equipped with a motorized focus and a DIC camera (Cohu). Additionally, a 60x immersion objective (Nikon) was used to identify individual cells for experiments. Fluorescent light of defined wavelength was applied to identify fluorescent astrocytes or oligodendrocytes. A detailed list of the equipment can be found in section 3.4.

The bath chamber was continuously perfused with carbogenized ACSF at room temperature by a peristaltic pump at 1-2 ml/min. The microscope was placed on a vibration isolation platform (Newport) to ensure stable measurements and placed inside a Faraday cage for electric shielding.
A hydraulically controlled micromanipulator MHW-3 (Narishige) was used to move the recording pipette which was connected to the head stage of the patch clamp amplifier. Currents were recorded in the voltage clamp mode employing an EPC-7 patch clamp amplifier and monitored by TIDA software (HEKA). Data were sampled at 6-30 kHz and filtered at 3-10 kHz.
Pipettes were fabricated from borosilicate glass and had a resistance of 2-6 MΩ when filled with internal solution. The recording electrode was a teflon-coated silver wire with a chlorinated tip. The reference electrode consisted of a silver/silver chloride pellet.
For extracellular recordings an electrically-driven micromanipulator was available to position the recording pipette connected to a bridge amplifier (SEC-05LX, npi). The bipolar stimulation electrode was positioned with the hydraulically controlled micromanipulator and connected to a stimulation generator (Multi Channel Systems).
For some experiments patch clamp technique and confocal laser scanning microscopy were combined. Therefore another patch clamp setup was used. In brief, the setup was equipped with an LSM SP5 (Leica) and electrically-driven micromanipulators. Currents were recorded using an EPC-800 patch clamp amplifier (HEKA).

4.1.3 Whole-cell patch clamp recording

The cells were electrophysiologically characterized by patch clamp technique (Neher and Sakmann, 1976). In brief, cells were approached with a patch pipette filled with internal solution. Obstruction of the pipette tip was prevented by applying overpressure while approaching the cell. When reaching the cell membrane the overpressure was immediately removed and low pressure was applied to obtain a close contact between the pipette tip and the cell membrane which is called the cell-attached mode. It is characterized by a high resistance above 1 GΩ and also known as Gigaseal. Next, short pulses of low pressure were applied to disrupt the cell membrane and obtain the whole-cell configuration.
Voltage clamp experiments were performed on cells identified by endogenous fluorescence or staining with the astrocyte marker SR101 (Nimmerjahn et al., 2004; Kafitz et al., 2008). All cells were analysed in whole-cell voltage clamp mode. Therefore the amplifier compares the resting potential of a patched cell with the selected holding potential. By current injection the cell is kept at its desired holding potential whenever the resting membrane differs from the holding potential. The current recorded by the amplifier represents the current flow over the cell membrane. Input and series resistance were regularly checked by applying 10 mV pulses for 50 ms (Fig. 4.1A). For analysis 10 traces were averaged and analysed using a custom made Igor Pro tool written by Ronald Jabs. In brief, the current at the beginning of the 10 mV pulse was used to

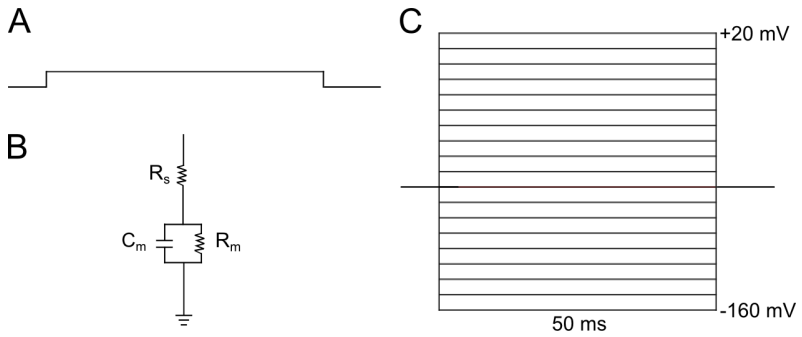

Figure 4.1 Whole cell patch clamp analysis. (A) 10 mV pulses of 50 ms duration were applied every 10 min to monitor the access resistance and electrophysiological properties of the patched cell. (B) Circuit diagram of the whole cell mode, R_s originates at the pipette tip and R_m depends on the cell membrane properties, e.g. ion channel types and their density. The capacity C_m depends on the membrane surface area (1 $\mu F/cm^2$). (C) Stimulation protocol applying de- and hyperpolarizing voltage steps between -160 mV to +20 mV for 50 ms to identify cell-types, 10 mV increment.

calculate the series resistance, a measure for the access quality. The constant current after decline of the capacitive current was used to calculate the membrane resistance, see the circuit diagram in Figure 4.1B. The series resistance was calculated by the equation $R_s = \Delta U/I(t_0)$ and the membrane resistance was obtained by $R_m = \Delta U/I(t_1) - R_s$.
The holding potential was -80 mV. During the 20 min experiments the membrane potential was monitored and all cells with a membrane potential above -60 mV were excluded from analysis. Cells were electrophysiologically identified by applying voltage steps between -160 mV to +20 mV, as shown in Figure 4.1C.
Intracellular solutions were based on a K-gluconate solution causing a liquid junction potential which was compensated during measurements by adjusting the holding potential. Tracer filling with biocytin or 2-NBDG was performed for 20 min. Afterwards, slices were fixed in 4% PFA in 1x PBS, pH 7.4 at 4°C. Slices used for fluorescent glucose analysis with 2-NBDG were not fixed as the 2-NBDG is not PFA fixable.
In some experiments cells were harvested for subsequent RT-PCR analysis. These cells were morphologically and electrophysiologically characterized and extracted from the tissue under optical supervision. The internal pipette solution was a standard KCl-solution. The harvested cytoplasm in the tip of the pipette was transferred into a tube with DEPC-water and immediately frozen in liquid N_2.

4.1.4 Extracellular field potential recordings

Field potentials were recorded in 300 µm thick horizontal slices tilted 30° to the horizontal plane (Fig. 4.2A). Synaptic stimulation of the corticothalamic pathway was achieved with a computer-controlled constant current isolated stimulator (STG4004 and 2004) and bipolar electrodes. Stimulation electrode and field potential recording pipette were placed several 100 µm away from each other. The bipolar electrode was placed in the

internal capsule and field potentials were recorded in the ventrobasal thalamus (Fig. 4.2B) with a SEC05-LX (npi). The bridge balance was adjusted and the capacity was compensated. Stimulation responses of the corticothalamic pathway were obtained by applying stimuli of 100 µs duration as a train of 5 stimuli at 20 Hz. Train stimuli were repeated every 15 s and resulted in stable responses. Furthermore the afferent synaptic input parameters allowed for long term recordings without inducing LTP or LTD, but to monitor the direct synaptic effects of the stimulation. The stimulation intensity was set to 80% of the maximally elicited postsynaptic responses.
Recorded field potentials were characterized by application of synaptic blockers and the sodium channel blocker tetrodotoxin (TTX). The receptor antagonist 2,3-dihydroxy-6-nitro-7-sulfamoyl-benzo[f]quinoxaline-2,3-dione (NBQX) was applied to block AMPA receptors and D-2-amino-5-phosphonopentanoate (D-AP5) blocked NMDA receptors. Picrotoxin-supplemented (100 µM) ACSF was used during the entire experiment to block $GABA_A$ receptor channels. At the end of every experiment TTX (0.5 µM) was applied to block action potentials and for artefact compensation for subsequent field potential analysis. After a 10-20 min baseline recording, either synaptic activity was blocked by bath application of synaptic blockers (10 µM NBQX and 20 µM D-AP5) or glucose deprivation was induced by wash-in of ACSF without glucose. Control experiments of glucose deprivation were always performed on slices from the same animal in Picrotoxin-supplemented ACSF. A scheme of the experimental procedure is shown in Fig. 4.2C, D.
Data analysis was performed with a custom made tool written by Ronald Jabs using Igor Pro software. Field potential traces were averaged as sets of 10 recordings and the corresponding TTX file was subtracted to eliminate stimulation artefacts. Three parameters were analysed, the delay of the popspike, the slope and the amplitude of the postsynaptic field potential (Fig. 4.2E). The slope of the postsynaptic potential was obtained by linear regression using all data points between two points of measurement on the descending slope of the postsynaptic potential. Using the custom made Igor Pro tool these two points were manually set on the recorded trace, the first one on the recorded maximum peak after the popspike and the second point was set close before reaching baseline levels again (Fig. 4.2E). All data points between the measuring points were included to make a linear fit of the postsynaptic potential. The amplitude of the popspike was measured from the fitted line to the peak amplitude, therefore a third measuring point was manually positioned on the peak of the popspike (Fig. 4.2E). This third point was also used to measure the delay of the popspike after the stimulation time point (Fig. 4.2E). The acquired data sets were analysed for changes over time during blocker application or glucose deprivation. The postsynaptic response after the third stimulus in a train of five stimuli was compared between all experiments.

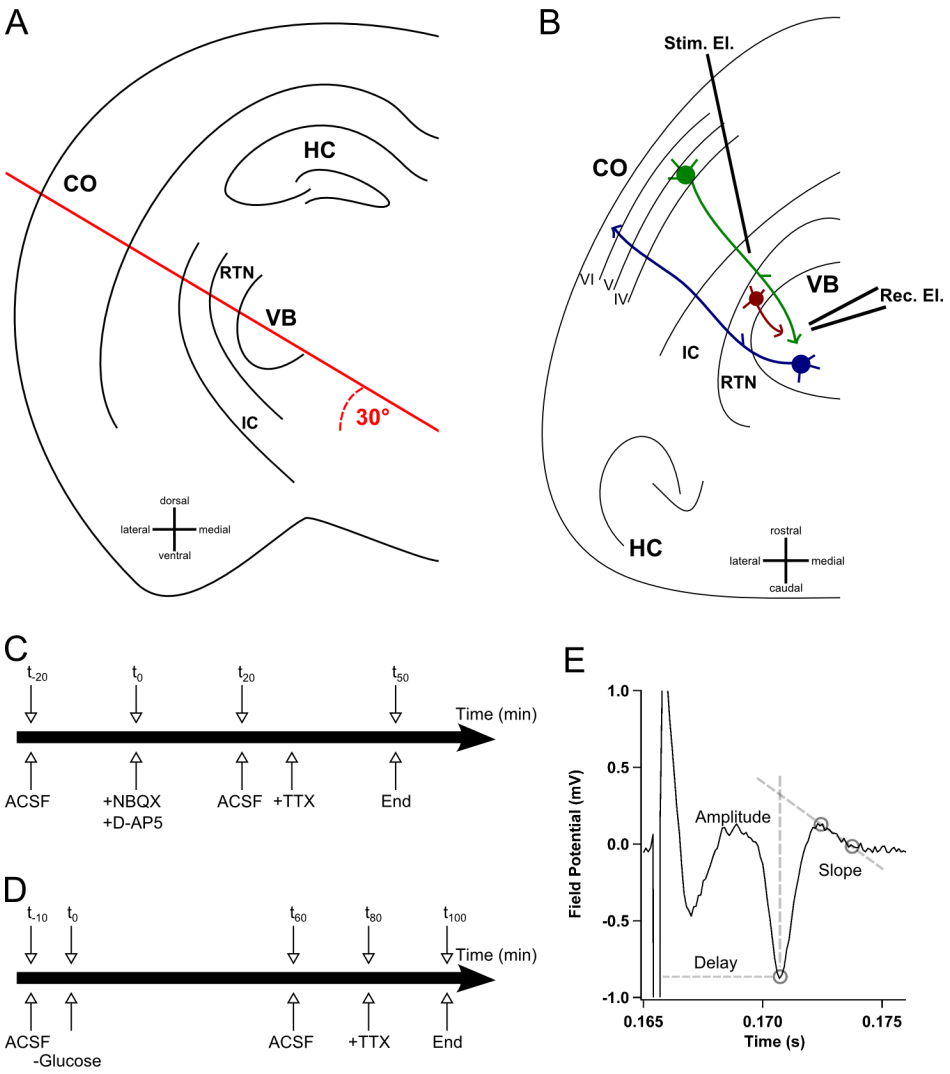

Figure 4.2 Field potential recordings in the ventrobasal thalamus. (A) Coronal section of a mouse brain, the cutting plane at a 30° angle with the horizontal plane is indicated by a red line. The plane contains the cortex (CO), the internal capsule (IC), the reticular thalamic nucleus (RTN) and the ventrobasal thalamus (VB). Additionally, the hippocampus (HC) is displayed and a cross indicating the slice orientation (bottom). Modified after Mouse Brain Atlas, mbl.org. (B) Scheme of a horizontal, 30° tilted brain slice. The corticothalamic pathway is indicated by a green neuron, additionally the thalamocortical pathway is shown in blue and the GABAergic neurons of the reticular thalamic nucleus (RTN) are displayed in brown colour. Modified after Grant et al., 2012. (C and D) Time lines of the experimental protocols applied for synaptic blocker analysis (C) and the glucose deprivation experiments (D). (E) Scheme depicting the FP analysis by a custom made Igor Pro tool, by placing three measuring points on the trace (grey circles). The parameters slope, amplitude and delay (dashed grey lines) of the postsynaptic response were analysed.

4.2 Confocal and 2-photon microscopy of acute slices

Electrophysiological recordings combined with 2-NBDG diffusion were imaged online employing a Leica SP5 laser scanning microscope (LSM) equipped with an infrared ultra-short-pulse laser. Before starting the patch clamp experiment, stacks of optical sections were obtained with a continuous wave laser to visualize the $SR101^+$ astrocytes and the PLP-GFP^+ cells in the ventrobasal thalamus. One $SR101^+$ astrocyte was patched and dialysed with 2-NBDG for 20 min. Employing the infrared laser, it was possible to separate the 2-NBDG fluorescence from the GFP signal. Therefore 2-photon absorption was achieved by excitation of the fluorochromes with femtosecond pulses of infrared light with repetition rates of 80 MHz. The wave length for the excitation was adjusted for best signal to noise ratio: GFP/SR101 710 nm (1.15 W). Reflected and transmitted light was collected with two channel non-descanned detectors in each light pathway. For GFP/SR101 signals reflected emission light was separated with a FITC-TRITC filter cube. Volumes of 258.33x258.33x28-33 μm^3 were scanned with a resolution of 1024x1024x29-34 pixels. Images of 2-NBDG diffusion were acquired 3 min and 20 min after patching the astrocyte. Combining the continuous wave laser images acquired before patching the astrocyte and the 2-NBDG filled network images, the number of PLP-GFP^+ cells and $SR101^+$ cells filled with 2-NBDG were quantified.

4.3 Immunohistochemistry

4.3.1 Tissue preparation

Mice were deeply anaesthetized by intraperitoneal injection of 80 mg/kg Ketamine hydrochloride and 1.2 mg/kg Medetomidine hydrochloride and transcardially perfused with 30-50 ml 1x PBS followed by 30-50 ml 4% PFA. Brains were removed, postfixed overnight in 4% PFA and washed the next day with 1x PBS.
Brains were prepared as described in section 4.1.1 and cut on a vibratome VT1200S (Leica) into horizontal slices (40 µm) in 1x PBS at 4°C and stored in 1x PBS with sodium azide at 4°C for subsequent staining.

4.3.2 Staining

Brain slices were stained to visualize tracer filled networks and for characterization of cell-types in the VB compared to hippocampal CA1 region.
The tissue was stained using a free floating method in 24-well plates. Slices were permeabilized and blocked for 2-4 h at room temperature in 1x PBS containing 0.5-2% TritonX-100 and 10% normal goat serum (NGS). The first antibodies were incubated in 1x PBS containing 0.1% TritonX-100 and 2% NGS at 4°C overnight on a shaker, some antibodies were incubated at room temperature overnight. The next day slices were

washed 3 times for 10 min in 1x PBS and incubated with the corresponding secondary antibodies in the antibody solution for 1.5 h at room temperature on a shaker. Afterwards slices were washed again 3 times for 10 min and incubated with Hoechst (1:100 in dH_2O) or Draq5 (1:1000 in 1x PBS) for nuclei staining. After a final washing step slices were mounted on object slides with Aquapolymount for further confocal or fluorescence microscopy analysis. See section 3.9.2 for a detailed list of the solutions.
Biocytin was visualized with Streptavidin-Cy3, -Cy2, -Cy5 or -A647 applied in the staining protocol above. Additionally, for the immunohistochemical analysis of the biocytin injected cells 2-5% bovine serum albumin (BSA) was added to the blocking and antibody solutions, secondary antibodies were incubated for 2 h at room temperature.
The applied antibodies are listed in section 3.5, for double and triple immunostainings suitable first and corresponding secondary antibodies were used.

4.3.3 Microscopy

Immunofluorescence stainings were analysed by microscopy. Images were acquired at a 1 µm interval using either a fluorescence microscope Axiophot employing MetaVue software or confocal LSMs Leica TCS NT or Leica SP8. Fluorescence image resolution was 2084x2084 pixels and LSM images were acquired at 1024x1024 pixels. Tracer filled networks were imaged employing a 20x objective. For colocalization studies confocal images were acquired. Cell type analysis in different brain areas was performed on image stacks of 500x500x10-15 μm^3 volumes. Aldh1L1 analysis was performed on 290x290x15 μm^3 volumes. The images obtained were analysed using Fiji software and Figures were edited using Inkscape.

4.3.4 Data analysis

The immunohistochemical stainings were quantified to assess the protein expression profile and to further characterize glial cells in different brain regions. The number of cells expressing one or more proteins were counted and cell densities were calculated. All quantification results were counted by two different persons, by myself and another person namely Sebastian Ebert, Ina Fiedler, Simon Höft or Anja Matijevic. Glial networks were analysed by counting manually all tracer filled cells using the Fiji plugin Cell-Counter. Cells were identified by their morphology and soma size. In some experiments co-labelling of biocytin and antibody stainings was assessed by counting co-labelled cells. Characterization of cell-types in the thalamus and hippocampus were performed on three image stacks with identical volumes from three mice each, a total of nine images were quantified. All cells of interest in the image were counted and analysed for colocalization with cell-type markers, subsequently cell densities were calculated. Data are displayed as mean ± SEM and were statistically analysed by analysis of variance (ANOVA) and *post-hoc* Tukey. Differences between means were regarded as significant at $p<0.05$ (*); $p<0.01$ (**).

4.4 Protein chemistry

4.4.1 Tissue lysis

Western blot analysis of connexin expression was performed using wild-type C57/Bl6J mice. Animals were sacrificed by cervical dislocation, and the brains were immediately isolated. Brain tissue samples of hippocampus and thalamus were isolated, transferred into a tube and frozen in liquid N_2. The tissue samples were stored at -80°C or immediately lyzed in protein lysis buffer supplemented with protease and phosphatase inhibitor single-use cocktail (100 µl/10 ml). The tissue samples were homogenized with a pestle, then disrupted with a prechilled 27 gauge needle and supersonic slat until homogeneous and incubated on ice for 30 min. Samples were centrifuged for 30 min at 13,000x g at 4°C and the supernatants were transferred into new tubes. Total protein content was assayed with bicinchoninic acid (BCA) using 5 µl of each sample, according to the manufacturer's instructions.

4.4.2 SDS-PAGE and Western blot

Connexin protein analysis was performed using sodium dodecyl sulfate polyacrylamide gel electrophoresis (SDS-PAGE), therefore 30-50 µg of total protein per lane was used. With this method, proteins are separated in a polyacrylamide gel according to their size, smaller molecules travel faster than larger proteins through the acrylamide pores. Potential charge interferences were excluded by adding SDS; the dodecyl sulfate surround the proteins with an equal negative charge.
Lysates were mixed with Laemmli sample buffer and denatured by heat-incubation for 10 min at 65°C before they were shortly centrifuged at 4°C. Proteins were separated with standard 10% or 12% SDS-PAGE under denaturing conditions for 1-1.5 h at 60 mA. To estimate the protein size, Novex Sharp Protein Standard was loaded along with the samples and lysate of a $Cx30^{LacZ/LacZ}$;$Cx43^{fl/fl}$:hGFAP-Cre mouse was loaded as a negative control for antibody specificity.
Polyvinylidene difluoride (PVDF) membranes were used for electroblotting of separated proteins for 2 h at 500 mA running condition. The electric field was applied vertically to the gel and allowed the transfer of proteins from the gel to the membrane. The proteins adhere to the membrane by hydrophobic and polar interactions. Membranes were blocked with 5% milk powder in Tris-buffered saline (TBS) containing 0.05% Tween-20 and incubated overnight at 4°C on a rotator with primary antibodies: rabbit polyclonal anti-Cx43CT (1:5,000), rabbit polyclonal anti-Cx30 (1:250) and mouse monoclonal anti-α-tubulin (1:10,000). Secondary antibodies used: goat-anti-mouse- horse radish peroxidase (HRP) conjugate (1:10,000) and goat-anti-rabbit-HRP conjugate (1:10,000). All antibodies, including secondary antibodies, were diluted in 5% milk powder in TBS containing 0.05% Tween-20. Equal loading of the lanes was confirmed by α-tubulin staining of the same membrane.
For stripping, Pierce Restore stripping buffer was used for all blots for 20 min at room

temperature. Membranes were usually re-blocked after stripping for 2 h at room temperature. For visualisation of HRP, the SuperSignal West Dura substrate was used and chemiluminescence was detected with the GeneGnome digital documentation system. SDS-PAGE and Western blotting were performed by Jiong Zhang.

4.4.3 Data analysis

Raw data analysis and densitometry were performed with GeneTools quantification software (Synoptics). After subtracting the background ratio for each band, the intensity of the target proteins was normalized to the values from their α-tubulin loading controls, respectively. For each sample the mean of two blots was calculated. The normalized values of control samples were set to 100%. Data are given as mean $\pm$ SEM. The statistical analysis employed the Mann-Whitney U-test, differences between means were regarded as significant at $p<0.05$ (*); $p<0.01$ (**). Data analysis was performed by Jiong Zhang.

4.5 Molecular biology

4.5.1 DNA extraction

Genomic DNA was obtained from small tail tips of 3 weeks old mice. Samples were incubated in 300 µl Laird buffer supplemented with Proteinase K (20 U/ml) at 55°C overnight in a water bath. The next day lysates were vortexed and centrifuged at 13,000 rpm for 10 min at room temperature. The supernatant was transferred to a new tube and the DNA was precipitated by adding 300 µl isopropanol and gently mixing the solutions. After another centrifugation step at 13,000 rpm for 10 min at room temperature the supernatant was discarded. The DNA pellet was washed in 70% ethanol (500 µl) and centrifuged again at 13,000 rpm for 10 min at room temperature. The supernatant was discarded and the DNA pellet was air dried for 1 h and dissolved in 50 µl of ddH_2O. The genomic DNA was subsequently used for routine genotype analysis with different primers.

4.5.2 Polymerase chain reaction

DNA samples were amplified by polymerase chain reaction (PCR). The method relies on several thermal cycling reactions for melting, primer annealing and subsequent replication of the target DNA. Primers were designed to bind at the 3'-end of the sense and antisense strands of the DNA sequence to be amplified. Employing a heat-stable *Taq* polymerase the DNA strands were amplified by elongation of the primers in 5'-3' direction. This enzyme was originally isolated from the bacterium *Thermus aquaticus*. The following Tables 4.1, 4.2 and 4.3 show the PCR mix and the applied PCR protocols for genotyping animals of the Cx26fl/fl:Nestin-Cre mouse line; the presence of a floxed Cx26 was detected by Cx26fl PCR, a successful excision of the gene was verified by

analysis with Cx26del PCR and the presence of a Cre recombinase gene was detected by Nestin-Cre PCR. The total volume of the PCR mix was 24 µl and 1-2 µl DNA were added.

Table 4.1 Cx26fl PCR and protocol

PCR mix	**Volume [µl]**
ddH_2O	11.3
PCR buffer 5x	5
$MgCl_2$ (25 mM)	2.5
Primer E3 (10 pmol/µl)	2
Primer E5 (10 pmol/µl)	2
dNTP (each 10 mM)	1
Taq polymerase	0.2

Step	**Temp. [°C]**	**Time [min]**	**Cycles**
1	94	5	1
2	94	0:45	2-4 35x
3	63	0:45	
4	72	0:45	
5	72	7	1
6	8	∞	1

Table 4.2 Cx26del PCR and protocol

PCR mix	**Volume [µl]**
ddH_2O	11.3
PCR buffer 5x	5
$MgCl_2$ (25 mM)	2.5
Primer E3 (10 pmol/µl)	2
Primer A5 (10 pmol/µl)	2
dNTP (each 10 mM)	1
Taq polymerase	0.2

Step	**Temp. [°C]**	**Time [min]**	**Cycles**
1	94	5	1
2	94	0:45	2-4 35x
3	55	0:45	
4	72	2:20	
5	72	7	1
6	8	∞	1

Table 4.3 Nestin-Cre PCR and protocol

PCR mix	**Volume [µl]**
ddH_2O	14.8
PCR buffer 5x	5
$MgCl_2$ (25 mM)	2
Primer Nestin-Cre us (25 pmol/µl)	0.5
Primer Nestin-Cre ds (25 pmol/µl)	0.5
dNTP (each 10 mM)	1
Taq polymerase	0.2

Step	**Temp. [°C]**	**Time [min]**	**Cycles**
1	95	5	1
2	94	0:30	2-4 34x
3	62	0:50	
4	72	1:30	
5	72	10	1
6	8	∞	1

4.5.3 Agarose gel electrophoresis

The PCR products were separated by agarose gel electrophoresis. The cDNA samples were separated by their size and charge, therefore a 1.5% agarose gel containing 0.8 µg/ml ethidium bromide was prepared. Due to the phosphate groups negatively charged DNA moved to the anode and the migration velocity was proportional to their molecular mass. Ethidium bromide was added to visualize the DNA under ultraviolet light; it intercalates double stranded DNA. Gel electrophoresis was performed at 110 V for 0:45-1 h. At the same time, a 100 bp DNA ladder was run along with the samples to estimate the molecular size of the amplified DNA fragments.

4.5.4 Single-cell RT-PCR

Reverse transcription

Thalamic astrocytes in p9-12 old hGFAP-EGFP mice were electrophysiologically characterized. After recording, the cytoplasm of individual cells was harvested under microscopic control and cytoplasm and pipette solution (3 µl) was expelled into a thin-walled reaction tube filled with 3 µl DEPC-water. The cytoplasm was frozen in liquid N_2 and stored at -20°C until reverse transcription (RT) was performed. For single-strand cDNA synthesis 5.5 µl RT-PCR mix (Tab. 4.4) was added to the tubes (final volume about 10 µl). The reaction was performed at 37°C for 1 h. All experiments employing single-cell mRNA were performed by Gerald Seifert.

Table 4.4 Reverse transcription mix

RT Mix	**Volume** [µl]
First strand buffer	2
$MgCl_2$ (25 mM)	1
dNTPs (4x 2.5 mM)	1
Random hexamer primer (1 mM)	0,5
RNasin RNase inhibitor (40 U/µl)	0.5
GoScript reverse transcriptase (160 U/µl)	0.5

Multiplex PCR

A multiplex 2-round single-cell PCR was performed with primers for either GluA1-4 AMPA receptors subunits or α-, β-, γ- and δ-$GABA_A$ receptor subunits respectively, together with the housekeeping gene S100β. The sequences of the primers are shown in section 3.7. The first PCR was performed after adding first round PCR mix to the RT product (final volume 50 µl); the PCR mix and protocol are shown in Table 4.5.
An aliquot (2 µl) of the PCR product was used as template for the second PCR employing nested, subunit-specific primers as shown in section 3.7. Furthermore a nested PCR for the astrocyte housekeeping gene S100β was performed. The conditions were the same as described for the first round, with addition of dNTPs and a Platinum *Taq* polymerase. Products were identified by gel electrophoresis using the Low Molecular Weight DNA ladder (New England Biolabs).
Specificity of primers was tested with total mRNA prepared from freshly isolated mouse brain. For optimization, a 2-round RT-PCR was performed with 2 ng of total RNA and primers as described above. The primers for the targets were located on different exons to prevent amplification of genomic DNA. Omission of the RT-enzyme and substitution of template by bath solution served as negative controls for RT and PCR amplification.

Restriction digest of PCR products

The splice variants flip and flop of the AMPA recepors were discriminated by restriction digest of PCR products. Therefore the second PCR (GluA1-4) was repeated. The PCR product was purified using the MinElute PCR Purification Kit (Qiagen), and dissolved in 30 µl H_2O. Eight µl of the PCR product were incubated with restriction enzymes (10 U, 6 h, 37°C, total volume 15 µl). cDNA fragments were analysed by gel electrophoresis (3% Agarose 1000) using a 50 bp ladder. The PCR products for GluA receptors were digested by the splice variant-specific restriction endonucleases BsaHI (cut GluA1 flip, yielding a 230 bp and a 45 bp fragment), TspRI (GluA2 flip 210 and 50 bp; GluA3 flip, 208 and 50 bp; and GluA4 flip, 235 and 50 bp), MseI (GluA1 flop, 221 and 64 bp; GluA4 flop, 207, 64 and 14 bp) and HpaI (GluA2 flop, 192 and 68 bp; GluA3 flop, 181 and 77 bp). See also section 3.8 for restriction enzyme properties.

Table 4.5 First round PCR and protocol

PCR Mix	**Volume µl**
dH_2O	29
PCR buffer	5
$MgCl_2$ (50 mM)	2.5
Primers receptor se (10 pmol/µl)	1
Primers receptor as (10 pmol/µl)	1
Primers S100β se (10 pmol/µl)	0.5
Primers S100β as (10 pmol/µl)	0.5
Taq polymerase (5 U/µl)	0.5

Step	**Temp. [°C]**	**Time [min]**	**Cycles**
1	94	0:25	1-3 5x
2	49	2	
3	72	0:25	
4	94	0:25	4-6 45x
5	49	0:45	
6	72	0:25	
7	72	7	1
8	4	∞	1

Table 4.6 Nested PCR and protocol

PCR Mix	**Volume [µl]**
dH_2O	37
PCR buffer	5
$MgCl_2$ (50 mM)	2.5
dNTPs (4x 2.5 mM)	1
Primer nested se (10 pmol/µl)	1
Primer nested as (10 pmol/µl)	1
Platinum *Taq* polymerase (5 U/µl)	0.5

Step	**Temp. [°C]**	**Time [min]**	**Cycles**
1	94	0:25	1-3 5x
2	54	2	
3	72	0:25	
4	94	0:25	4-6 30x
5	54	0:45	
6	72	0:25	
7	72	7	1
8	4	∞	1

5 Results

Astroglial networks have been extensively studied in the hippocampus, but little is known about glial cells in the thalamus. In a study by Parri et al. (2001) thalamic astrocytes displayed no Lucifer yellow diffusion to neighbouring cells. The apparent absence of an astroglial network was an unexpected observation and questioned the concept of an astroglial network throughout the brain.
The thalamus consists of several nuclei with different functions in sensory information processing. In this study, all experiments were performed in the ventrobasal thalamus, specifically the VPL and VPM nuclei to avoid potential regional effects. The ventrobasal thalamus plays an important role in transduction of somatosensory information from the whiskers to the somatosensory cortex (Haidarliu and Ahissar, 2001).

5.1 Properties of thalamic astroglial networks

Astrocytes are connected with each other via GJC in many brain regions (Wallraff et al., 2006; Houades et al., 2008; Roux et al., 2011). In the first set of experiments, the size of these GJN was analysed in the ventrobasal thalamus during mouse development. Therefore, a single astrocyte was patched using a pipette solution supplemented with biocytin, a tracer small enough to diffuse through GJC. Biocytin was chosen over Lucifer yellow as it diffuses further into the network (Rouach et al., 2008). The extent of tracer diffusion after 20 min filling was analysed to assess network sizes.
In Figure 5.1A and B two exemplary GJN in hGFAP-EGFP mice are displayed. The patched cells were electrophysiologically characterized and displayed large passive current patterns typical for astrocytes (Fig. 5.1A_1, B_1; Wallraff et al., 2006). Subsequent tracer visualization revealed large networks which displayed a round shape as shown in Figure 5.1A_2 or an elongated shape (Fig. 5.1B_2). The lateral part of the ventrobasal thalamus contains densely packed myelinated fibre tracts. Tracer spread from the astrocyte into myelin fibres was observed in several cases (see inset in Figure 5.1B_2).
Developmental analysis was performed at four different time points from young to adult mice. Thalamic astrocytes filled with biocytin always revealed large GJN which increased between early juvenile and two weeks old animals (p9-11, 84 $\pm$ 13 cells; p13-15, 111 $\pm$ 8 cells; p35-56, 108 $\pm$ 11 cells; p90-120, 95 $\pm$ 8 cells; tested by ANOVA and *post-hoc* Tukey's test, $p<0.01$ (**); Fig. 5.1C). The p9-11 cells were patched by Anna Beinhauer; 10 of 20 cells at p13-15, 6 of 14 cells at p35-56 and cells at p90-120 were patched by Simon Höft (see also Griemsmann et al., 2014).

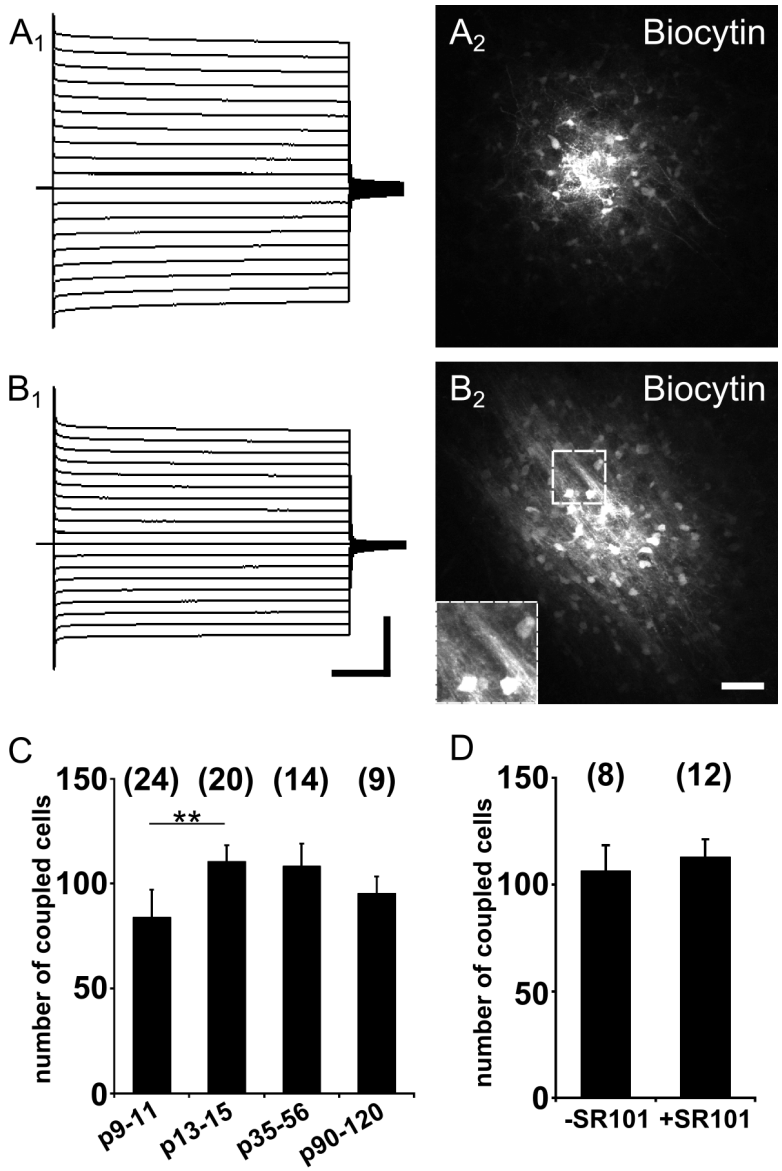

Figure 5.1 Astroglial networks in the ventrobasal thalamus have distinct properties. (A, B) Representative examples of tracer-filled networks after patching an EGFP fluorescent astrocyte in hGFAP-EGFP mice. (A_1, B_1) Current patterns of astrocytes induced by de- and hyperpolarization of the membrane between -160 and +20 mV evoked a passive current pattern in whole-cell voltage clamp mode (10 mV increment, holding potential -80 mV). Scale bar, 10 ms, 5 nA. (A_2, B_2) Biocytin always spread from the initial cell into neighbouring cells and revealed large glial networks. In some cases the tracer also diffused into myelinated fibre tracts, see higher magnification of boxed area in the inset in B_2. Scale bar, 50 µm. (C) Quantification of network sizes at different time points. The average GJN size was constant after the second postnatal week (mean ± SEM). (D) Analysis of the influence of the widely used fluorescent dye SR101 on GJNs revealed no influence on network sizes. Asterisks indicate statistical significance. Number of experiments is given in parentheses. See also Griemsmann et al., 2014.

The red fluorescent dye sulforhodamine 101 (SR101) is an efficient and reliable astrocyte marker, but it also affects neuronal activity (Nimmerjahn et al., 2004; Kafitz et al., 2008; Kang et al., 2010). Furthermore, it was still unclear whether SR101 influences astrocyte network sizes. To answer this question, brain slices were incubated with SR101 and GJNs compared with those observed in slices without dye incubation (Fig. 5.1D). Tracer coupling in the thalamus was not influenced by SR101 staining (SR101 incubation, 113 ± 8 cells, n = 12; control, 106 ± 12 cells, n = 8; ANOVA; see also Griemsmann et al., 2014). SR101 proved to be a reliable astrocyte marker in the thalamus.
In conclusion, astrocytes in the ventrobasal thalamus form glial networks via gap junction channels which are already fully developed at p13-15. The astrocyte marker SR101 does not influence network sizes which is therefore a valuable tool for further experiments.

5.2 Connexin expression in astrocytes

5.2.1 The impact of Cx30 and Cx43 on astroglial networks

The first part of the present study employing biocytin as a tracer revealed large glial networks in the thalamus (Section 5.1). Astrocytes express three different connexin isoforms: Cx26, Cx30 and Cx43. In the hippocampus Cx43 is the main GJ protein and loss of Cx30 was reported to have a minor or equal influence (Wallraff et al., 2006; Gosejacob et al., 2011; Theis and Giaume, 2012; Pannasch et al., 2014). The impact of Cx26 expression on networks sizes has not been analysed so far in mice lacking this connexin. It was of special interest which connexins are involved in the formation of GJC in thalamic glial networks. Therefore, further experiments were performed employing connexin knock-out mice at the age p30-60 which applies for all following experiments, if not stated otherwise. Experiments performed in the institute employing heterozygous $Cx43^{ECFP/+}$ mice revealed that a moderate proportion of the cells express ECFP in thalamic GJNs (Griemsmann et al., 2014). In addition, transcript levels of Cx30 mRNA were increased in thalamic samples in sqRT-PCR analysis compared to hippocampus of wild-type mice (Griemsmann et al., 2014), indicating that Cx43 plays a less important role in the thalamus. Still, the functional role of Cx30 in the thalamus remained elusive. The impact of this isoform on thalamic coupling was investigated in Cx30kiLacZ mice, in which the coding region of the Cx30 gene was replaced by the reporter LacZ (Teubner et al., 2003). Thalamic astrocytes were filled with biocytin and displayed a strong decrease in coupling by 73% compared to littermate controls ($Cx30^{+/+}$, 81 ± 6 cells, n = 17; $Cx30^{LacZ/LacZ}$, 22 ± 3 cells, n = 15; Fig. 5.2A_{1-3}, B_1), employing ANOVA and *post-hoc* Tukey's test ($p<0.01$ (**)). Even complete uncoupling was observed in 25% of the cells (n = 5 of 20; Fig. 5.2A_3, B_2; see also Griemsmann et al., 2014) which differed from control littermates employing $\mathcal{X}^2$-test ($p<0.05$ (*)). In $Cx30^{LacZ/LacZ}$ mice the tracer-filled cell was always brightly fluorescent with a few or no weakly fluorescent cells around it. The tracer barely diffused into neighbouring cells.

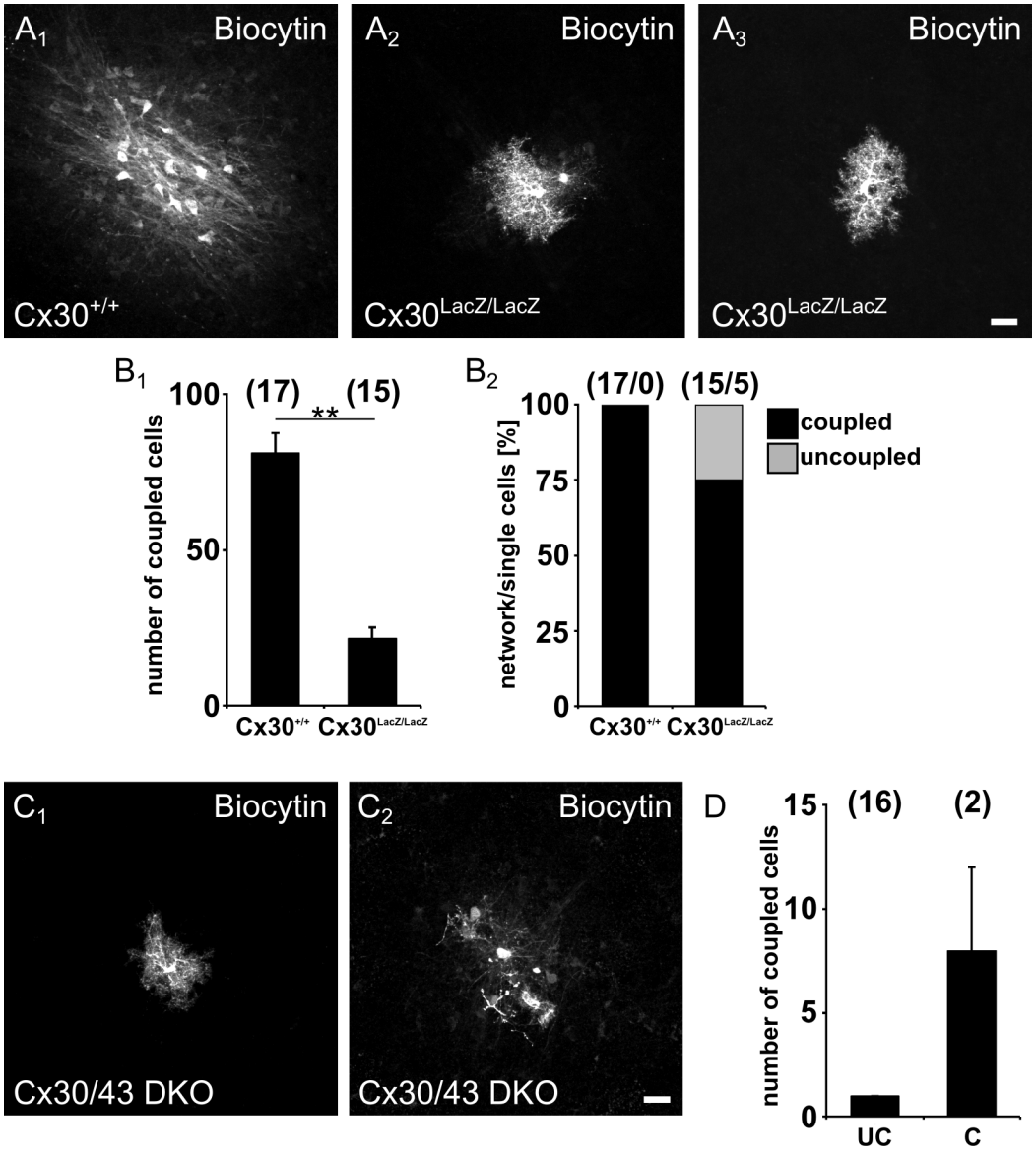

Figure 5.2 Functional analysis of the gap junction protein Cx30 in the thalamus. (A) Confocal images show biocytin diffusion in the thalamus of $Cx30^{+/+}$ mice (A_1) and $Cx30^{LacZ/LacZ}$ littermates (A_2 and A_3). Tracer-filled cells in $Cx30^{LacZ/LacZ}$ mice were connected to few (A_2) or no neighbouring cells (A_3). The initial cell was always brightly fluorescent with weakly labelled neighbouring cells. (B_1) Network sizes were strongly decreased (by -73%) in $Cx30^{LacZ/LacZ}$ vs. $Cx30^{+/+}$ mice. (B_2) Percentage of injected cells which were coupled to at least one other cell and thereby formed a network (black) versus injected uncoupled cells (grey). (C) Additional deletion of Cx43 in astrocytes abolished coupling of the cells (C_1). Only in 2 cases residual networks were observed (C_2). (D) Summary of the network analysis in Cx30/43 DKO mice. UC, uncoupled cells; C, coupled cells. Asterisks indicate statistical significance. Number of experiments is given in parentheses. Scale bar, 20 µm. See also Griemsmann et al., 2014.

The observed difference between thalamic and hippocampal networks regarding the importance of Cx30 for GJN formation, led to the question whether an additional deletion of Cx43 would completely abolish coupling as observed in the hippocampus (Wallraff et al., 2006). Tracer-filled astrocytes in mice deficient for Cx30 and Cx43 (Cx30/43 DKO) revealed complete disruption of inter-cellular gap junctions in 16 out of 18 biocytin-filled thalamic $SR101^+$ cells in contrast to $Cx30^{+/+}$ and $Cx30^{LacZ/LacZ}$ mice ($\mathcal{X}^2$-test, $p<0.05$ (*)). Tiny networks (8 ± 6 cells) were only observed in two experiments (Fig. 5.2C_{1-2}, D). Some cells were patched by Simon Höft (5 of 16 uncoupled and 1 of 2 coupled cells; see also Griemsmann et al., 2014).
In conclusion, astrocytic coupling in the adult thalamus is mediated predominantly by Cx30. The additional deletion of Cx43 leads to a complete disruption of the glial network, though the residual coupling in some cases might involve a third connexin, e.g. Cx26.

5.2.2 Molecular analysis of Cx30 and Cx43 expression

The functional analysis revealed distinct properties of astroglial networks in the thalamus compared to the hippocampus. In the following experiments these two brain regions were analysed for developmental differences in connexin expression on protein level in C57/Bl6 mice.
Western blot analysis revealed differential connexin expression between brain regions, additionally, proteins were developmentally up-regulated (Fig. 5.3A_{1-2}, B_{1-2}). Two age groups were compared: p14, when Cx30 expression increases (Kunzelmann et al., 1999) and p53 which is in the age group of tracer-filled mice. Western blots were performed by Jiong Zhang and statistically analysed employing Mann-Whitney U-test, $p<0.05$ (*), $p<0.01$ (**). Cx30 protein levels increased more than threefold during this period in the thalamus, while in the hippocampus Cx30 increased twofold between age groups. In young mice Cx30 protein levels were equal. Cx43 increased twofold in the hippocampus and thalamus. Protein amounts were equal between brain regions in adult mice, but differed at p14. In summary, in the adult brain Cx30 protein levels are higher in the thalamus, while Cx43 protein content does not differ (Fig. 5.3A_2, B_2; see also Griemsmann et al., 2014). These data corroborate the important role of Cx30 in the thalamus.
On a cellular level connexin expression was further analysed by reporter gene analysis in $Cx43^{ECFP/+}$;$Cx30^{LacZ/+}$ mice. Experiments were performed only in the thalamus, as the reporter LacZ is not expressed in the hippocampus of these mice (Fig. 5.3C; Gosejacob et al., 2011). Quantification was performed on 3 image stacks in 3 different mice, therefore a total of 9 images were quantified by two persons each (see also Section 4.3.4). The Cx30-β-Gal signal contains a nuclear localization signal and antibody staining revealed abundant expression in the thalamus (Fig. 5.3C_1). Cx43-$ECFP^+$ cells were visualized in green (Fig. 5.3C_2), in the overlay co-expressing cells appear yellow, but also some single-labelled cells were observed (Fig. 5.3C_3).

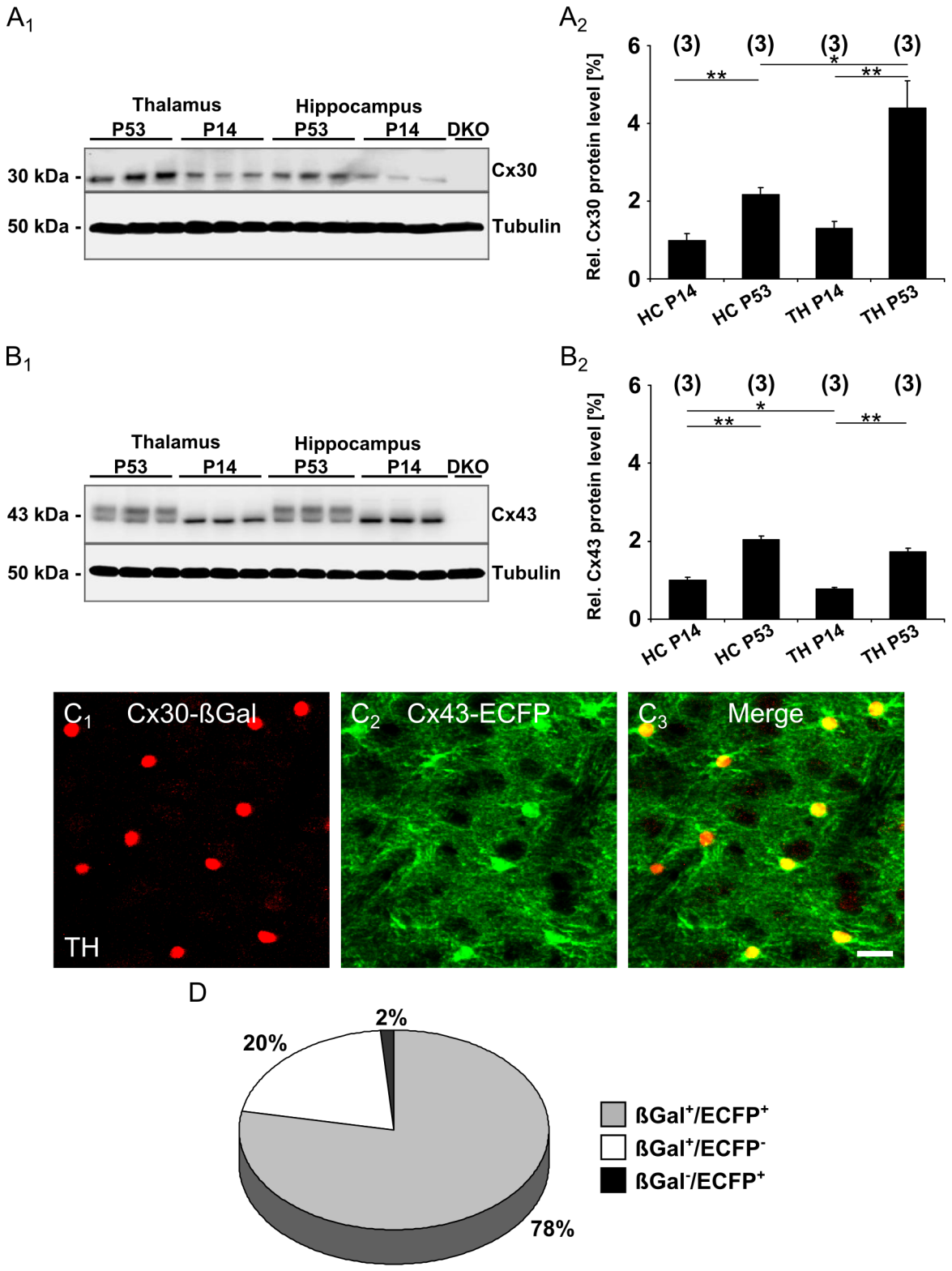
A1
Thalamus
Hippocampus
P53
P14
P53
P14
DKO
30 kDa -
Cx30
50 kDa -
Tubulin
A2
Rel. Cx30 protein level [%]
(3)
(3)
(3)
(3)
**
*
**
HC P14
HC P53
TH P14
TH P53
B1
Thalamus
Hippocampus
P53
P14
P53
P14
DKO
43 kDa -
Cx43
50 kDa -
Tubulin
B2
Rel. Cx43 protein level [%]
(3)
(3)
(3)
(3)
*
**
**
HC P14
HC P53
TH P14
TH P53
C1 Cx30-ßGal
TH
C2 Cx43-ECFP
C3 Merge
D
2%
20%
78%
ßGal+/ECFP+
ßGal+/ECFP-
ßGal-/ECFP+

Figure 5.3 ***(previous page)*** **Protein expression of Cx30 and Cx43.** (A_1) Cx30 protein levels analysed by Western blot in the thalamus (TH) and hippocampus (HC) of C57/Bl6 mice at two different time points. Cx30 protein levels increased between p14 and p53 and were higher in the adult thalamus. A Cx30/43 DKO mouse was used as negative control and α-tubulin as a loading control. (A_2) Normalised protein levels confirmed the increase of Cx30 levels during development with a stronger upregulation in the thalamus. (B_1) Western blot analysis of Cx43 in wild-type mice. The different phosphorylation status led to two bands in adult mice. (B_2) Cx43 protein levels, which were normalised to α-tubulin levels, were higher in the juvenile hippocampus than in thalamus. Protein levels increased during development and were equal between brain regions at p53. (C) Immunohistochemical analysis of reporter gene expression in mice heterozygous for $Cx30^{LacZ/+}$ (C_1) and for $Cx43^{ECFP/+}$ (C_2). In the thalamus, different astrocyte populations were observed according to their connexin expression profile. (C_3) Colocalization of the reporters was observed in most cells (yellow in merge), but single-labelled cells expressing only one reporter gene were also present (red or green). (D) Quantification of connexin reporter expression revealed three different astrocyte populations in the thalamus (β-Gal^+/$ECFP^+$, 78.1 ± 2.6%; β-Gal^+/$ECFP^-$, 20.4 ± 2.4%; β-Gal^-/$ECFP^+$, 1.5 ± 0.7%, n = 9 from 3 mice). Asterisks indicate statistical significance. Number of mice is given in parentheses. Scale bar, 20 µm. See also Griemsmann et al., 2014.

The quantified overlap of ECFP and β-Gal signal revealed that almost all (98.5%, 43,051 ± 1,627 β-Gal^+ cells/mm^3 of 43,719 ± 1,457 total cells/mm^3) of the astrocytes expressed Cx30, while one fifth lacked Cx43 (20%, 8,904 ± 1,117 β-Gal^+/$ECFP^-$ cells/mm^3; Fig. 5.3D). The uncoupled cells found in the thalamus of $Cx30^{LacZ/LacZ}$ mice probably belong to this group (see Section 5.2.1). Furthermore, a minor proportion of 1.5% only expressed Cx43 (667 ± 309 β-Gal^-/$ECFP^+$ cells/mm^3; ANOVA and *post-hoc* Tukey, $p<0.01$ (**); see also Griemsmann et al., 2014).
Summarizing, Western blot analysis and reporter gene expression verified the prominent expression of Cx30 in the thalamus, although Cx43 is also widely expressed.

5.2.3 The role of Cx26 in glial networks

Astrocytes express three connexins: Cx26, Cx30 and Cx43. While the latter 2 have been extensively studied in many brain regions (Wallraff et al., 2006; Houades et al., 2008; Pannasch et al., 2011; Roux et al., 2011), the influence of Cx26 on network formation is highly debated in the field. In the hippocampus of Cx30/43 DKO mice, astrocytes were uncoupled and also in the thalamus coupling was mostly abolished (see Section 5.2.1). A recent study revealed a negative impact of the Cx30 knock-out on Cx26 expression (Lynn et al., 2011). Hence, it was of major interest to study the effect of Cx26 on network size directly by taking advantage of the $Cx26^{fl/fl}$:Nestin-Cre mouse line (Tronche et al., 1999; Cohen-Salmon et al., 2002).
Astrocytes were identified by SR101 labelling in acute slices. Tracer-filled cells displayed similar resting membrane potentials in both genotypes in the thalamus(control, -71 ± 1.5 mV, n = 9; $Cx26^{fl/fl}$:Nestin-Cre, -70 ± 1.6 mV, n = 11) and hippocampus (control, -73 ± 1.6 mV, n = 8; $Cx26^{fl/fl}$:Nestin-Cre, -69.4 ± 2.3 mV, n = 9; ANOVA).

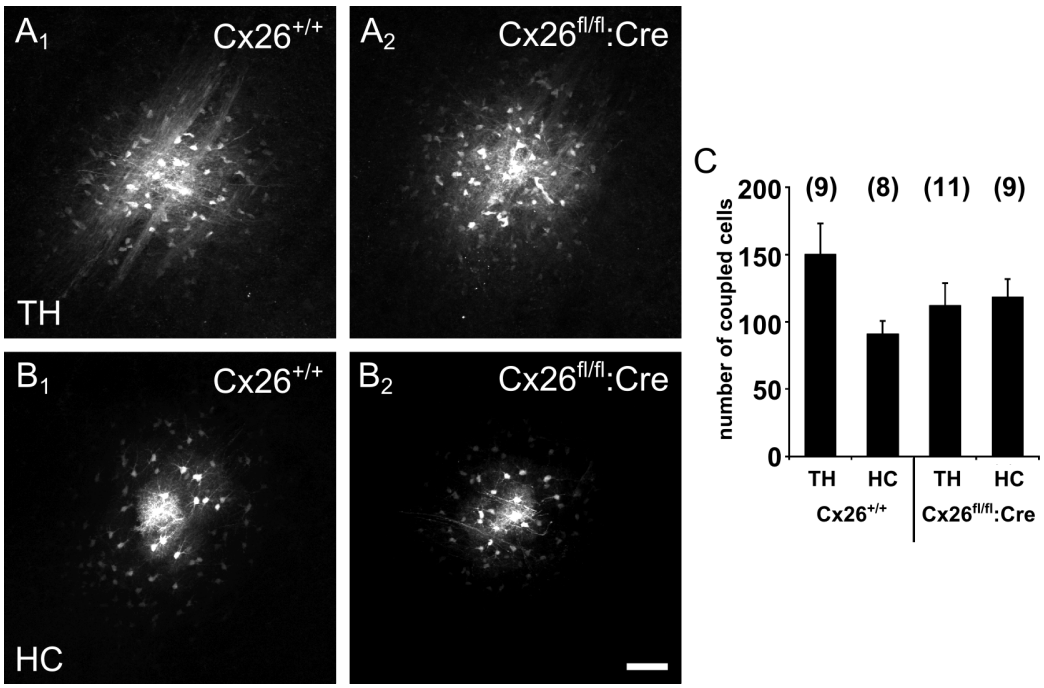

Figure 5.4 Cx26 does not contribute to astrocyte networks. (A, B) The impact of Cx26 deletion on coupling was analysed in $Cx26^{+/+}$ and $Cx26^{fl/fl}$:Nestin-Cre mice. In both thalamus (A, TH) and hippocampus (B, HC) large networks were observed in $Cx26^{+/+}$ (A_1, B_1) and $Cx26^{fl/fl}$:Nestin-Cre mice (A_2, B_2). (C) Network sizes were equal between all genotypes and brain regions analysed (ANOVA). Number of experiments is given in parentheses. Scale bar, 50 µm.

Biocytin diffusion and subsequent visualization revealed large networks in the thalamus of both control and conditional knock-out mice (Fig. 5.4A_{1-2}). Similar results were obtained when analysing hippocampal networks (Fig. 5.4B_{1-2}). Equal network sizes were observed in control and Cx26 knock-out mice (TH, control, 150 ± 23 cells, n = 9; $Cx26^{fl/fl}$:Nestin-Cre, 112 ± 17 cells, n = 11; HC, control, 91 ± 9 cells, n = 8; $Cx26^{fl/fl}$:Nestin-Cre, 118 ± 14 cells, n = 9; Fig. 5.4C; ANOVA; see also Griemsmann et al., 2014). Hence, Cx26 is not involved in GJN formation in these brain areas.
The $Cx26^{fl/fl}$:Nestin-Cre mouse line does not express a reporter gene, when the floxed gene is deleted. It is very important to closely monitor Cre activity to obtain the required conditional knock-out. Both an inactive Cre and an ectopic Cre activity have been described earlier (Requardt et al., 2009; Zhang et al., 2013). Therefore, the genotype of all animals used for the tracer study described above were re-genotyped. The PCR strategy applied here involved three PCRs, a first Cx26fl PCR to detect the Cx26wt and Cx26fl allele, a second PCR to detect the Nestin-Cre gene and finally a third Cx26del PCR to confirm the deletion of Cx26fl in the presence of Cre (Fig. 5.5). In Figure 5.5 four genotypes are depicted, #1 is a $Cx26^{+/+}$:Nestin-Cre mouse which expresses the wt Cx26 protein. Mouse #2 is $Cx26^{+/fl}$, but lacks Cre recombinase, #3 is a $Cx26^{+/fl}$:Nestin-Cre mouse with deletion of the floxed allele and

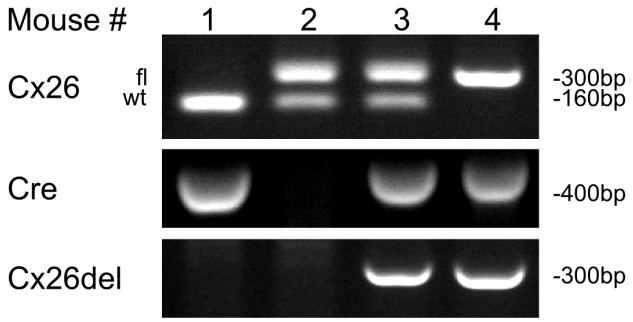

Figure 5.5 Genotyping PCR of the Cx26$^{fl/fl}$:Nestin-Cre mouse line. The conditional deletion of the floxed Cx26 allele was monitored by genotyping PCR. Animals were tested for the presence of a wt or a fl Cx26 allele (upper row), the presence of the Nestin-Cre transgene and additionally the deletion of the Cx26fl allele by a new Cx26del PCR. Mouse #1 has a Cx26$^{+/+}$:Nestin-Cre genotype, #2 is a Cx26$^{+/fl}$, #3 is a Cx26$^{+/fl}$:Nestin-Cre with Cx26 deletion, and #4 is a Cx26$^{fl/fl}$:Nestin-Cre with Cx26 deletion. The mouse #4 is a conditional Cx26 knock-out.

therefore heterozygous for Cx26. Mouse #4 has a Cx26$^{fl/fl}$:Nestin-Cre genotype, also containing the deletion of Cx26fl and is a conditional knock-out of Cx26. A deletion of Cx26fl was only observed in the presence of Nestin-Cre, as shown for mouse #3 and #4 (10 litters of 4 matings were analysed). Noticeably, in the tail tip PCR both the deleted and the floxed Cx26 allele were detected. Nestin is expressed in neural precursor cells, but also in vascular endothelial cells, at the neuromuscular junction and many precursor cells, e.g. in kidney, muscle, testis and heart (Klein et al., 2003; Mohseni et al., 2011).
The Cx26$^{fl/fl}$:Nestin-Cre mouse line proved to be a reliable tool to study the physiological role of Cx26 in the brain. An influence of Cx26 on GJN formation was not observed, indicating that inter-cellular GJs in astrocytes are composed of Cx30 and Cx43.

5.2.4 Cx43 variants reveal impact on RG-like cell networks

RG-like cells are neuronal precursor cells which still reside in the mature brain in neurogenic niches. They share many properties with astrocytes and express a similar pattern of connexins (Kunze et al., 2009). Here, the impact of Cx43 mutations on RG-like cell coupling was investigated.
Earlier studies showed that Cx30 has no influence on adult neurogenesis (Liebmann et al., 2013). Therefore, all knock-out mice used in the network analysis were Cx30 knock-outs and additionally carried different Cx43 modifications to study the influence of the Cx43 channel vs. regulatory effects influencing Cx43 localization. Wild-type (C57/Bl6) animals were compared to mice carrying a floxed point mutation Cx43G138R leading to closure of the channel pore. Additionally, a mouse line carrying a truncation of the cytoplasmic C-terminal tail was analysed. Adult mice between p90-120 were used for the study.

RG-like cells display rather small networks compared to astrocytes, the average network size was 12 ± 1 in $Cx30^{+/+}$;$Cx43^{+/+}$ mice (wt, n = 5). Mice carrying the point mutation Cx43G138R displayed smaller network sizes compared to wild-type animals (Mann-Whitney U-test, $p<0.05$ (*)). No difference was observed between animals with Nestin-Cre ($Cx30^{-/-}$;$Cx43^{flG138R/flG138R}$:Nestin-Cre, 8 ± 2, n = 4) which expressed the point mutation, and those without Cre ($Cx30^{-/-}$;$Cx43^{flG138R/flG138R}$, 8 ± 1, n = 3; Mann-Whitney U-test; Fig. 5.6A). Compared to $Cx30^{+/+}$;$Cx43^{+/+}$ mice the occurrence of networks was equal for RG-like cells carrying the point mutation Cx43G138R (wt, 83%, n = 5 coupled cells and n = 1 single cell; $Cx30^{-/-}$;$Cx43^{flG138R/flG138R}$:Nestin-Cre, 50% coupled cells, n = 4 coupled cells and n = 4 single cells; $\mathcal{X}^2$-test). Mice negative for Nestin-Cre displayed an equal network/single cell ratio compared to wild-type and point mutation mice (60% coupled cells; n = 3 coupled cells and n = 2 single cells; $\mathcal{X}^2$-test; Fig. 5.6B).
Mice with a truncation of the cytoplasmic tail were heterozygous for this knock-out (Cx43K258stop) and carried a floxed Cx43 on the other allele, otherwise the truncation is lethal (Maass et al., 2007). The floxed Cx43 was deleted employing a hGFAP-Cre recombinase. These $Cx30^{-/-}$;$Cx43^{fl/K258stop}$:GFAP-Cre animals displayed significantly smaller networks compared to $Cx30^{+/+}$;$Cx43^{+/+}$ animals (5 ± 1, n = 5; Mann-Whitney U-test, $p<0.05$ (*)), but were equal to GFAP-Cre negative mice ($Cx30^{-/-}$;$Cx43^{fl/K258stop}$, 8 ± 2, n = 4; Mann-Whitney U-test). Analysing the ratio of networks vs. single cells when patching an RG-like cell, the truncated Cx43K258stop did not differ from wild-type, GFAP-Cre negative mice or Cx43G138R mice. RG-like cells in $Cx30^{-/-}$;$Cx43^{fl/K258stop}$ mice were coupled in 80% of the experiments (n = 4 coupled cells and n = 1 single cell) and in $Cx30^{-/-}$;$Cx43^{fl/K258stop}$:GFAP-Cre mice 63% of the tracer filled RG-like cells were coupled (n = 5 coupled cells and n = 3 single cells; $\mathcal{X}^2$-test; Fig. 5.6B). The RG-like cell networks were analysed in collaboration with Jiong Zhang, who stained and co-counted the networks. Part of the data were published in the PhD thesis by Zhang, 2013.
In conclusion, RG-like cells in the subgranular zone of adult mice were coupled to other cells. The networks were however much smaller compared to astrocyte networks in the CA1 st. rad. (Fig. 5.6A, 5.1C). Modifications of the Cx43 protein led to changes in RG-like networks. The point mutation in the pore domain often led to uncoupling, while the truncation of the cytoplasmic tail with its regulatory phosphorylation sites decreased network sizes compared to wild-type mice.

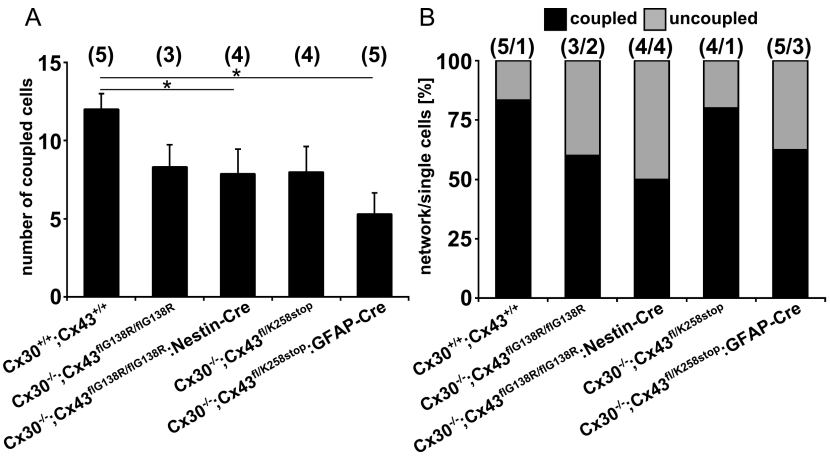

Figure 5.6 Impact of Cx43 modifications on gap junctions in RG-like cells. (A) Network sizes of RG-like cells in five different genotypes, in $Cx30^{+/+}$;$Cx43^{+/+}$ the average number of coupled cells was 12 ± 1. Mice expressing the Cx43G138R point mutation have smaller networks. Also cells containing a C-terminal truncated Cx43K258stop on one allele and a floxed wt allele displayed decreased network sizes. Mice expressing only the truncated Cx43K258stop displayed the smallest networks compared to $Cx30^{+/+}$;$Cx43^{+/+}$ animals. (B) Most RG-like cells are coupled, though some cells were not connected to other cells. No difference between genotypes was observed. Asterisks indicate statistical significance. Number of experiments is given in parentheses.

5.3 Astrocytes and oligodendrocytes form a panglial network in the murine brain

5.3.1 Indications for panglial networks from immunohistochemistry

The differential connexin expression between hippocampus and thalamus, and even within thalamic astrocytes, revealed a considerable astrocyte heterogeneity. Furthermore, the network analysis revealed tracer diffusion into myelinated fibre tracts. The latter observation led to the question how the tracer could diffuse into the myelin sheath and questioned the concept of a pure astrocytic network. In the following experiments the cell-type composition of these physiological networks was investigated by immunohistochemistry.

The membrane potential of tracer-filled astrocytes was equal between brain regions (TH, -76.55 ± 1.34 mV, n = 11; HC, 78.7 ± 1.34 mV, n = 10), while the membrane resistance was slightly lower in the thalamus (TH, 1.58 ± 0.23 MΩ, n = 11; HC, 3.28 ± 0.46 MΩ, n = 10).

Characterization of cell identity in GJNs was performed employing hGFAP-EGFP mice and subsequent antibody staining. Many $EGFP^{+}$ cells were observed in both thalamus and hippocampus (Nolte et al., 2001), although GFAP antibody staining in the thalamus labels only very few cells (not shown; see Frassoni et al., 2000; Parri and Crunelli, 2002). Instead of GFAP the enzyme GS was used as a marker for astrocytes (Norenberg, 1979;

Sonnewald et al., 1997; Coulter and Eid, 2012). Glutamine synthetase is an enzyme involved in detoxification of ammonia, metabolises glutamate to glutamine and is located in the cytoplasm of astrocytes (Norenberg, 1979). Antibody staining revealed many GS^+ cells in both thalamus and hippocampus and was therefore considered a good astrocyte marker for GJN analysis. Immunostaining of tracer-coupled networks revealed many co-labelled cells, but some biocytin filled cells were not stained for GS (Fig. 5.7A_{1-3}, B_{1-3}). This marker was expressed by less than half of the biocytin-coupled cells in the thalamus (TH, 49 ± 8 of 100 ± 13 cells, n = 10), while most of the coupled cells in the hippocampal CA1 region were GS^+ (HC, 106 ± 10 of 129 ± 11 cells, n = 7; Fig. 5.7). The amount of GS^+ cells differed significantly (by 35%) between networks in the two brain regions. In the thalamus 46.4 ± 5.4% and in the hippocampus 81.6 ± 2% of the tracer filled cells were GS^+ (ANOVA and *post-hoc* Tukey's test, $p<0.01$ (**); Fig. 5.7C_{1-2}). In summary, glial networks contain distinct amounts of GS^+ cells in the thalamus and hippocampus (see also Griemsmann et al., 2014).

A marker for oligodendrocytes was employed in a second study to investigate the cell-identity of GS^- cells in these networks. The transcription factor Olig2 is expressed in cells of the oligodendrocyte lineage (Marshall et al., 2005; Nishiyama et al., 2009; Trotter et al., 2010) and was therefore considered a suitable tool to look for mature and immature oligodendrocytes. Thalamic networks abundantly contained $Olig2^+$ cells (49 ± 8 of 75 ± 7 cells, n = 10; Fig. 5.8A_{1-3}). In contrast, in hippocampal GJNs Olig2 labelling was much less prevalent (19 ± 4 of 129 ± 18 cells, n = 7; Fig. 5.8B_{1-3}). The fraction of $Olig2^+$ cells differed significantly between the two brain regions. While in the thalamus a majority of cells expressed Olig2 (62.2 ± 8.4%, n = 10), in the hippocampus only a minor fraction of cells displayed Olig2 (17.5 ± 4.6%, n= 7; ANOVA and *post-hoc* Tukey's test, $p<0.01$ (**); Fig. 5.8C_{1-2}). Immunostainings suggested participation of astrocytes and oligodendrocytes in GJNs in both brain regions, though at variable amounts. While GS and Olig2 label distinct cell populations in the hippocampus (Fig. 5.7C_2, 5.8C_2), they were not cell-type specific in the thalamus. There was a considerable overlap in staining as derived from cell counting (Fig. 5.7C_1, 5.8C_1; see also Griemsmann et al., 2014).

Recent observations in white matter areas of the brain described NG2 cells as part of glial networks (Maglione et al., 2010). The Olig2 labelling might include NG2 cells as the transcription factor Olig2 labels the entire oligodendrocytes lineage, including $NG2^+$ cells (Trotter et al., 2010). A potential role of these cells in grey matter areas of the hippocampus and thalamus was investigated in the next set of experiments. In contrast to recent findings in the corpus callosum (Maglione et al., 2010), we never observed $NG2^+$ cells within thalamic or hippocampal GJNs (TH, 0 of 117 ± 11 cells, n = 8; HC, 0 of 136 ± 18 cells, n = 8; Fig. 5.9A_{1-3}, B_{1-3}). In conclusion, GJNs in both brain regions did not contain $NG2^+$ cells and indicate differences between grey and white matter areas (see also Griemsmann et al., 2014).

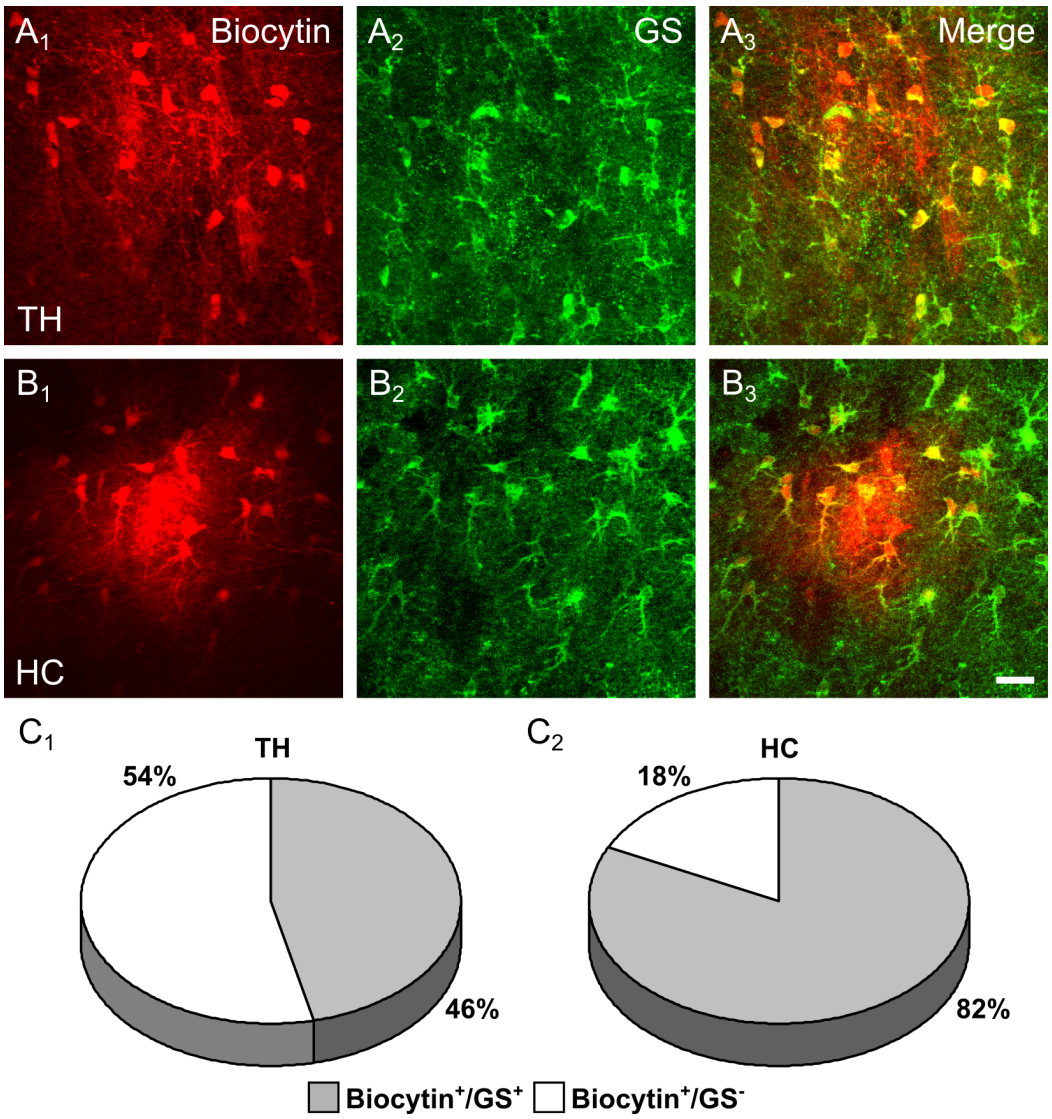

Figure 5.7 GS expressing cells in tracer-coupled networks. (A, B) Immunostainings of GJNs (A_1, B_1) in the thalamus (TH) and hippocampus (HC) with the astrocyte marker GS (A_2, B_2). Merged images (A_3, B_3) show colocalization of biocytin (red) and GS staining (green) in yellow. (C) Thalamic networks contained less than 50% GS^+ cells (C_1, 46.4 ± 5.4%, n = 10), while most cells in hippocampal GJNs were GS^+ (C_2, 81.6 ± 2%, n = 7). Scale bar, 20 µm. See also Griemsmann et al., 2014.

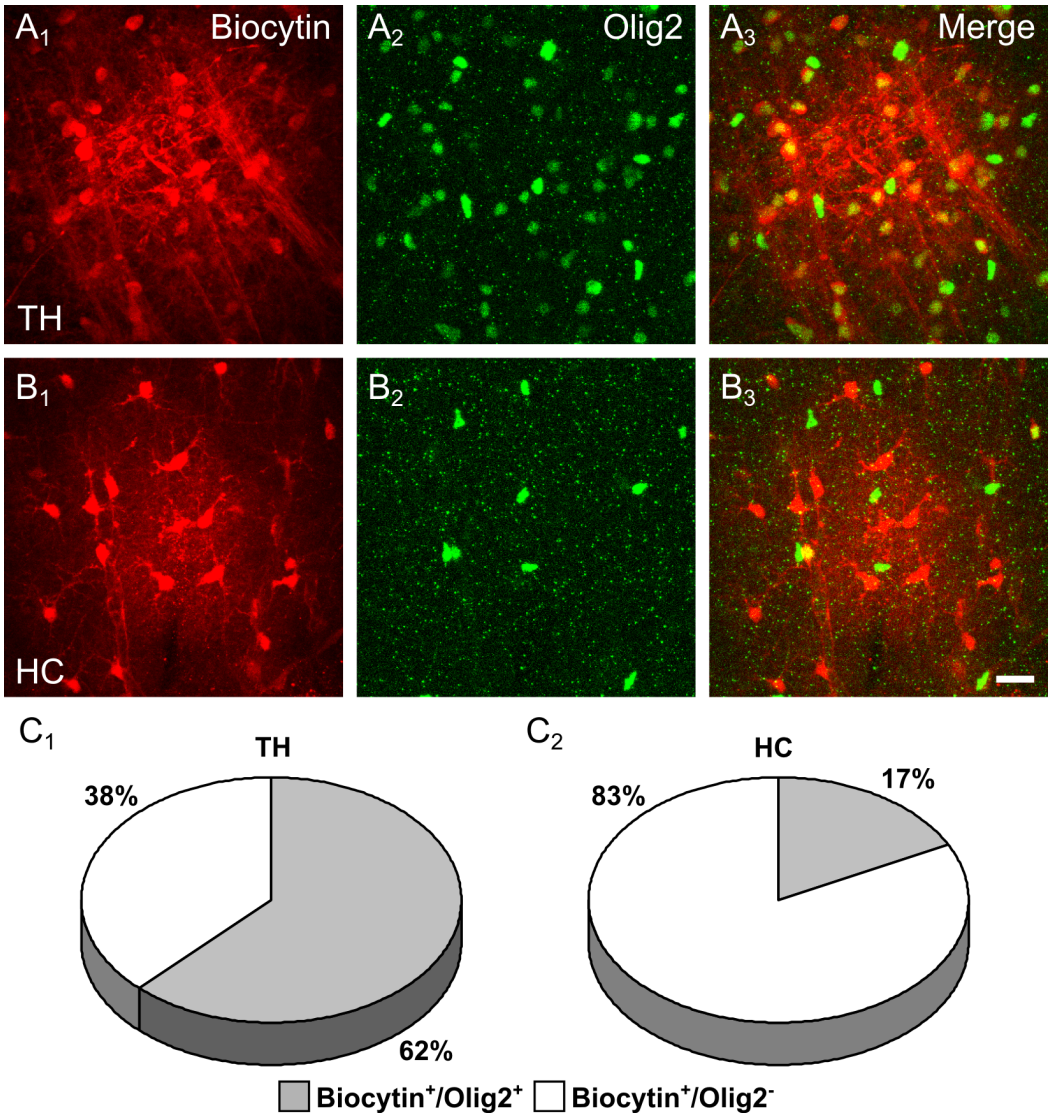

Figure 5.8 Glial networks contain differential amounts of Olig2 expressing cells. (A, B) Immunostainings of thalamic (TH) and hippocampal (HC) networks (A_1, B_1) in hGFAP-EGFP mice using antibodies against Olig2 (A_2, B_2). Merged images in the thalamus (A_3) display many Olig2$^+$ cells in tracer coupled networks, while in the hippocampus only few Olig2$^+$ and biocytin double labelled cells were observed (B_3). (C) Most coupled cells in the thalamus were Olig2$^+$ (C_1, 62.2 ± 8.4 %, n = 10). In the hippocampus only a few Olig2$^+$ cells (C_2, 17.5 ± 4.6 %, n= 7) were observed in GJNs. Scale bar, 20 µm. See also Griemsmann et al., 2014.

Microglia express Cx43 under certain conditions, e.g. inflammation, and are dye-coupled *in vitro* (Eugenín et al., 2001). To check whether microglia participate in GJNs, networks were stained for Iba1. In both brain regions Iba1$^+$ microglia (TH, n = 9; HC, n = 8) were never part of the tracer-filled networks (Fig. 5.9C$_{1-3}$, D$_{1-3}$; see also Griemsmann et al., 2014).
In the thalamus and the hippocampal CA3 region Cx45 mediated gap junction coupling between neurons has been described in adulthood (Maxeiner et al., 2003). Accordingly, a potential contribution of neurons was investigated immunohistochemically study by labelling neuronal nuclei (NeuN). In the ventrobasal thalamus no NeuN$^+$ cells were found in GJNs, when patching an astrocyte, and also in the hippocampal CA1 region no indications for a neuronal contribution to glial GJNs was observed (TH, n = 9; HC, n = 6; Fig. 5.9E$_{1-3}$, F$_{1-3}$; see also Griemsmann et al., 2014).
Thus, the immunohistochemical study of physiological tracer-coupled networks *in situ* revealed a heterogeneous cell population in both brain regions. GJNs are not exclusively formed by astrocytes, but also include oligodendrocytes. While in the hippocampus the networks contain around 80% GS$^+$ astrocytes and 20% Olig2$^+$ oligodendrocytes, the thalamic networks differ in their properties regarding GS$^+$(46%) and Olig2$^+$(62%) cells. Furthermore, thalamic networks contain a population of cells that, according to cell counting, expresses both astrocytic and oligodendrocytic markers.

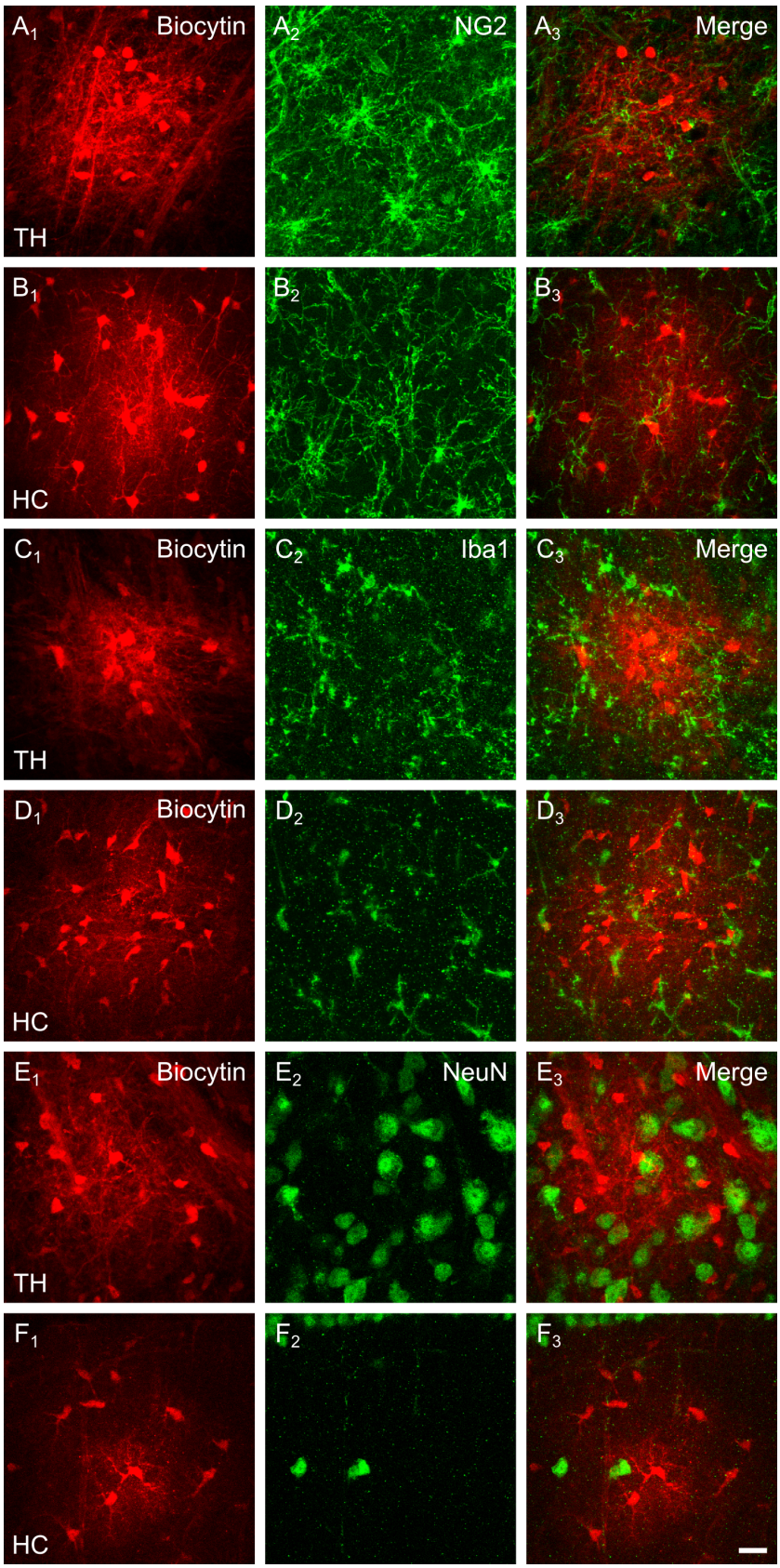
A1
Biocytin
TH
A2
NG2
A3
Merge
B1
HC
B2
B3
C1
Biocytin
TH
C2
Iba1
C3
Merge
D1
Biocytin
HC
D2
D3
E1
Biocytin
TH
E2
NeuN
E3
Merge
F1
HC
F2
F3

Figure 5.9 ***(previous page)*** **Biocytin-filled networks are devoid of NG2 cells, microglia and neurons.** Immunostainings of GJNs (A_1-F_1)in the thalamus (TH) and hippocampus (HC) using antibodies against NG2 (A_2, B_2), Iba1 (C_2, D_2) and NeuN (E_2, F_2). The merged images (A_3-F_3) show no overlap of biocytin with the cell-type specific antibody staining for NG2 cells (A_3, B_3), Iba1$^+$ microglia (C_3 and D_3) or NeuN$^+$ neurons (E_3, F_3) in any of the analysed brain regions. (A_3, B_3) show only one optical section, the other images are projections of 10 µm z-stacks. Scale bar, 20 µm.

5.3.2 Tracer diffusion is bidirectional in panglial networks

The prevalence of both GS$^+$ and Olig2$^+$ cells in glial networks in the thalamus and hippocampus challenged the concept of pure astrocytic networks (Section 5.3.1; Blomstrand et al., 2004; Houades et al., 2008). It is known from *in vitro* studies that astrocytic connexins form heterotypic channels with oligodendrocytic connexins (Orthmann-Murphy et al., 2007b; Magnotti et al., 2011b).
Putative astrocyte-oligodendrocyte coupling was further investigated using PLP-GFP mice. In these mice mature oligodendrocytes expressing the myelin protein phospholipoprotein (PLP) also express the reporter GFP (see Section 3.10). Networks were analysed in juvenile and adult mice.
In juvenile mice, panglial coupling was investigated before the expected onset of Cx30 protein expression (Kunzelmann et al., 1999). Thalamic SR101$^+$ astrocytes in p9-11 PLP-GFP mice were abundantly coupled to other cells, including PLP-GFP$^+$ cells (total, 87 ± 18 coupled cells, among them 34% GFP$^+$ cells, n = 14; Fig. 5.10; Griemsmann et al., 2014). Still, at this age prior to onset of myelination only few PLP-GFP$^+$ cells can be observed, the amount of oligodendrocytes might thus be underestimated.

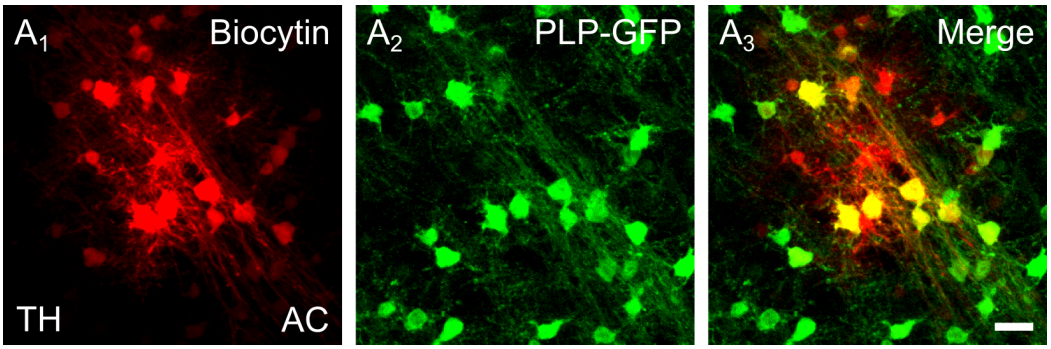

Figure 5.10 Panglial tracer diffusion in juvenile (p9-11) mice. SR101$^+$ astrocytes were filled with biocytin (A_1, indicated by AC) and subsequently co-immunostained for GFP (A_2) revealing diffusion from astrocytes to PLP-GFP$^+$ oligodendrocytes (A_3) in the thalamus. Scale bar, 20 µm. See also Griemsmann et al., 2014.

In adult mice (p30-60) either PLP-GFP$^+$ oligodendrocytes or SR101$^+$ astrocytes were tracer-filled in both brain regions. In Figure 5.11 tracer-coupled networks are shown for the 4 experimental conditions. Always large networks were observed when patching an astrocyte or an oligodendrocyte (Fig. 5.11A$_1$-D$_1$). Filling of SR101$^+$ astrocytes with biocytin in the thalamus and hippocampus revealed abundant coupling (TH, 118 ± 15, n = 16; HC, 133 ± 16, n = 16; Fig. 5.12A). Network sizes were equal, when filling oligodendrocytes with the tracer (TH, 87 ± 14, n = 6; HC, 82 ± 15, n = 8), and coupling did not differ between brain regions (ANOVA; Fig. 5.12A; see also Griemsmann et al., 2014). Biocytin diffusion is therefore bidirectional in the panglial network.
The proportion of PLP-GFP$^+$ cells was assessed in the four groups and significant differences between brain regions were observed. The GFP reporter fluorescence was enhanced by immunostaining and visualized many GFP$^+$ cells in the ventrobasal thalamus (Fig. 5.11A$_2$, B$_2$). In contrast, only few PLP-GFP$^+$ cells were observed in the hippocampus (Fig. 5.11C$_2$, D$_2$). The merged images show colocalization of biocytin and PLP-GFP in all experimental settings (Fig. 5.11A$_3$-D$_3$). Thalamic networks contained more than 50% GFP$^+$ cells, while in the hippocampus only a minor proportion stained for GFP (<14%; ANOVA and *post-hoc* Tukey, p<0.01 (**)). Interestingly, the contribution of GFP$^+$ cells was equal in one brain region irrespective of the patched cell-type (TH-AC, 53.1 ± 6.4%, n = 16; TH-OL, 66.5 ± 8.4%, n = 6; HC-AC, 12.4 ± 1, n = 16; HC-OL, 13.4 ± 1.4, n = 8; ANOVA and *post-hoc* Tukey; Fig. 5.12B; see also Griemsmann et al., 2014). The tracer spread is therefore not unidirectional from astrocytes to oligodendrocytes, but diffuses in both directions in the panglial network regardless of the brain region. The proportions of PLP-GFP$^+$ cells in GJNs differs between thalamus and hippocampus and might reflect the different densities of PLP-GFP$^+$ cells observed in the PLP-GFP images (Fig. 5.11A$_2$-D$_2$; Fig. 5.12B).
In summary, astrocytes and oligodendrocytes form panglial GJNs in the thalamus and hippocampus. The diffusion of the tracer biocytin is bidirectional as indicated by equal network sizes and similar proportions of PLP-GFP cells in these networks in each region. Molecules can therefore pass in both directions through channels between the two cell-types. Furthermore, panglial networks are already prevalent during early postnatal development.

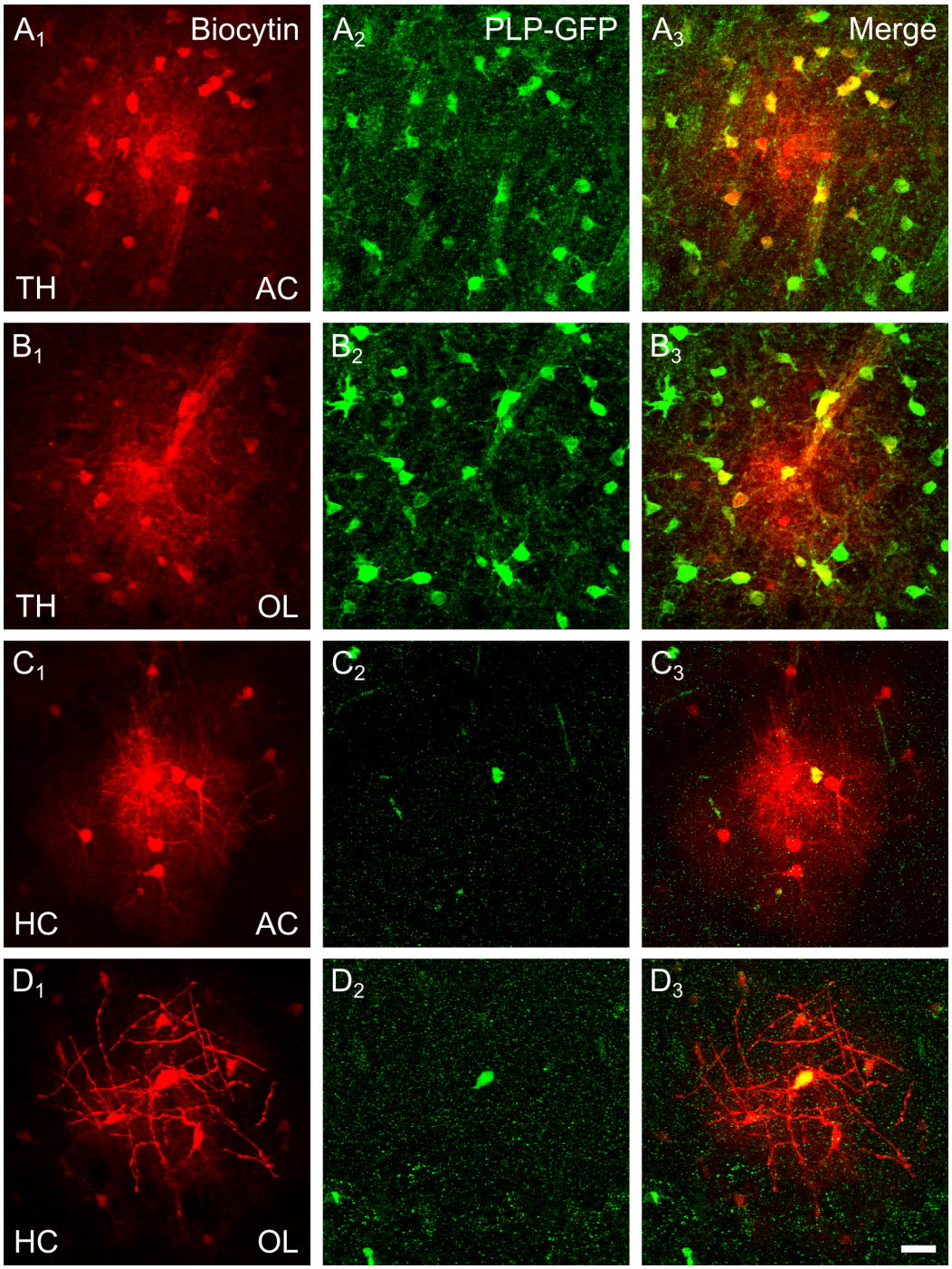

Figure 5.11 Tracer diffusion in adult (p30-60) PLP-GFP mice reveals panglial networks. (A-D) $SR101^+$ astrocytes (A, C; indicated by AC) and PLP-GFP^+ oligodendrocytes (B, D; as indicated by OL) in the thalamus and hippocampus of PLP-GFP mice were tracer-filled. Immunostaining for GFP (A_2-D_2) always revealed biocytin spread into PLP-GFP^+ oligodendrocytes (A_3-D_3). Tracer-injected PLP-GFP^+ cells always exhibited inter-cellular coupling in thalamus and hippocampus (B_3, D_3). Scale bar, 20 µm. See also Griemsmann et al., 2014.

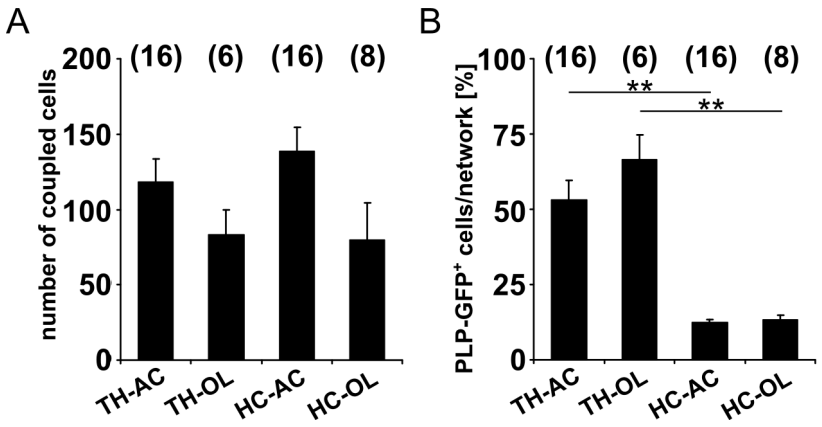

Figure 5.12 Quantification of panglial networks in adult PLP-GFP mice. (A) Graph summarizing the network sizes in the thalamus (TH) and hippocampus (HC) for injected astrocytes (AC) and oligodendrocytes (OL). Network sizes were equal between the four groups. (B) Thalamic networks contained more PLP-GFP$^+$ cells, irrespective of the cell-type initially filled with biocytin (TH, 53.1 ± 6.4% and 66.5 ± 8.4%, HC: 12.4 ± 1 and 13.4 ± 1.4, injection into AC or OL respectively). Number of experiments is given in parentheses. Asterisks indicate statistical significance. See also Griemsmann et al., 2014.

5.3.3 Heterotypic channels containing Cx30 are mainly responsible for panglial coupling

Astrocytes and oligodendrocytes express a distinct set of connexins (see Section 1.4). *In vitro* studies confirmed functional heterotypic channels composed of Cx30 and Cx32, while Cx47 forms GJCs with Cx43 (Orthmann-Murphy et al., 2007b; Theis and Giaume, 2012). The experiments so far confirmed the presence of panglial networks in both regions (see Sections 5.3.1 and 5.3.2). The molecular basis of these networks was investigated in mice with deletion of Cx30 and Cx47 (Tress et al., 2012).
Networks were analysed by tracer injection in SR101-labelled astrocytes from Cx30$^{+/LacZ}$; Cx47$^{EGFP/EGFP}$, Cx30$^{LacZ/LacZ}$;Cx47$^{EGFP/EGFP}$ and Cx30$^{LacZ/LacZ}$;Cx47$^{+/EGFP}$ mice in the thalamus (Fig. 5.13A-C) and hippocampus (Fig. 5.13D-F).
The cell-type specific reporter gene expression provided an insight into panglial network composition. Antibody staining for β-Gal$^+$ astrocytes and Cx47-EGFP$^+$ oligodendrocytes revealed abundant panglial GJC between both cell-types in the thalamus of Cx30$^{+/LacZ}$; Cx47$^{EGFP/EGFP}$ mice (Fig. 5.13A$_{1-4}$).
Unexpectedly, in double knock-out Cx30$^{LacZ/LacZ}$;Cx47$^{EGFP/EGFP}$ mice astroglial networks were almost completely abolished (Fig. 5.13B$_1$, 5.14A). In addition, no panglial networks were observed in these mice, only β-Gal$^+$ astrocytes were found (Fig. 5.13B$_{1-4}$). This observation led to the question whether an oligodendrocytic connexin might rescue the glial network. Therefore, we tested mice expressing on one allele Cx47, but completely lacking Cx30 expression (Cx30$^{LacZ/LacZ}$;Cx47$^{+/EGFP}$). Tracer coupling in these mice revealed panglial networks when patching SR101$^+$ astrocytes (Fig. 5.13C$_{1-4}$).

In the hippocampus panglial coupling was less abundant compared to thalamic networks (see Section 5.3.2). Though, as observed in thalamic networks, mice expressing one of the connexins on one allele displayed panglial coupling in the CA1 region (Fig. 5.13D_{1-3}, F_{1-3}). The double knock-out of Cx30 and Cx47 displayed no panglial coupling and no or only small networks (Fig. 5.13E_{1-3}, 5.14A).
Deletion of one Cx30 allele and both Cx47 alleles resulted in large networks (TH, 166 ± 16, n = 11; HC, 79 ± 14 coupled cells, n = 10; Fig. 5.14A). In double knock-out $Cx30^{LacZ/LacZ}$; $Cx47^{EGFP/EGFP}$ mice many biocytin-filled cells lacked coupling (TH, 43%, 3 of 7 cells; HC, 60%, 6 of 10; Fig. 5.14C), and the remaining filled cells showed only small networks (TH, 5 ± 1, n = 4; HC, 5 ± 2 coupled cells, n = 4; Fig. 5.14A). Mice being heterozygous for Cx47 and lacking Cx30 ($Cx30^{LacZ/LacZ}$;$Cx47^{+/EGFP}$) displayed only small networks (TH, 28 ± 11, n = 10; HC, 39 ± 19 coupled cells, n = 7; Fig. 5.14A; see also Griemsmann et al., 2014). Differences in network size and proportions of Cx47-EGFP cells were tested by ANOVA and *post-hoc* Tukey, $p<0.01$ (**).
Analysing the proportions of networks vs. single cells no difference between brain regions was observed ($\mathcal{X}^2$-test). In the thalamus these proportions differed between $Cx30^{LacZ/LacZ}$;$Cx47^{+/EGFP}$ (100% coupled cells) and $Cx30^{LacZ/LacZ}$;$Cx47^{EGFP/EGFP}$ mice (57% coupled cells), while in the hippocampus $Cx30^{+/LacZ}$;$Cx47^{EGFP/EGFP}$(100% coupled cells) displayed more networks compared to $Cx30^{LacZ/LacZ}$;$Cx47^{EGFP/EGFP}$ mice (40% coupled cells; $\mathcal{X}^2$-test, $p<0.05$ (*)).
Panglial coupling was quantified by determining the proportion of Cx47-$EGFP^+$ oligodendrocytes. As Cx30-LacZ is not expressed in the hippocampus, astrocytes were not quantified. The amount of oligodendrocytes varied considerably in GJNs of different genotypes (Fig. 5.14B). Networks in Cx30 and Cx47 double knock-out mice did not contain any Cx47-$EGFP^+$ cells (n = 4, each brain region). In the thalamus and hippocampus of $Cx30^{+/LacZ}$;$Cx47^{EGFP/EGFP}$ (TH, 60 ± 8.5%, n = 11; HC, 29 ± 3.3%, n = 10) and $Cx30^{LacZ/LacZ}$;$Cx47^{+/EGFP}$ mice (TH, 19 ± 5.9%, n = 10; HC, 19.9 ± 6.8%, n = 7) panglial coupling was always present, though less abundant in the thalamus of the latter genotype (see also Griemsmann et al., 2014).
Interestingly, one allele of either connexin was sufficient to promote panglial coupling, while the double knock-out of Cx30 and Cx47 was mainly devoid of any glial networks.

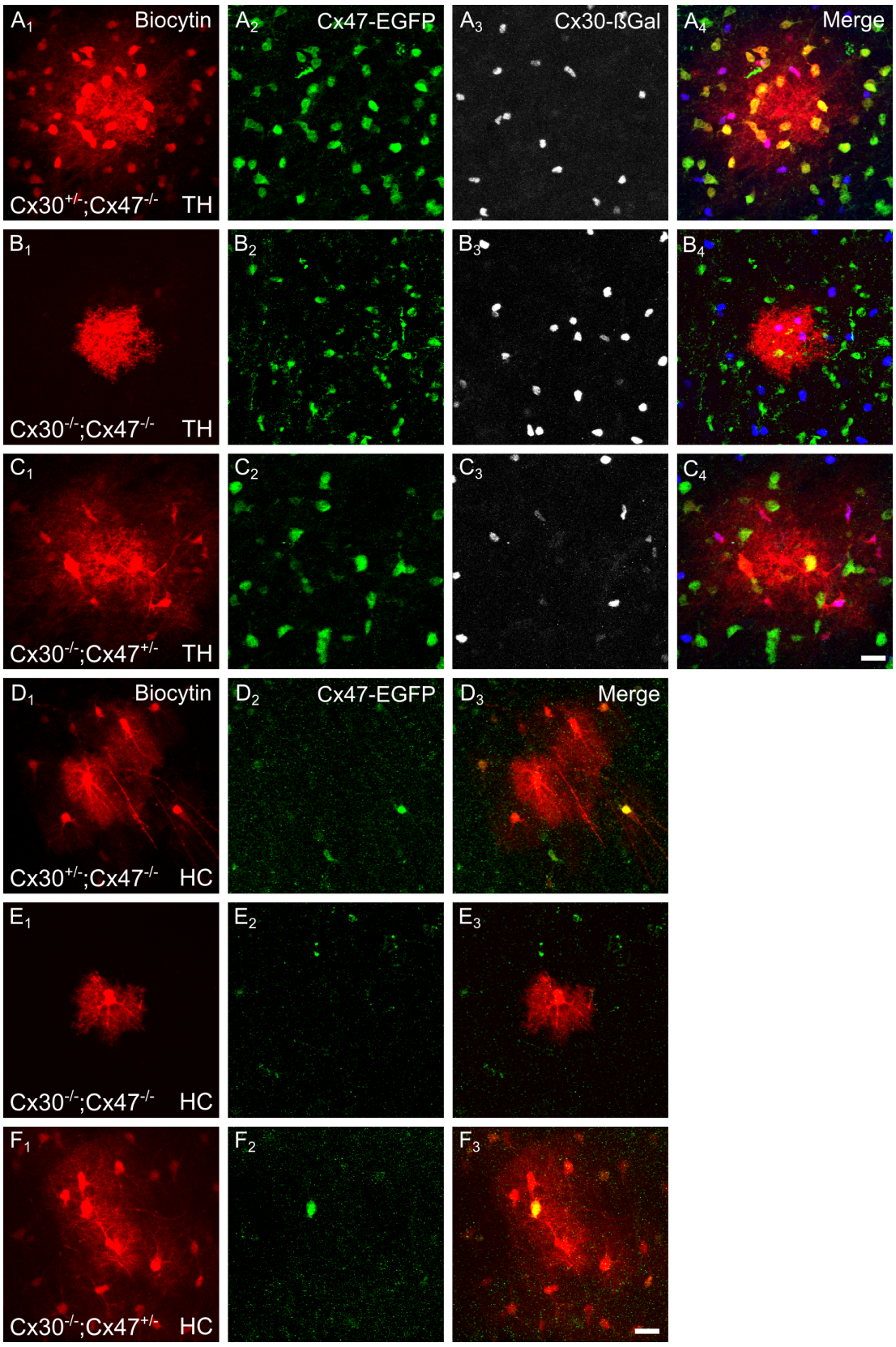
A1 Biocytin
A2 Cx47-EGFP
A3 Cx30-ßGal
A4 Merge
Cx30+/-;Cx47-/- TH
B1
B2
B3
B4
Cx30-/-;Cx47-/- TH
C1
C2
C3
C4
Cx30-/-;Cx47+/- TH
D1 Biocytin
D2 Cx47-EGFP
D3 Merge
Cx30+/-;Cx47-/- HC
E1
E2
E3
Cx30-/-;Cx47-/- HC
F1
F2
F3
Cx30-/-;Cx47+/- HC

Figure 5.13 ***(previous page)*** **Cx30 and Cx47 reporter gene expression in thalamic networks.** SR101$^+$ astrocytes in the TH and HC were tracer filled for 20 min (A_1-F_1) in 3 genotypes Cx30$^{+/LacZ}$;Cx47$^{EGFP/EGFP}$ (A, D), Cx30$^{LacZ/LacZ}$;Cx47$^{EGFP/EGFP}$ (B, E) and Cx30$^{LacZ/LacZ}$;Cx47$^{+/EGFP}$ (C, F). Cx47-EGFP$^+$ oligodendrocytes are displayed in green (A_2-F_2) and β-Gal$^+$ astrocytes (A_3-C_3) in blue in the merged images (A_4-C_4; D_3-F_3). Notice that Cx30LacZ is not expressed in the hippocampus and β-Gal is therefore only displayed for thalamic networks. Colocalization of biocytin and Cx47-EGFP was observed in networks of heterozygous animals (A_4, C_4, D_3, F_3) and overlap with β-Gal was observed in all genotypes in the thalamus (A_4-C_4). Cx30/47 double knock-outs were devoid of Cx47-EGFP cells (B_4, E_3). Scale bar, 20 µm.

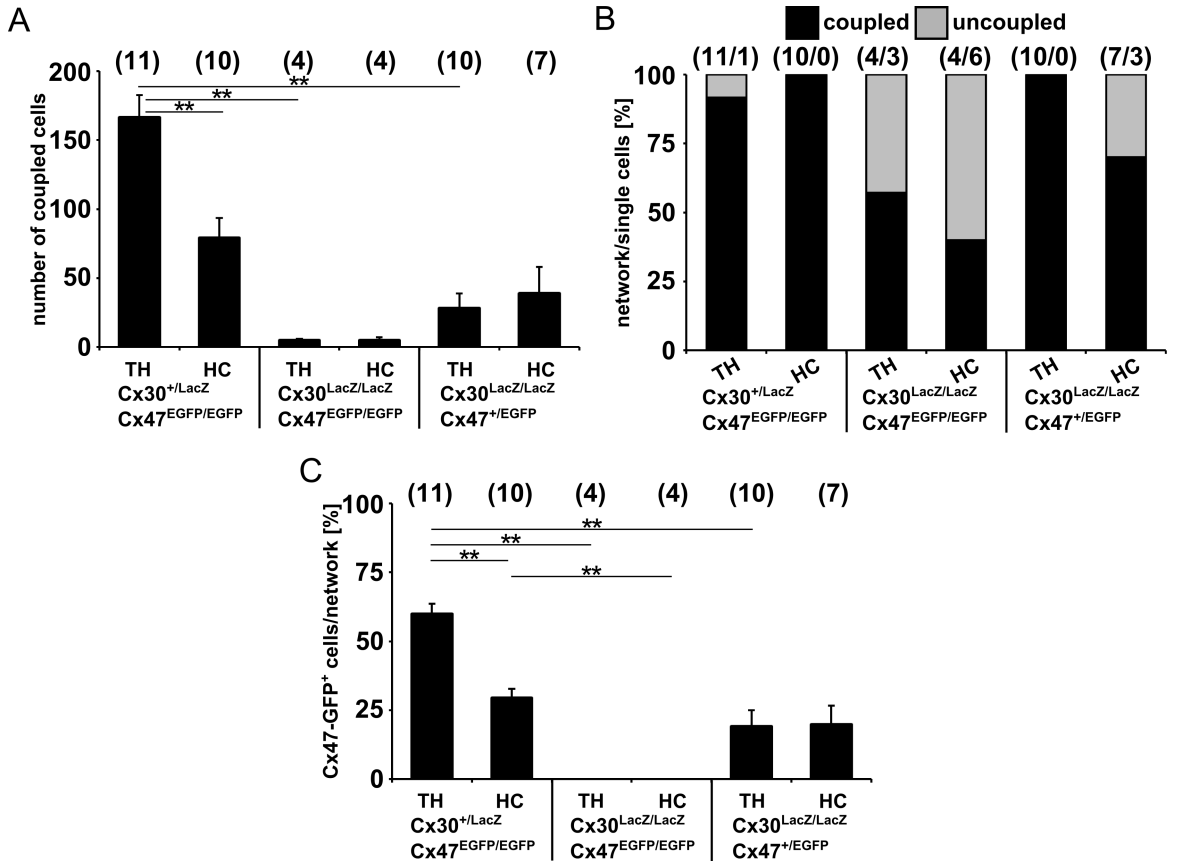

Figure 5.14 Summary of Cx30 and Cx47 impact on network properties. (A) Network sizes differed considerably between genotypes. Only minimal tracer spread was observed in Cx30/Cx47 deficient mice, in contrast to heterozygous mice. (B) The proportion of coupled vs. single cells was assessed in all genotypes both in hippocampus and thalamus. (C) Cx47-EGFP$^+$ oligodendrocytes were quantified in all networks. Many oligodendrocytes were observed in thalamic networks of Cx30$^{+/LacZ}$;Cx47$^{EGFP/EGFP}$ mice. The hippocampal networks contained less Cx47-EGFP$^+$ cells. Oligodendrocytes were absent in GJNs of Cx30/Cx47 deficient mice and panglial coupling was reduced in the thalamus of Cx30$^{LacZ/LacZ}$;Cx47$^{+/EGFP}$ mice. Asterisks indicate statistical significance. Number of experiments is given in parentheses. See also Griemsmann et al., 2014.

5.4 Expression profile of classical astrocyte markers in the thalamus

5.4.1 A cell-type marker study in PLP-GFP mice

The immunohistochemical analysis of glial networks revealed abundant GS expression in the thalamus, but the calculated overlap of GS and Olig2 questioned the concept of marker specificity in this brain region (see Section 5.3.1). Hence, GS expression and other markers were further analysed by immunofluorescence.
Brain slices from PLP-GFP mice were stained against GS. In the thalamus abundant overlap of GS and PLP-GFP was observed in confocal images (94.5%, 129,333 ± 8,616 GFP^+ and GS^+ cells/mm^3 from a total of 136,911 ± 9,363 GFP^+ cells/mm^3, n = 9 from 3 mice), while only few cells displaying weak GS immunoreactivity were visible (indicated with a star in Figure 5.15A_{1-3}; Griemsmann et al., 2014). Furthermore, the strongly GS fluorescent cells (Fig. 5.15A_1) possessed the typical morphology of PLP-GFP^+ oligodendrocytes (Fig. 5.15A_2), while the weakly fluorescent cells show GS immunoreactivity also in their main processes (see star-labelled cells in Figure 5.15A). In the green channel myelinated fibre bundles were visible, a characteristic property of the VB which was never observed in the CA1 region. In the hippocampus of the same slices the GS staining pattern was distinct from the thalamus. Many star-like cells, resembling astrocytes, with GS staining in their cytoplasm and main processes were observed. Notice that only in few cases PLP-GFP cells expressed GS (17.8%, 4,067 ± 692 GFP^+ and GS^+ cells/mm^3 from a total of 22,644 ± 1,573 GFP^+ cells/mm^3, n = 9 from 3 mice; Fig. 5.15B_{1-3}, 5.17A; see also Griemsmann et al., 2014). Some of the processes of PLP-GFP cells can be observed in the GFP staining (Fig. 5.15B_2). The density of PLP cells in the thalamus is significantly higher, by sixfold, compared to the hippocampus. In the CA1 region the population of GS^+ cells was significantly larger than the PLP-GFP^+ population (Fig. 5.17A). A complete list of cell densities obtained by immunohistochemistry is shown in table 9.1 in the appendix. Differences in cell densities in this and the following immunostainings were statistically analysed by ANOVA and *post-hoc* Tukey or Student's *t*-test as appropriate, $p<0.05$ (*).
PLP-GFP expression in mice has been described to exclusively label oligodendrocytes in selected brain areas including hippocampus, while the thalamus was not analysed (Fuss et al., 2000). Therefore, in addition to astrocyte markers also other cell-type specific markers were analysed for potential co-labelling with PLP-GFP. In a first set of experiments, GFP staining was analysed in neurons. Both, in the thalamus and hippocampus no co-staining with NeuN was observed (n = 3 from 3 mice; Fig. 5.15C_{1-3}, D_{1-3}; Fig. 5.17B).
The commonly used astrocyte marker GFAP was applied in another series of stainings, along with the microglia marker Iba1. GFAP antibodies only sparsely labelled cells in the thalamus (Fig. 5.16A_1), confirming earlier observations (Frassoni et al., 2000;

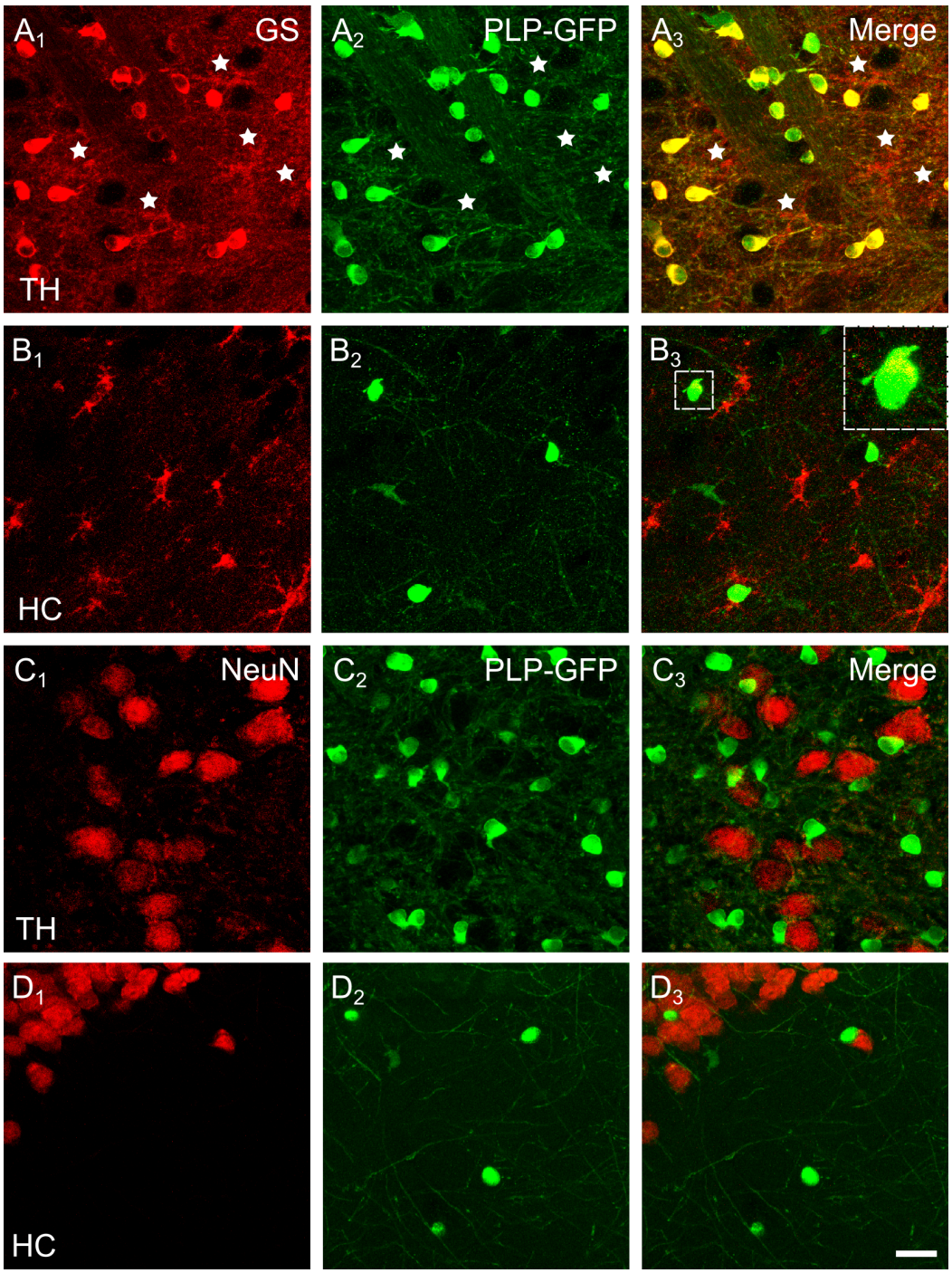

Figure 5.15 Immunohistochemical analysis reveals GS staining, but not NeuN in PLP-GFP cells. (A) Staining with antibodies against GS (A_1) in the thalamus (TH) revealed abundant colocalization with PLP-GFP (A_2)in the merged images (yellow cells in A_3). Few cells were only GS^+ (labelled with a star in A). (B) GS staining in the hippocampus (HC) of the same brain slices displayed the typical star-like morphology of astrocytes (B_1). Rarely colocalization of PLP-GFP (B_2) with GS was observed (inset in B_3). (C, D) Analysis of PLP-GFP expression (C_2, D_2) revealed no colocalization with neuronal nuclei (NeuN; C_1, D_1) in the overlay (C_3, D_3). Scale bar, 20 µm.

Parri and Crunelli, 2002). Interestingly, some of the GFAP$^+$ processes were arranged parallel to myelinated fibre bundles. In contrast, CA1 stratum radiatum GFAP$^+$ cells stretch their main processes perpendicular to stratum pyramidale (Fig. 5.16B$_1$). Microglia in both brain regions had similar morphologies (Fig. 5.16A$_3$,B$_3$) No colocalization of GFAP (Fig. 5.16A$_1$,B$_1$), nor Iba1 (Fig. 5.16A$_3$,B$_3$) with PLP-GFP (Fig. 5.16A$_2$,B$_2$) were observed in the merged images (n = 3 from 3 mice; Fig. 5.16A$_4$,B$_4$) in any of the two brain regions (Fig. 5.17C).
Another astrocyte marker, S100β (Ogata and Kosaka, 2002; Parri et al., 2010), was analysed in conjunction with NG2, a marker for oligodendrocyte precursor cells (Trotter et al., 2010). Images showed that in the thalamus S100β was not restricted to astrocytes, but some of the PLP-GFP cells also expressed this marker (17.5%, indicated with a ∧ in Fig. 5.16C$_{1-4}$). Colocalization of S100β with NG2 was a rare event in the VB (22 ± 31 cells/mm^3), also neither triple labelling (0.014%) nor overlap of PLP-GFP with NG2 (0.2% from 158,844 ± 4,092 GFP$^+$ cells/mm^3, n = 9 slices from 3 mice; Fig. 5.17D) was observed. In the hippocampal CA1 region only a minor fraction of PLP-GFP cells were labelled for S100β (18.1%, indicated with a "∧" in Fig. 5.16D$_{1-4}$). Interestingly, in this region NG2 cells were sometimes PLP-GFP$^+$ (17.9% from a total of 26,447 ± 1,434 GFP$^+$ cells/mm^3, n = 9 slices from 3 mice; indicated with a star in Fig. 5.16D$_{1-4}$). Some S100β$^+$ cells were NG2$^+$ (622 ± 227 cells/mm^3) and furthermore in rare cases triple labelling was detected (1.6%, indicated with an arrowhead in Fig. 5.16D$_{1-4}$). The population of PLP-GFP, S100β and NG2 labelled cells was significantly smaller than the PLP-GFP$^+$ population. Additionally, the cell density of PLP-GFP and S100β co-labelled cells was significantly larger in the thalamus, though ratios were similar (Fig. 5.17D; see also Griemsmann et al., 2014). In this region, a fraction of 25.1 ± 3.1% of S100β$^+$ cells was PLP-GFP$^+$, while in the hippocampus only 5.1 ± 1.9% of the S100β$^+$ cells expressed PLP-GFP.
Finally, we used the astrocyte marker Aldh1L1 which was described as a more global marker in a transcriptome study (Cahoy et al., 2008). Aldh1L1 was abundantly expressed in the thalamus of PLP-GFP mice. Extensive overlap of Aldh1L1 staining and PLP-GFP (52.2% overlap from a total of 65,422 ± 6,242 cells/mm^3; n = 9 slices from 3 mice; Fig. 5.16E$_{1-4}$, Fig 5.17E) was observed. Almost all of these cells also expressed Olig2 (97.2%). Only a minority of Aldh1L1$^+$ and PLP-GFP$^+$ cells lacked the transcription factor Olig2 (444 ± 522 cells/mm^3). The other half of the Aldh1L1 cells lacked PLP-GFP: 22.4% of all Aldh1L1 cells only expressed this marker and 25.3% co-expressed Olig2 (see also Griemsmann et al., 2014). An overlapping expression profile of astrocyte and oligodendrocyte markers was observed earlier in the immunohistochemical study of GJNs (see Section 5.3.1).
In summary, classical astrocyte markers are not expressed by oligodendrocytes in the hippocampus, though S100β is partially expressed in NG2 cells, while in the thalamus most markers are not astrocyte specific. The results indicate S100β as the most reliable astrocyte marker of all analysed proteins in the VB thalamus.

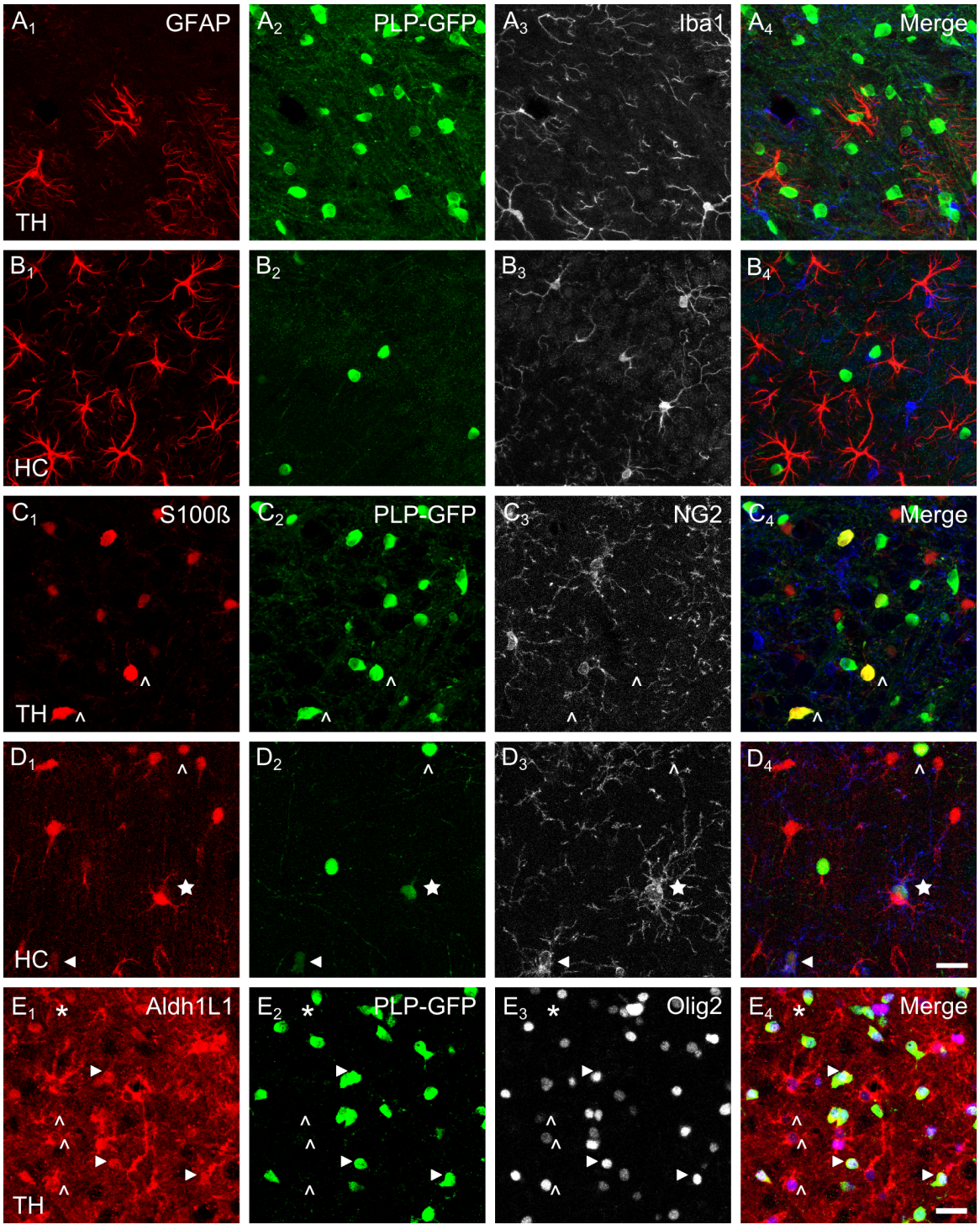
A1 GFAP
A2 PLP-GFP
A3 Iba1
A4 Merge
TH
B1
B2
B3
B4
HC
C1 S100ß
C2 PLP-GFP
C3 NG2
C4 Merge
TH
D1
D2
D3
D4
HC
E1 * Aldh1L1
E2 * PLP-GFP
E3 * Olig2
E4 * Merge
TH

Figure 5.16 ***(previous page)*** **Astrocyte markers are expressed by PLP-GFP cells.** (A, B) Stainings for GFAP (A_1, B_1) and Iba1 (A_3, B_3) revealed no overlap with PLP-GFP (A_2, B_2) in the merged images (A_4, B_4). There are only few GFAP labelled cells in the TH, displaying a distinct morphology from those in the HC. (C, D) Antibodies against S100β (C_1, D_1) were used along with NG2 (C_3, D_3). In some cases colocalization of S100β with PLP-GFP (C_2, D_2) was observed in merged images (yellow cells in C_4, D_4, labelled with ∧). No colocalization of S100β with NG2 or PLP-GFP with NG2 was observed in the TH, while in the HC some cells were triple labelled (arrowhead) or PLP-GFP was co-expressed with NG2 (star). (E) Aldh1L1 antibody staining (E_1) in the TH revealed that almost half of these cells were PLP-GFP$^+$ (E_2) and also Olig2$^+$ (arrowhead, E_3) in the merged images (E_4). Some cells were only Aldh1L1$^+$ (*), and some cells expressed Aldh1L1 and Olig2 (∧), though at variable amounts. Scale bar, 20 μm.

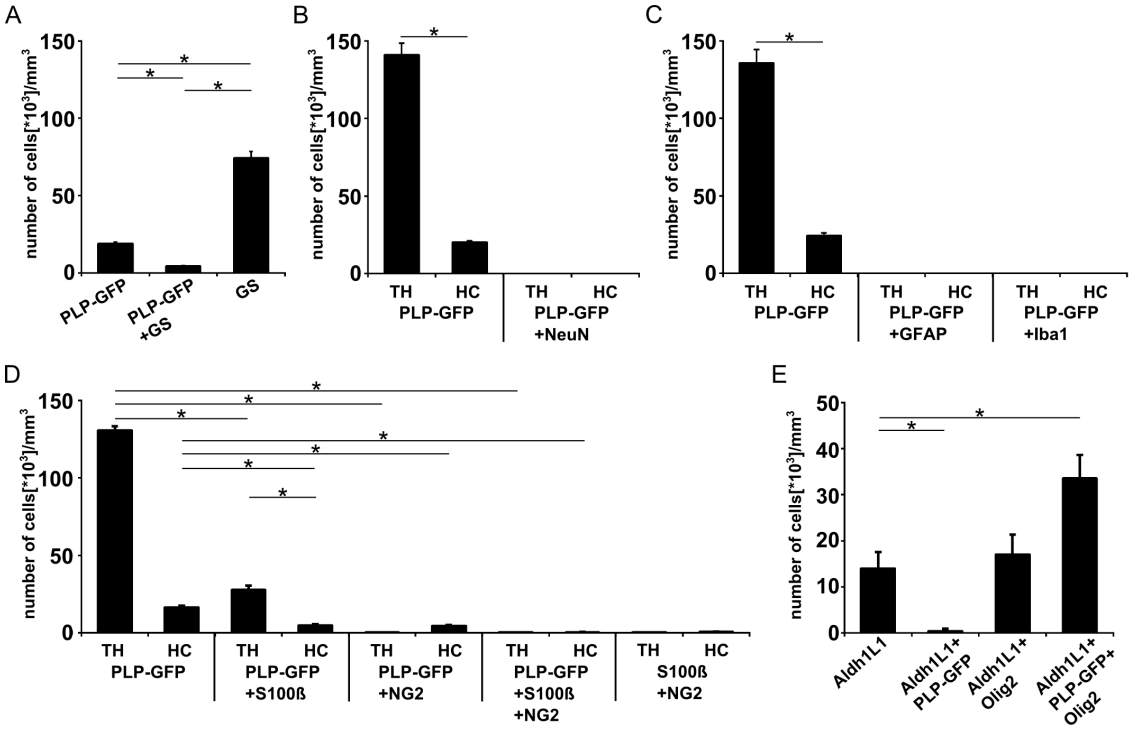

Figure 5.17 Graphs summarizing the immunohistochemical analysis in PLP-GFP mice. (A) Quantification of GS and PLP-GFP in the HC (n = 9 for each region from 3 mice). There are fourfold more GS cells than PLP-GFP cells. (B) PLP-GFP cells were never NeuN$^+$ (n = 3 for each region from 3 mice). There are almost sixfold more oligodendrocytes in TH compared to HC. (C) PLP-GFP never colocalized with GFAP nor Iba1 in both brain regions (n = 3 for each region from 3 mice). (D) Some of the PLP-GFP cells were S100β$^+$ in both TH and HC. Furthermore only in HC a few PLP-GFP cells were also NG2$^+$ and in rare cases triple labelled (n = 9 for each region from 3 mice). (E) Aldh1L1 is a more global astrocyte marker. In the TH four groups of cells were observed. Almost half of the cells were triple labelled for AldhL1, PLP-GFP and Olig2. Almost one fourth was only AldhL1$^+$, one fourth was AldhL1$^+$ and Olig2$^+$ and a minor population was AldhL1$^+$ and PLP-GFP$^+$ (n = 9 from 3 mice). Asterisks indicate statistical significance.

5.4.2 Immunohistochemical identification of thalamic glial cells

The results presented in the previous Section questioned the concept of cell markers in the thalamus as the observed co-expression of astrocyte and oligodendrocyte markers was unexpected. Employing the Cx43-ECFP knock-in mouse, the expression of Olig2 was studied. In these mice the reporter ECFP is expressed under the control of Cx43 regulatory elements (see also Section 3.10). Due to the similarities of ECFP with GFP it can be visualized using GFP antibodies.
Immunostaining of ECFP and Olig2 in the thalamus revealed that about half of the Cx43-ECFP$^+$ cells co-expressed the transcription factor Olig2 (20,267 $\pm$ 2,917 cells/mm^3 from a total of 38,563 $\pm$ 1,723 ECFP$^+$ cells/mm^3; Fig. 5.18A$_{1-3}$, C$_1$).
The total density of ECFP$^+$ cells was slightly higher in the hippocampus than in the thalamus, but in the latter ECFP$^+$ cells mostly lacked Olig2 (3,155 $\pm$ 1,107 ECFP$^+$/Olig2$^+$ cells/mm^3 from a total of 52,217 $\pm$ 3,215 ECFP$^+$ cells/mm^3; Fig. 5.18B). The two populations of ECFP$^+$ cells with or without Olig2 differed significantly in size (Fig. 5.18C$_2$). Furthermore, the cell density of solely ECFP$^+$ cells was significantly higher in the hippocampus, while the population of ECFP$^+$ and Olig2$^+$ cells was significantly increased in the thalamus (see also Griemsmann et al., 2014). All cell densities are listed in table 9.1 in the appendix. Differences in cell densities were analysed by ANOVA and *post-hoc* Tukey, $p<0.05$ (*).
Overlap of astrocyte (Cx43-ECFP, Degen et al., 2012) and oligodendrocyte markers (Olig2, Trotter et al., 2010) in these immunostainings and in PLP-GFP mice indicate the existence of an "intermediate" glial cell-type in the thalamus.
In a next step, the antigen expression profile in biocytin labelled networks in Cx43-ECFP mice was analysed in the thalamus. The "intermediate" glial cell-type was also part of glial networks in the thalamus (see merged image in Fig. 5.19). Tracer injection of a Cx43-ECFP expressing cell and subsequent visualisation confirmed the presence of a small population of ECFP$^+$ and Olig2$^+$ cells in these networks (14% of 58 $\pm$ 6 coupled cells, n =10; see also Griemsmann et al., 2014).
The immunohistochemical study in Cx43-ECFP knock-in mice confirmed the findings in PLP-GFP mice of an overlapping marker profile in the thalamus. Interestingly, the observed "intermediate" glial cells were gap junction coupled, a hallmark of mature cells.

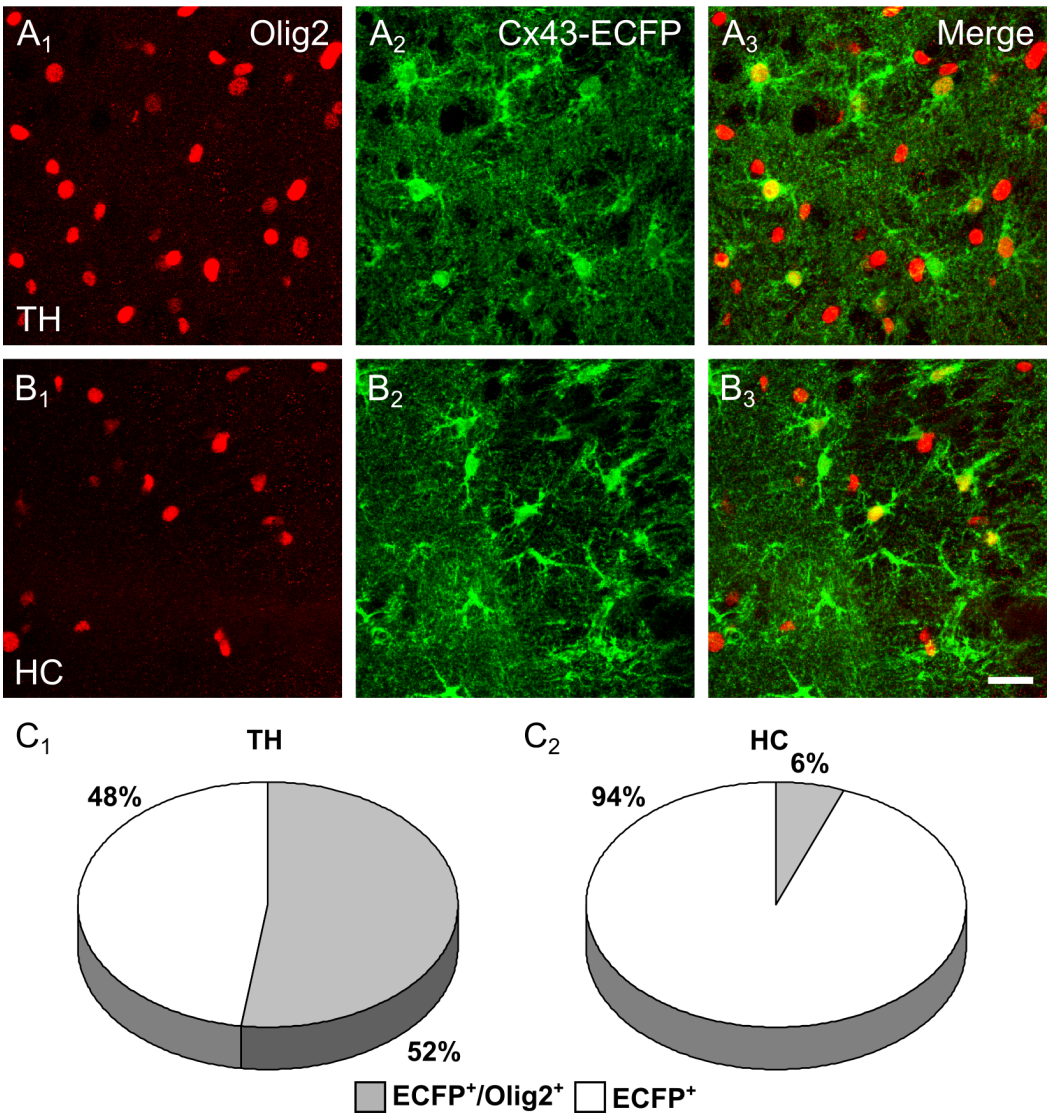

Figure 5.18 Cx43-ECFP cells express Olig2. (A) Immunostaining of Olig2 (A_1) in the thalamus (TH) revealed abundant co-labelling with Cx43-ECFP (A_2). These cells appear yellow in the merged image (A_3). (B) In contrast, in the hippocampus (HC) most $ECFP^+$ cells (B_2) lacked expression of the transcription factor Olig2 (B_1) in the merged image (B_3). (C) Quantification of the cell populations revealed significant differences between brain regions. In the thalamus the two populations were almost equal in size (52.2 ± 6% $ECFP^+/Olig2^+$), while in the hippocampus the population of ECFP cells outnumbered the population of $ECFP^+$ and $Olig2^+$ cells (5.9 ± 1.8% $ECFP^+/Olig2^+$; n = 9 from 3 mice for each region). Scale bar, 20 µm. See also Griemsmann et al., 2014.

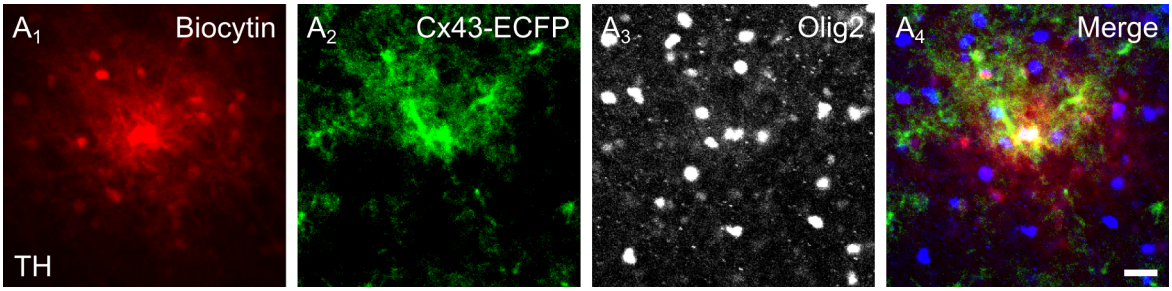

Figure 5.19 Thalamic glial networks include Cx43-ECFP$^+$ and Olig2$^+$ cells. Biocytin-filled networks (A_1) in the thalamus (TH) contained Cx43-ECFP$^+$ (A_2) and Olig2$^+$ cells (A_3), when patching an ECFP$^+$ astrocyte. Furthermore, in the merged image (A_4) triple-labelled cells are visible (white cells, centre). Scale bar, 20 µm. See also Griemsmann et al., 2014.

5.5 Physiological role of panglial networks

The results documented an unexpected heterogeneity of glial cells between brain regions. The well studied astrocytes in the hippocampus displayed known properties, while in the thalamus glial cells differ in their network properties and their marker expression. Here, an undocumented "intermediate" cell-type was observed. The observation of an extensive panglial network in the thalamus using the tracer biocytin was of special interest, but the functional role of this network remained elusive.

5.5.1 Metabolite diffusion in panglial networks

The tracer biocytin diffused into the panglial network irrespective of the patched cell-type and diffused along a concentration gradient into neighbouring cells. Recently, it was observed that oligodendrocytes support axonal function by transport of metabolites and therefore sustain neuronal activity (Fünfschilling et al., 2012; Lee et al., 2012). Physiologically active molecules likely diffuse to sites of local demand.
Since oligodendrocytes do not have a direct contact to blood vessels, the panglial network is a possible route of transport for energy metabolites from blood vessels to oligodendrocytes. In the hippocampus, glucose diffusion has been observed in the astroglial network (Rouach et al., 2008). Possible diffusion of glucose in thalamic panglial network was analysed in the following experiment.
For visualization of glucose diffusion, the fluorescent glucose analogue 2-NBDG (2-(N-(7-Nitrobenz-2-oxa-1,3-diazol-4-yl)Amino)-2-Deoxyglucose) was applied. Taking advantage of a confocal LSM equipped with an infrared laser, it was possible to image SR101$^+$ cells (excitation/absorption maxima ∼586/605 nm) and PLP-GFP$^+$ oligodendrocytes (excitation/absorption maxima ∼488/509 nm) with continuous wave lasers and isolate the fluorescence of the 2-NBDG (excitation/absorption maxima of ∼465/540 nm) employing a pulsed 2P laser. 2-NBDG was acquired with NDDs, while SR101 and PLP-GFP images were acquired with PMTs.

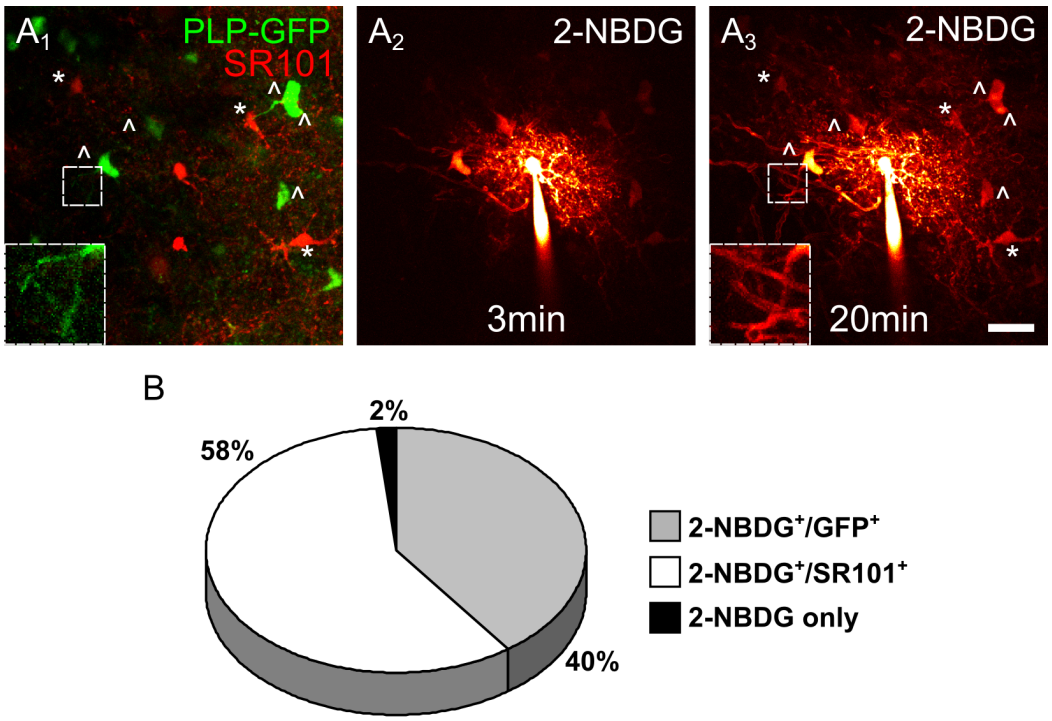

Figure 5.20 Metabolite transport in thalamic panglial networks. (A) Employing the green fluorescent glucose analogue 2-NBDG, it was possible to visualize glucose transport from an $SR101^+$ astrocyte (red, centre) to $PLP\text{-}GFP^+$ oligodendrocytes (green, labelled with a ∧) in the thalamus (A_1). Already after 3 min 2-NBDG diffusion into neighbouring cells was visible (A_2). After 20 min 2-NBDG diffused into neighbouring astrocytes (*) and oligodendrocytes (∧). Furthermore, 2-NBDG diffused into myelinating processes of oligodendrocytes (see insets in A_1, A_3, showing a higher magnification of boxed areas). Scale bar, 20 µm. (B) The 2-NBDG-filled network comprised of 40 ± 9.4% $PLP\text{-}GFP^+$ cells, 58.4 ± 9.5% $SR101^+$ cells and 1.6 ± 1% only $2\text{-}NBDG^+$ cells (n = 6).

Before starting glucose filling a z-stack of the SR101 and PLP-GFP cells (Fig. 5.20A_1) was acquired and after 3 min (Fig. 5.20A_2) and 20 min (Fig. 5.20A_3) z-stacks of 2-NBDG fluorescence were imaged. Already after 3 min glucose diffused into an average of 14 ± 0.7 cells (n = 6; Fig. 5.20A_2). The 2-NBDG further spread into the network and after 20 min 36 ± 5 cells were filled (n = 6; Fig. 5.20A_3). The networks were smaller than those visualized with biocytin (see Section 5.1) which might be due to the difference in size of the molecules. Additionally, the tracer diffused into the processes of oligodendrocytes and into the myelin sheath (see insets in Fig. 5.20A_1, A_3).
Employing the images taken before tracer diffusion and the 2-NBDG images after 20 min, the panglial diffusion was assessed (Fig. 5.20A). The networks contained 58.4 ± 9.5% $SR101^+$ astrocytes, 40 ± 9.4% $PLP\text{-}GFP^+$ oligodendrocytes and 1.6 ± 1% only $2\text{-}NBDG^+$ cells (n = 6; Fig. 5.20B).
The experiments with the glucose-derived tracer 2-NBDG confirmed diffusion of metabolites through the panglial network and moreover into the myelin sheath. The panglial network might therefore be important for nutrient supply to neuronal axons.

5.5.2 Cortico-thalamic pathway stimulation

The extensive panglial network in the thalamus might be crucial in sustaining neuronal activity. A protocol for field potential recordings in the VB on nearly horizontal slices was established. In the following experiments field potentials of neuronal activity were recorded as it allows for monitoring the activity of entire neuronal populations.
The ventrobasal thalamus has two inputs. One is the lemniscal pathway which sends the sensory information from the whiskers to the VB. The information is then propagated towards the cortex via the thalamo-cortical pathway and there is a feedback circuit to the VB, the cortico-thalamic (CT) pathway (Parri et al., 2010; Pinault, 2011; Grant et al., 2012). For further experiments the CT pathway was stimulated and a protocol for stimulation on horizontal slices was established.
Stimulation of the CT pathway was achieved on horizontal slices with a 30° angle to the horizontal plane (Fig. 4.2A). The recording electrode was placed in the VB and the bipolar stimulation electrode was located in the internal capsule to stimulate CT afferents. The stimulation protocol consisted of train stimuli of 5 pulses at 20 Hz which were repeated every 15 s. To obtain stable responses for almost 2 h the stimulation intensity was set to 80% of the maximally elicited peak amplitude.
The recorded field potentials in the VB displayed two peaks with increasing amplitude over 5 pulses (Fig. 5.21A). After the first pulse only one peak was observed directly after the stimulus (indicated by arrows in Fig. 5.21). The second response displayed a first larger and a small second peak, for the following stimuli the second peak increased in amplitude (Fig. 5.21A). The trace shown in Figure 5.21B is a blow up of the field potentials for the third and fourth stimulus shown in A. The first negative peak appeared very fast directly after the stimulus (arrow). Between the two peaks the field potential did not reach baseline levels again, but instead a positive potential was observed during which a second negative peak appeared. Only afterwards the signal reached baseline levels again.
The field potentials were recorded in the presence of picrotoxin to block GABAergic inhibitory innervation of the VB from the RTN (see Section 1.1.1; Pinault, 2011). In some cases weak epileptiform activity was observed, as can be seen after the second stimulus in Figure 5.21A. In case epileptiform activity interfered with the stimulation responses, the experiments were excluded from further analysis.
The stimulation parameters of the recorded field potentials were designed to avoid metaplasticity. The train stimulation proved to be a reliable tool to record neuronal activity in the VB thalamus.
The field potentials were further characterized by applying blockers to inhibit neuronal excitation. Therefore the CT pathway was stimulated and fEPSPs recorded in normal ACSF for 20 min. Afterwards D-AP5 and NBQX were applied to block NMDA and AMPA receptors (Fig. 5.22A). Blockers were applied for 20 min and the field potential was continuously recorded. At the end of the experiment the voltage-gated Na^+ channel blocker TTX was applied. The application of D-AP5 and NBQX led to loss of the

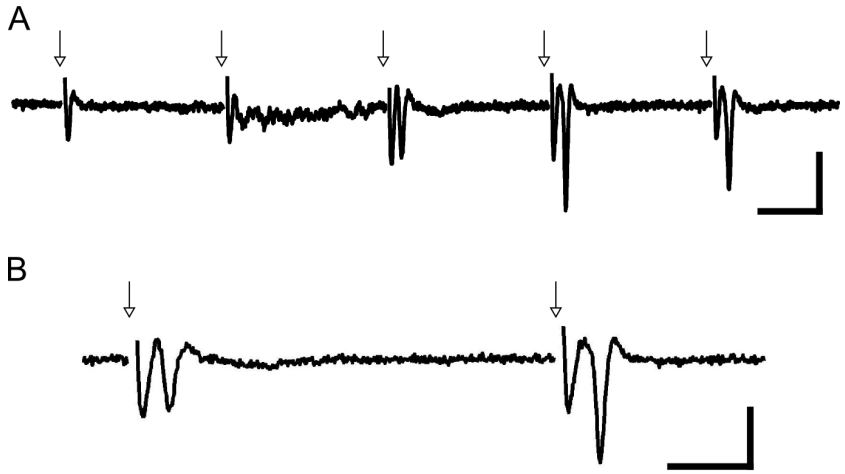

Figure 5.21 Field potentials in the ventrobasal thalamus. (A) The CT pathway was stimulated in the internal capsule and the neuronal activity was recorded in the VPL and VPM nuclei. Stimulation trains of 5 pulses at 20 Hz (indicated with arrows) were applied and repeated every 15 s. Traces show averages of 10 recordings. Field potentials in the VB displayed increasing responses over 5 stimuli. The first peak slightly increased in amplitude during the train, while the second peak only appeared after the second stimulus and then increased in amplitude. Scale bar, 20 ms, 0.5 mV. (B) Blow up of the third and fourth response shown in A. Scale bar, 10 ms, 0.5 mV.

second peak of the field potential, while the first peak was still present. The remaining amplitude is therefore induced by presynaptic neuronal excitation. Application of TTX completely blocked action potentials and led to loss of both pre- and postsynaptic responses. The residual signals were stimulation artefacts (Fig. 5.22A).
Field potentials were analysed using a custom written Igor tool (by Ronald Jabs). Figures 5.22B_1 and B_2 illustrate the field potential analysis for the third pulse. In Figure 5.22B_1 the raw data of one response are displayed, a recording in ACSF (black), after blocker application (blue) and after TTX application (red). The overlay nicely shows the loss of the second peak after D-AP5 and NBQX application and the complete loss of both peaks after TTX application. In Figure 5.22B_2 two methods to compensate for the artefact are displayed. The blue trace displays the resulting field potential after subtraction of the D-AP5 and NBQX recording from the ACSF recording. The red trace indicates the subtraction of the TTX recording. In the following analysis, the artefact was eliminated by subtraction of the TTX recording.
Quantification of the field potentials revealed fast changes in fEPSPs upon blocker application. Data were normalized to the average amplitudes and delay in ACSF (t_{-20min}−t_{0min}). Analysing the amplitude of the postsynaptic peak a slight increase in normalized amplitude was observed during the first 20 min of recording to 127.1 ± 5.2%. Shortly after bath application of the blockers the amplitude decreased, 4 min after incubation the amplitude size dropped to 53.9 ± 6.3% and further diminished to 14.9 ± 2% at 6.5 min. After 14 min the second peak completely disappeared (n = 4; Fig. 5.22C_1).

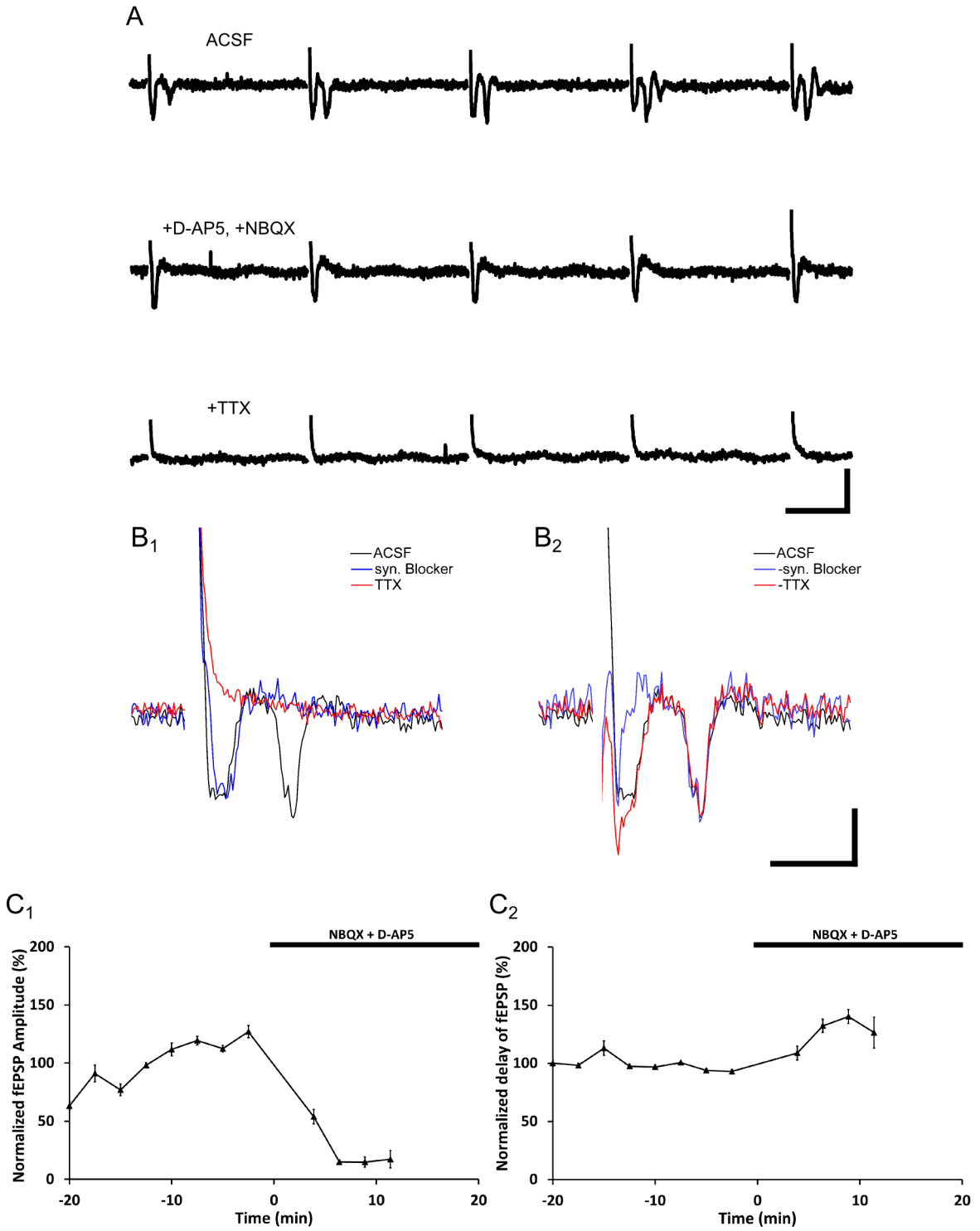
A
ACSF
+D-AP5, +NBQX
+TTX
B1
ACSF
syn. Blocker
TTX
B2
ACSF
-syn. Blocker
-TTX
C1
NBQX + D-AP5
Normalized fEPSP Amplitude (%)
200
150
100
50
0
-20
-10
0
10
20
Time (min)
C2
NBQX + D-AP5
Normalized delay of fEPSP (%)
200
150
100
50
0
-20
-10
0
10
20
Time (min)

Figure 5.22 ***(previous page)*** **Properties of field potentials in the ventrobasal thalamus.** (A) fEPSPs were sensitive to blocker application. The upper trace is a recording in ACSF supplemented with picrotoxin. The middle trace was recorded after bath application of D-AP5 and NBQX which inhibit synaptic transmission. The lower trace shows a recording after TTX application which blocks action potentials. The residual signals are stimulation artefacts. Scale bar, 20 ms, 0.2 mV. (B) Signals before and after analysis with the Igor tool are shown. In B_1 the raw data for one stimulus are displayed, an ACSF recording (black), a response after D-AP5 and NBQX application (blue) and a recording in the presence of TTX (red). In B_2 the ACSF recording was separated by subtracting recordings in the presence of blockers, to either isolate the fEPSP (blue), or the pre- and postsynaptic responses (red). Scale bar, 5 ms, 0.1 mV. (C_1) The normalized fEPSP amplitudes during ACSF recordings ($t_{-20min}-t_{0min}$) and during D-AP5 and NBQX application ($t_{0min}-t_{20min}$) are displayed. The fEPSP amplitude slightly increased during the first 20 min and rapidly decreased after blocker application (n = 4). (C_2) The normalized delay of the postsynaptic potential was constant prior to blocker application and afterwards the delay increased (n = 4). After 14 min fEPSPs completely disappeared. Traces show averages of 10 recordings.

In addition to the amplitude the time interval from the stimulus to the amplitude peak of the postsynaptic response was measured, termed the delay of the fEPSP. The normalized data show a constant delay of the fEPSP. At the end of recording in normal ACSF the normalized delay amounted to 93 ± 1.4% of the average delay in ACSF. After 4 min blocker application the delay was constant at 109 ± 6%, afterwards the delay increased to 132.4 ± 5.6% after 6.5 min. After 14 min the fEPSP was completely abolished (n = 4; Fig. 5.22C_2). Changes in fEPSP amplitude and delay were analysed by ANOVA and *post-hoc* Tukey, $p<0.05$ (*).
In summary, field potentials on nearly horizontal slices in the VB consist of pre- and postsynaptic responses as identified by blocker application. The newly established method is a reliable tool to monitor neuronal activity in the VB.

5.5.3 Impact of glucose deprivation on neuronal activity

The experiments so far demonstrated extensive panglial networks in the thalamus and a potential role in metabolite supply to neurons.
Neuronal activity is sensitive to extracellular glucose deprivation (GD) and has been extensively studied in optic nerve and hippocampus (Wender et al., 2000; Brown et al., 2001; An et al., 2008; Rouach et al., 2008). In the following experiments a method to monitor neuronal glucose sensitivity in the thalamus in acute horizontal slices was established. Therefore, experiments were conducted in the VB to analyse the effects of long-time GD. At the beginning a recording in ACSF with picrotoxin was recorded for 10 min and subsequently glucose-free ACSF with picrotoxin was applied for 1 h. Afterwards, field potentials were recorded during 20 min re-perfusion with ACSF, see also timeline in Figure 4.2D. Additionally, control experiments in ACSF with picrotoxin over the same time period were performed on slices from the same animals. Three GD and three control experiments were recorded in n = 3 animals.

At the beginning, the fEPSP was recorded in ACSF and displayed the typical two peaks in response to the stimulus. Already 20 min after the start of GD the postsynaptic amplitude decreased. After 62 min the postsynaptic response was almost abolished (Fig. 5.23A).
Data were normalized to the mean amplitude and delay in ACSF (t_{-10min}−t_{0min}). At the end of recordings in ACSF the normalized fEPSP amplitude was at 92.7 ± 4.3% ($t_{-2.5min}$) of the mean signal over 20 min in ACSF. After 21 min of GD the amplitude decreased to 50.3 ± 16%, further decreased until the end of GD to 11 ± 2.2% (t_{62min}), and did not recover during re-perfusion with glucose (t_{78min}, 17.1 ± 0.4%,n = 3; ANOVA and *post-hoc* Tukey, p<0.05 (*); Fig. 5.23B_1). On the other hand the neuronal activity is not completely abolished, most likely there is some glucose storage in cells. Control experiments on another slice from the same animal over 90 min in ACSF displayed constant amplitude sizes ($t_{-2.5min}$, 108.2 ± 1.2; t_{21min}, 110.6 ± 7.9; and t_{62min}, 110.3 ± 9%; n = 3 controls; ANOVA; Fig. 5.23B_1). The fEPSP amplitudes were similar during recordings in ACSF at the beginning of the experiments. After 16 min of GD the amplitude was significantly smaller compared to control fEPSPs in ACSF (ANOVA and *post-hoc* Tukey,, p<0.05 (*); Fig. 5.23B_1).
The delay of the postsynaptic peak varied during GD, but did not differ from prior recordings in ACSF ($t_{-2.5min}$, 101 ± 0.4%; t_{62min}, 148.8 ± 9.5%; ANOVA). The delay of the postsynaptic potential did also not recover during re-perfusion (t_{78min}, 119.3 ± 8.5%; ANOVA; Fig. 5.23B_1). In control experiments on another slice from the same animal the normalized delay was stable during the entire recording time in ACSF ($t_{-2.5min}$, 100.6 ± 0.3%; t_{62min}, 97 ± 0.9%; t_{78min}, 97.6 ± 1%; n = 3 each; ANOVA; Fig. 5.23B_2). The delay in GD and control recordings was equal at the beginning of the recording in ACSF. After 18 min the delay was increased compared to the delay in control recordings and remained high. Some time points were not significantly different from control recordings, due to the higher variability of the delay during GD (ANOVA and *post-hoc* Tukey, p<0.05 (*); Fig. 5.23B_2).
In conclusion, thalamic neurons are sensitive to GD. The amplitude of fEPSPs decreased to 50% after 21 min, while the delay was unchanged. Recordings in ACSF over 90 min were stable and differed both in amplitude and delay from recordings in glucose-free ACSF.

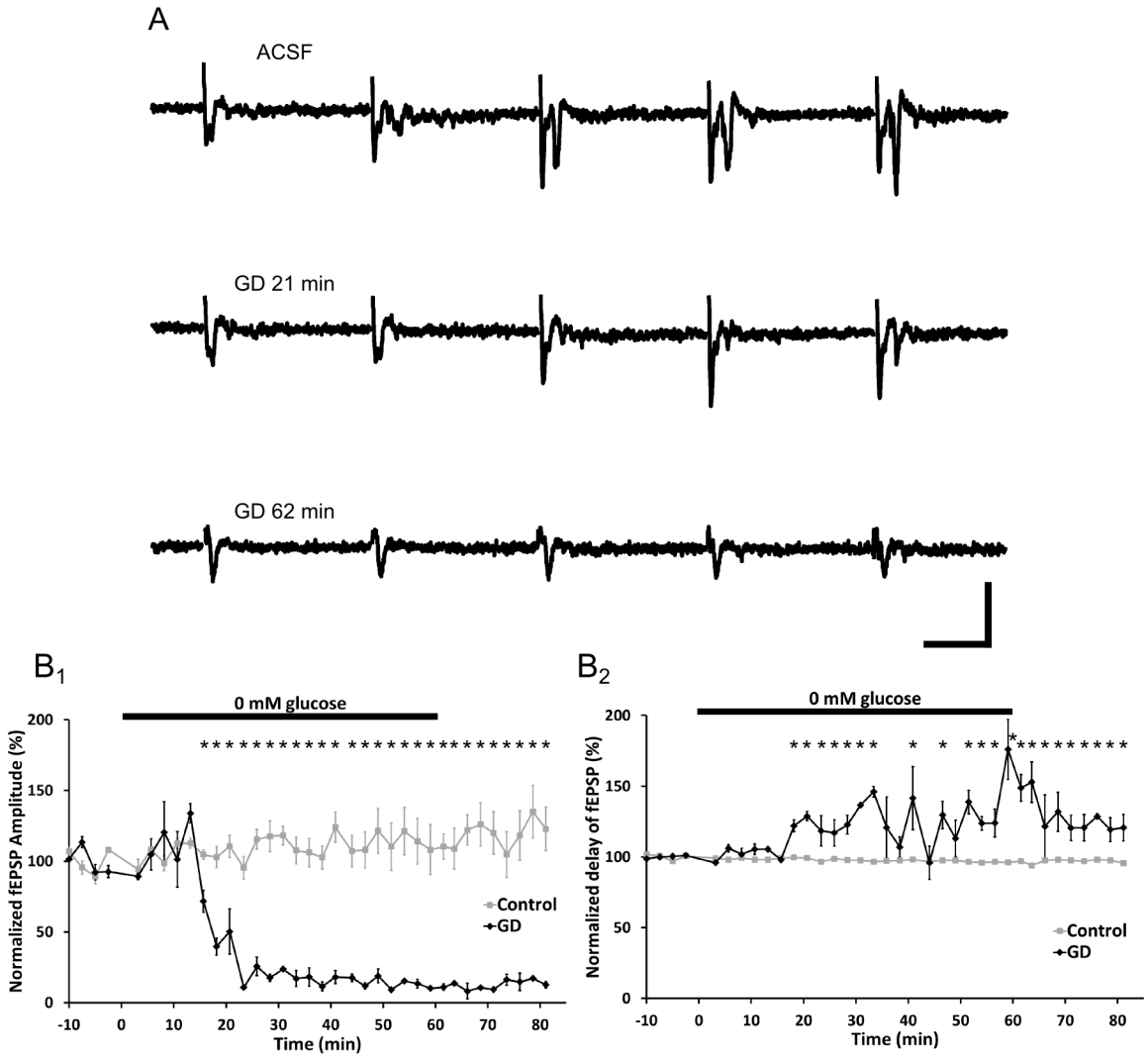

Figure 5.23 Impact of glucose deprivation on thalamic fEPSPs. (A) GD led to changes in fEPSPs. The upper trace is a recording in ACSF supplemented with picrotoxin. The middle trace was recorded 21 min after GD. After 62 min only presynaptic responses were observed (lower trace). Scale bar, 20 ms, 0.4 mV. (B_1) Normalized fEPSP amplitudes were sensitive to GD. After 10 min recording in ACSF, 60 min GD was performed. Subsequently, 20 min in normal ACSF were recorded, but no recovery was observed. In contrast, recordings in normal ACSF over 90 min showed no changes in amplitude (n = 3 each). (B_2) Additionally to the decreased amplitude the neuronal postsynaptic response appeared later after the stimulus. In control slices in normal ACSF the delay was constant over 90 min (n = 3 each). Traces show averages of 10 recordings. Asterisks indicate statistical significance of differences between GD and control experiments.

5.6 Molecular analysis of ionotropic receptor expression in thalamic astrocytes

Astrocytes express several other channels and receptors on their cell surface in addition to connexins. In this study, we focused on AMPA and $GABA_A$ receptors and investigated the subunit expression pattern in VB astrocytes. The cells were identified by their bright GFAP-EGFP fluorescence, a passive current pattern and typical negative resting membrane potentials. Subsequently, the cytoplasm was harvested for further RT-PCR analysis performed by Gerald Seifert.

5.6.1 Astrocytic AMPA receptor subunit expression

The RNA of harvested cells was used for reverse transcription and subsequent multiplex PCR for different AMPA receptor subunits. The typical astrocytic current pattern and the PCR result for a cell are shown in Fig. 5.24A, B. S100β was used as an astrocytic marker. A total of 23 cells expressed AMPA receptors in this study, 4 cells expressed the GluA1 subunit (17%), 22 cells expressed GluA2 (96%), 10 cells expressed GluA3 (43%) and only 8 cells expressed the GluA4 subunit (35%; Fig. 5.24C). Additionally, 5 cells did not contain AMPA receptor subunit specific mRNAs, but expressed S100β.
All AMPA receptor subunits have different splice isoforms, termed flip and flop. The second PCR of the two-round multiplex PCR was repeated and the cDNA used for a restriction enzyme digest. Characteristic splice fragments were obtained and separated by gel electrophoresis. The flip GluA1 subunit was only observed in 1 of 4 cells, the other 3 cells contained the flop splice variant. Most astrocytes expressed both splice variants of GluA2 (flip, 18 of 22 cells; flop, 17 of 22 cells). The GluA3 splice variants were also often both present in the cells, all cells contained the flop variant (flip, 5 of 10 cells; flop, 10 of 10 cells). Both splice variants of GluA4 were found in most cells (flip, 6 of 8 cells; flop 6 of 8 cells; Fig. 5.24D).
In summary, single-cell RT-PCR revealed two astrocyte populations lacking or expressing AMPA receptors. The latter group abundantly expressed the AMPA receptor GluA2 subunit.

5.6.2 Astrocytic $GABA_A$ receptor subunit expression

In the second part of the molecular analysis the $GABA_A$ receptors were analysed. The RT-PCR study on harvested cells focused on the subunit composition of the receptors. There are different subunit isoforms which can be further differentiated, e.g. five different α-$GABA_A$ receptor subunits (Fig. 5.25A). In Figure $5.25A_{1,2}$ one exemplary cell is shown. It displayed a passive current pattern and expressed four of the five α subunits. As for the AMPA receptor study S100β was used as a cell-type marker. A total of 18 cells was analysed and 33% expressed the subunit α1 (6 of 18 cells), 50% expressed the

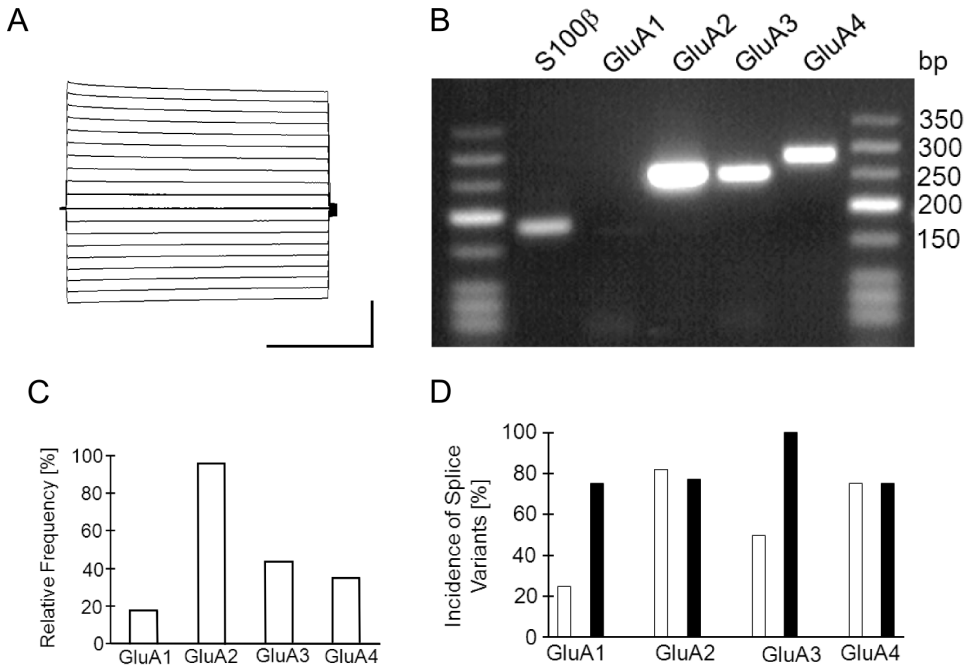

Figure 5.24 Single cell RT-PCR reveals AMPA receptor subunit expression in thalamic astrocytes. (A) Typical passive astrocyte current pattern of a harvested cell. Scale bar, 20 ms, 5 nA. (B) Reverse transcription and subsequent multiplex PCR for different AMPA receptor subunits. The exemplary cell expressed the subunits GluA2, GluA3 and GluA4, but lacked GluA1. Additionally, the astrocyte specific S100β was expressed and used as a control. (C) Summary of the data of the RT-PCR, almost 20% of the cells expressed GluA1, almost all cells expressed GluA2, the GluA3 subunit was expressed by 40% and GluA4 was found in 30% of the cells. (D) The subunits exist as splice variants flip and flop, therefore the PCR product of the second PCR round was digested. Except for GluA1, cells mostly contained both splice variants. White bars indicate flip variants and black bars indicate flop variants.

α2 subunit (9 of 18 cells) and no cell expressed the α3 subunit. The $GABA_A$ α4 subunit was expressed in 39% of the cells (7 of 18 cells) and the α5 subunit was detected in 56% (10 of 18 cells; Fig. 5.25A_3).
Furthermore, the RT-PCR study revealed expression of β1 in 86% of the cells (6 of 7 cells) and β2/3 in 43% (3 of 7 cells; Fig. 5.25B). The $GABA_A$ δ subunit was less expressed in astrocytes (14%, 1 of 7 cells; Fig. 5.25B).
A total of 9 cells were used for γ subunit expression. All of the cells expressed the γ1 subunit(100%, 9 of 9 cells), γ2 was rarely expressed (11%, 1 of 9 cells) and the γ3 subunit was abundantly expressed in 89% of the cells (8 of 9 cells).
In conclusion, all VB astrocytes expressed $GABA_A$ receptors and abundantly expressed the γ1 subunit and lacked the α3 subunit.

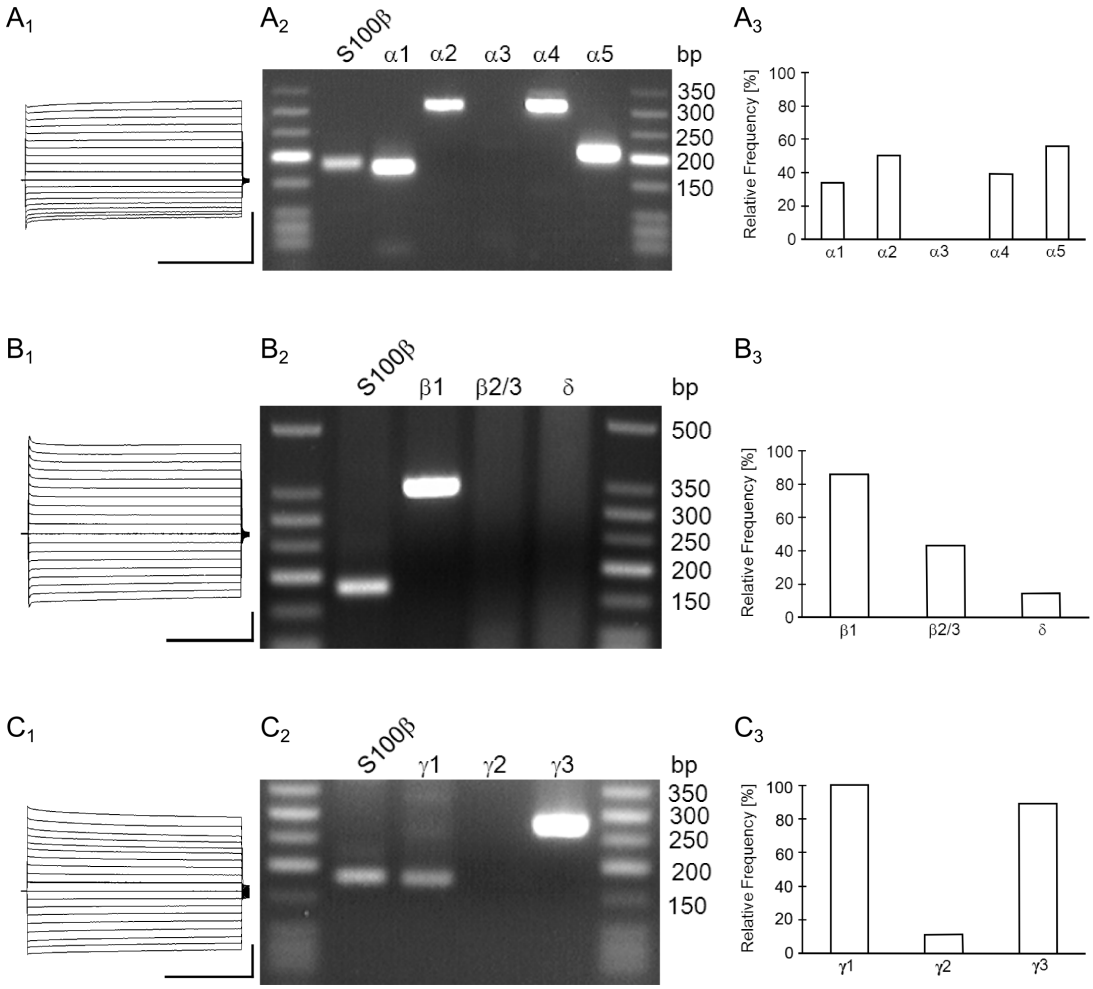

Figure 5.25 Thalamic astrocytes express different $GABA_A$ receptor subunits as revealed by single cell RT-PCR. (A) α subunit expression in astrocytes. (A_1) Typical passive astrocyte current pattern of a harvested cell. Scale bar, 20 ms, 2 nA. (A_2) The astrocyte shown in A_1 expressed all α subunits, except for α3. S100β served as a control for astrocyte specific expression. (A_3) Summary of the data of the RT-PCR. Almost 33% of the cells expressed α1, 50% expressed α2, no cell expressed α3. The subunit α4 was expressed by 39% of the analysed cells and α5 was found in 56% of the cells (n= 18 cells). (B) $GABA_A$ receptor subunit β and δ expression in astrocytes. (B_1) Current pattern of an astrocyte. Scale bar, 20 ms, 2 nA. (B_2) The passive cell was an S100β^+ astrocyte expressing the subunit β1, but lacked the other isoforms. (B_3) In summary, 86% of the analysed cells expressed the β1 isoform, 43% expressed β2/3 subunit and only 14% expressed the δ subunit (n = 7). (C) $GABA_A$ receptor subunit γ expression in astrocytes. (C_1) Typical passive astrocyte current pattern. Scale bar, 20 ms, 5 nA. (C_2) The S100β positive cell expressed the subunits γ1 and γ3. (C_3) Quantification of single-cell RT-PCRs of 9 cells showed expression of γ1 in all cells, γ2 was only present in 11% and γ3 in 89% of the cells.

6 Discussion

Glial cells were seen as the passive glue, "Nervenkitt", between neurons for a long time (Virchow, 1846). Today we know that these cells fulfil a variety of functions in the brain. The present study aimed at characterizing glial cells in a subcortical brain structure, the thalamus, often referred to as the "gate to consciousness". The ventrobasal thalamus receives somatosensory input and relays information to the cortex. It consists of grey matter and myelinated fibres extending to and arriving from the cortex and brain stem. Glial cells are active partners in neuronal signalling and were analysed in this study for their protein and ionotropic receptor expression profile and network properties. Furthermore, a method to analyse neuron-glia interactions on a network level was established in this study. The results of the present study revealed heterogeneous expression profiles and properties within and between brain regions, enhancing our understanding of glial heterogeneity.

6.1 Properties of glial networks in the VB

Astrocytes were widely studied in the hippocampus and cortex, but little is known about thalamic glial cells. In a previous study by Parri et al. (2001) astrocytes lacked gap junction coupling. This surprising observation initialised a first set of experiments to study glial networks in the VB. In adult mice biocytin-filled networks revealed large GJN with a round shape as observed in the hippocampus (Fig. 5.1A_2; Wallraff et al., 2004). Furthermore, network sizes were similar to hippocampal networks (Section 5.3.1). GJNs close to myelinated fibres often displayed tracer spread into the myelin sheath with the GJs responsible for this tracer spread being unknown (Fig. 5.1B_2). This aspect will be further discussed in the following Section.
For network analysis astrocytes were identified by their bright fluorescence in transgenic hGFAP-EGFP mice (Nolte et al., 2001; Matthias et al., 2003), or labelled with the fluorescent dye SR101. This marker is specifically taken up by astrocytes in acute slices and *in vivo* (Nimmerjahn et al., 2004; Kafitz et al., 2008). It is taken up by the thyroid hormone transporter, an organic anion transporter protein (OATP1C1), expressed in astrocytes in several brain regions like cortex and hippocampus, but not in the ventrolateral medulla (Schnell et al., 2012; Schnell et al., 2013). This expression profile reveals a heterogeneous astrocyte population in the brain. A study performed earlier in the lab confirmed the specific uptake of SR101 by thalamic astrocytes, but not oligodendrocytes which is in contrast to findings in the cortex (Wasseff and Scherer, 2011;

Griemsmann et al., 2014). Recently, an *in vivo* study by Hill and Grutzendler (2014) reported SR101 uptake by oligodendrocytes, but this study employed 200x more SR101 than applied by Nimmerjahn et al. (2004) and 50-100x more SR101 than Kafitz et al. (2008), Schnell et al. (2012) and Griemsmann et al. (2014). This high concentration of SR101 might have caused non-specific oligodendrocyte staining. In the cortex a time dependent diffusion of SR101 through panglial GJCs was described (Wasseff and Scherer, 2011). Another study revealed an impact of SR101 on neuronal activity (Kang et al., 2010). In the present study, a potential influence of the marker SR101 on astrocytic networks was analysed in SR101 incubated slices vs. control slices. Tracer diffusion revealed no impact of SR101 on GJ mediated tracer transfer, and is therefore a reliable astrocyte marker in this brain region (Fig. 5.1D).
The tracer biocytin was employed as it was shown to diffuse furthest into the network compared to other dyes like Sulforhodamine B or Lucifer yellow (Rouach et al., 2008). *In vitro* studies confirmed reliable diffusion of a structurally similar molecule, neurobiotin, through astrocytic GJCs (Yum et al., 2007). Thus, the absence of coupling in the thalamus in a previous study by Parri et al. (2001) is likely due to distinct properties of the channel pore resulting in a selective permeability for tracers regarding size, structure and charge. Likewise, the tracer Lucifer yellow employed by Parri et al. (2001) does not diffuse through Cx30 channels (Yum et al., 2007). Selective permeability was observed for both Cx30 and Cx43 channels, while Cx26 seems to form non-selective channels (Elfgang et al., 1995; Yum et al., 2007).
Glial networks in the VB were analysed during development and further experiments were performed in adult mice between p30-60. Astrocytic networks were already present at p9-11 and increased in size until the end of the second postnatal week (Fig. 5.1C). All astrocytes showed GJ mediated tracer diffusion. In comparison, hippocampal networks were found already shortly after birth and reached their maximum size at the end of the second postnatal week, though the frequency of coupling was highly variable in rat brain (Schools et al., 2006). In the cortex a similar timeline was described at p5 small networks were observed which increased until the age of p10 in the mouse brain (Houades et al., 2008).
In conclusion, thalamic astrocytes form glial networks in contrast to previous observations by Parri et al. (2001). The frequency of coupling is higher in the thalamus compared to hippocampus during postnatal development. The maximum network size is established later in the thalamus compared to the cortex.

6.2 The role of connexins in astroglial networks

6.2.1 Cx30 is the main gap junction protein in thalamic astrocytes

The time course of network formation likely reflects the high impact of Cx30 observed in thalamic networks (Fig. 5.2A_{1-3}, B_{1-2}) and its late upregulation in the second postnatal week (Kunzelmann et al., 1999). In the thalamus loss of Cx30 resulted in dramatically reduced networks compared to wild-type littermates (Fig. 5.2B_1). In the hippocampus the Cx30 knock-out had a weaker impact between 22% and 50% (Gosejacob et al., 2011; Pannasch et al., 2014). In the olfactory glomeruli Cx43 was more important than Cx30 for network sizes (Roux et al., 2011). Cx43 expression starts already during embryonal development and remains high after birth (Dermietzel et al., 1989). Brain regions mainly expressing Cx43 might therefore establish large glial network earlier than brain regions expressing mainly Cx30, although not all cells are part of a network at early developmental stages. The impact of Cx30 and Cx43 on network formation is region dependent and reflects the heterogeneous properties of these cells in the brain. The VB contains a somatotopic map of the whisker field. Mice use their whiskers for exploration of new territories (Erzurumlu et al., 2010). These signals arrive in the VB before they are relayed to the somatosensory cortex. Interestingly, Cx30 levels increased in animals exposed to enriched environment (Rampon et al., 2000). This is in line with the high impact of Cx30 in the thalamus (Fig. 5.2A_{1-3}, B_{1-2}). As reported for hippocampal networks (Wallraff et al., 2006), the Cx30/43 DKOs mostly lacked GJC in the thalamus (Fig. 5.2C_{1-2}, D). Residual coupling is likely mediated by cells devoid of hGFAP-Cre activity as GFAP is only weakly expressed in the thalamus (Frassoni et al., 2000; Wallraff et al., 2006; Requardt et al., 2009; Pannasch et al., 2011).
Likewise, these small networks might be mediated by another connexin, Cx26, which is also expressed by astrocytes and was reported to be abundantly present in thalamic nuclei (Nagy et al., 2011). On the other hand, it was reported that the Cx30LacZ mouse line additionally lacks Cx26, probably due to the Cx30 knock-out strategy and the close proximity of the two loci on one chromosome (Lynn et al., 2011). Concluding, the 30/43 DKO mice additionally lack Cx26 expression. Employing the mouse line Cx26fl:Nestin-Cre used by Nagy et al. (2011), biocytin diffusion did not reveal any functional impact of Cx26 on intercellular coupling in thalamus nor hippocampus in the present study (Fig. 5.4). Therefore Cx30 and Cx43 are the main GJ proteins in astrocytes required for network formation in the hippocampus and thalamus, although with a different impact. The role of Cx26 expression in the thalamus remains elusive. Nagy et al. (2011) reported an immunohistochemical colocalization of Cx26 with Cx43 and Cx47. This is in contrast to the findings of the present study. The immunohistochemically identified channels seem to be non-functional as loss of Cx26 did not influence network sizes (Fig. 5.4C). Similarly, *in vitro* studies found no functional channels between Cx26 and Cx43, nor Cx26 and Cx47 (Elfgang et al., 1995; Magnotti et al., 2011b). Cx26 might be located at autologous GJs between processes of one cell. Another explanation

might be that potential intercellular GJ between different cells were replaced by Cx30 and Cx43 in Cx26$^{fl/fl}$:Nestin-Cre mice in the present study. Cx26 formed functional channels with Cx26, Cx30 and Cx32 *in vitro* (Elfgang et al., 1995; Yum et al., 2007; Magnotti et al., 2011b). A comparative study by Nagy et al. (2011) revealed higher Cx26 protein levels in the rat brain compared to mouse brain. Thus, a functional role in brains with morphologically more complex astrocytes (Nedergaard et al., 2003) cannot be excluded and requires further analysis. The secondary effect caused by the Cx30LacZ knock-out strategy can be circumvented by using the new Cx30 knock-out mouse line generated by Boulay et al. (2013).

It is unlikely that the results in Cx26$^{fl/fl}$:Nestin-Cre mice were due to incomplete recombination. Unfortunately, the Cx26fl:Nestin-Cre mouse line lacks a reporter to confirm successful excision of the floxed gene. In the present study, Cre recombinase activity was confirmed by a newly generated Cx26Del PCR detecting the deleted floxed Cx26 in tail tip PCRs (Fig. 5.5). Due to Nestin expression in other tissues like endothelial cells, it was possible to determine the deleted genotype (Klein et al., 2003; Mohseni et al., 2011). These control PCRs were required as several reports demonstrated both the inactivity of Cre and the ectopic Cre activity (Requardt et al., 2009; Zhang et al., 2013). For future studies it would be advantageous to use reporter genes to confirm the status of the floxed gene.

The relevance of Cx30 in the thalamus was further supported by increased protein levels in Western blot analysis compared to hippocampus and reporter gene expression in the thalamus. Interestingly, the Cx43 protein levels did not differ between thalamus and hippocampus in the adult brain, but a substantial astrocyte population lacked Cx43 reporter gene expression (Fig 5.3). This observation is in line with the observation of a subpopulation of uncoupled cells in Cx30$^{LacZ/lacZ}$ mice in the thalamus (Fig 5.2B$_2$). Another study performed in the lab employing heterozygous Cx43-ECFP mice confirmed the strong impact of Cx43 on network size in the hippocampus, but no change in network size was observed in cortex nor thalamus. In addition, the ECFP expression in glial networks was higher in the hippocampus compared to thalamus and cortex (Griemsmann et al., 2014). The different expression levels of Cx43 might reflect functional differences and regional specializations of astrocytes which adapted to their environment and local requirements. Cx30 was shown to mediate astrocyte process extension into synaptic clefts by a non-channel adhesive function, while Cx43 hemichannels play a role in presynaptic glutamate release (Pannasch et al., 2014; Chever et al., 2014; Chever et al., 2014).

Biocytin is a widely used tracer for network analysis. Due to its good diffusion properties it passes equally well through most connexin GJC. On the other hand, the analysis by counting biocytin-labelled cells has its limitations. No information about the preferential direction of the tracer diffusion in glial networks nor about the quantity of gap junctions between adjacent cells is gained. For further analysis of spatial properties of glial networks a diffusion model was simulated and analysed in the hippocampus. Quantifying network sizes by the coupling length constant and network anisotropy revealed a

temperature dependence in dye diffusion which could not be detected by cell counting (Anders et al., 2014). For future network studies it would be advantageous to analyse diffusion parameters based on fluorescence intensities in addition to cell counting.
In summary, connexin expression in astroglial cells differs between all brain regions analysed so far, revealing considerable heterogeneity between astrocytes throughout the brain. The impact of Cx30 and Cx43, the main connexins for GJC formation, differs between brain regions. In the present study, a predominating role for Cx30 in thalamic glial networks was observed. In addition, some astrocytes in the thalamus express only one connexin. This is in contrast to previous assumptions of general Cx43 expression in all astrocytes (Giaume et al., 1991). Most likely these differences reflect functional and regional specializations of these cells.

6.2.2 The role of Cx43 in RG-like cell proliferation

The functional role of Cx43 was further studied in neural stem cells in the mature brain. A study by Elias et al. (2007) demonstrated the importance of extracellular adhesive functions of Cx26 and Cx43 GJC expressed in neuronal precursors migrating along the radial scaffold during embryonal development. This effect did not depend on connexin expression and intracellular scaffolding in RG-like cells as shown by transplantation of Cx26-shRNA or Cx43-shRNA treated neuronal precursors into wild-type brains (Elias et al., 2007). In contrast, a study by Cina et al. (2009) showed that the intracellular C-terminal domain is essential for neuronal migration. In the mature brain neuronal precursors were not coupled to RG-like cells (Kunze et al., 2009).
The present study aimed at identifying the key function, adhesion or gap junction coupling, of Cx43 for proliferation in adult neurogenesis. RG-like cells are neuronal precursors which reside in neurogenic niches, the SVZ and the SGZ, in the adult brain. They share many properties with astrocytes, e.g. they express GFAP and are connected to neighbouring cells via GJC formed by Cx30 and Cx43. Cx30/43 DKO mice displayed reduced adult neurogenesis and uncoupled RG-like cells (Kunze et al., 2009). Though, few RG-like cells expressed Cx26 in the above-mentioned study, a functional analysis in Cx26fl:Nestin-Cre mice was not performed so far. Recently, a study in this lab and by another group showed that Cx30 is not important for adult neurogenesis (Liebmann et al., 2013; Zhang, 2013). Hence, due to the findings in RG-like cells, Cx43 is a likely candidate to regulate proliferation and is known to be tightly regulated, e.g. by phosphorylation of the cytoplasmic C-terminal tail. To decide whether Cx43 mediated regulation of adult neurogenesis relies on a channel mediated effect or adhesion to the intracellular cytoskeleton of RG-like cells we employed mice carrying two different Cx43 mutations. In this study, Cx43G138R mice were employed which carry a point mutation in the cytoplasmic loop. This mutation leads to channel closure and changes in phosphorylation status, but Cx 43 traffic to the membrane is preserved as revealed in cardiomyocytes (Dobrowolski et al., 2008). In addition, Cx43K258stop mice were studied. These mice lack the entire C-terminal tail and in consequence adhesion to the cytoskeleton by ZO-

proteins and all phosphorylation sites, but display an intact GJC pore (Maass et al., 2007; see also3.10). Compensation of Cx43 function by Cx30 expression was circumvented as both genotypes additionally lacked Cx30.
The two mouse lines displayed significantly reduced network sizes compared to wild-type mice, but not in comparison to their Cre negative controls (Fig. 5.6A). The ratio of coupled to uncoupled cells was unaffected by Cx43 mutations (Fig. 5.6B). The observation of coupled RG-like cells in Cx43G138R mice was an unexpected finding as this mutation was shown to inhibit GJ coupling in the heart. The mutation is not located in the channel pore itself, but in the cytoplasmic loop. The loop of Cx43G138R folds into the channel pore, this process might be sterically hindered in brain cells in contrast to cardiomyocytes. Another explanation would be an incomplete excision status of the floxed Cx43G138R due to Cre inactivity in some cells or Cx26 mediated GJC (Kunze et al., 2009; Requardt et al., 2009). Although, the latter case is unlikely due to side-effects of the Cx30LacZ knock-out on Cx26 expression as discussed above. RG-like cells carrying the other mutation Cx43K258stop were coupled, although network sizes were reduced compared to wild-type mice. Due to the observed residual coupling in Cx43G138R mice, the data do not allow for a definite conclusion on the decisive effect, adhesion or GJ coupling, for adult neurogenesis. Both gap junction coupling and adhesive properties to the intracellular cytoskeleton might play role in adult neurogenesis.
Unfortunately, both floxed Cx43 mutations displayed strongly reduced protein levels compared to wild-type protein expression, but no further reduction upon excision of the mutation sites (Maass et al., 2007; Dobrowolski et al., 2008). The observations on network size level rather reflect the diminished Cx43 protein levels in the Cx43 mutated mouse lines than mutation specific effects on network sizes. Regulatory effects by phosphorylation might also play a role in regulating proliferation as the Cx43G138R mutation showed a shift in phosphorylation in Western blots and the Cx43K258stop mouse lacks the entire C-terminus including all phosphorylation sites.
In this context, further experiments are required to understand the role of gap junctions in adult neurogenesis. A suitable tool would require mutated protein levels as in wild-type mice. Employing the Cx43 mutant Cx43flD378stop, which just lacks the binding site for ZO-1 protein, might be helpful to exclude side-effects by changes in the phosphorylation status (Lübkemeier et al., 2013). In conclusion, Cx43 expression seems to be required for proliferation of RG-like cells as shown by Liebmann et al. (2013), although the mechanism remains elusive.

6.3 Panglial networks in the brain

The initial experiments in this study often displayed tracer spread into myelinated fibres in the thalamus (Fig. 5.1B_2). The GJC involved in this transfer from astrocytes to the myelin sheath were unknown and questioned the concept of a purely astrocytic network. So far, studies in the hippocampus and cortex always described purely astroctyic networks (Houades et al., 2008; Rouach et al., 2008).

6.3.1 Astrocytes and oligodendrocytes form functional networks

Analysing glial networks in the thalamus for the first time in the present study, immunohistochemical analysis was carried out to characterize the protein expression profile of cells involved in tracer-coupled networks. There is only little information available for suitable glial markers in the thalamus. A study by Frassoni et al. (2000) showed that GFAP is only weakly expressed in the adult thalamus. Therefore GS was chosen to identify astrocytes in GJNs which was shown to be a good marker in other areas. Olig2 was used to label the oligodendrocyte lineage. This comparative study in hippocampus and thalamus revealed considerable heterogeneity regarding the expression profile of the tracer-filled cells. Half of the cells expressed GS and over 60% expressed Olig2 in the thalamus , while in the hippocampus the majority of cells expressed GS and only a minority was Olig2-labelled (Fig. 5.7; 5.8). This indicated the presence of panglial networks, though to a different extent in both brain regions. The expression of these two proteins was further studied by immunohistochemistry on transgenic mice with astrocyte or oligodendrocyte specific fluorescence. A cell-type specific expression of GS and Olig2 could not be observed in the thalamus, in contrast to the hippocampus (Fig. 5.15A_{1-3}, B_{1-3} 5.18). In conclusion, the immunohistochemical analysis indicated the presence of a panglial network in both brain regions.
In contrast to white matter networks studied by Maglione et al. (2010) the presence of NG2 cells was not observed in glial networks in the grey matter areas thalamus and hippocampus (Fig. 5.9A_{1-3}, B_{1-3}). This observation was further confirmed by a previous study demonstrating that NG2 cells in the hippocampus are uncoupled (Wallraff et al., 2004). During embryonic development neurons express connexins and possess electrical synapses which are later on mostly replaced by chemical synapses. In some regions, e.g. in the RTN, GJs between neurons are present throughout life (Lee et al., 2014). Despite the presence of neuronal GJ in neighbouring thalamic nuclei, no tracer spread from glia to neurons was observed and also microglia were not involved in network formation (Fig. 5.9C_{1-3}, F_{1-3}). These findings are in line with previous observations in the healthy and lesioned cortex and striatum (Richter et al., 2014; Wasseff and Scherer, 2014). Hence, the network is limited to astrocytes and oligodendrocytes.
The protein expression of tracer-coupled cells was indicative for a panglial network. To further confirm this hypothesis transgenic PLP-GFP mice with fluorescence labelled

oligodendrocytes were employed (Fuss et al., 2000). Network analysis in PLP-GFP mice confirmed the findings of the immunohistochemical network study employing GS and Olig2. Thalamic networks consist of almost equal numbers of astrocytes and oligodendrocyte, while in the hippocampus only a minor population of cells in these networks are oligodendrocytes (Fig 5.11, 5.12B). In contrast, when injecting an oligodendrocyte in the white matter region corpus callosum the ratio of astrocytes and oligodendrocytes was opposite to hippocampal networks, because only a minority of astrocytes were observed in these networks (Maglione et al., 2010). In the cortex similar numbers of Olig2 labelled cells were found in glial networks compared to thalamic glial networks, but fewer Cx43-ECFP$^+$ co-expressed Olig2 compared to the thalamus (Griemsmann et al., 2014). Cortical glial networks comprise of an astrocyte to oligodendrocyte ratio in between hippocampus and thalamus. The thalamus has an even cell-type ratio of astrocytes and oligodendrocytes which corresponds well with a grey matter regions which contains myelinated fibre bundles. The contribution of oligodendrocytes to glial networks additionally reflects the different densities of oligodendrocytes in different brain regions, as observed by immunohistochemistry (Fig. 5.17B). Interestingly, tracer diffusion was independent of the cell-type initially patched, PLP-GFP$^+$ cells or SR101$^+$ cells. This indicates bidirectional diffusion of biocytin through GJC between astrocytes and oligodendrocytes. Further studies are required to analyse potential physiological influences on diffusion of active molecules which likely diffuse towards sites of higher demand and away from sites with excess concentrations.
Thalamic panglial networks were already present in the second postnatal week (Fig. 5.10). Still, the number of PLP-GFP$^+$ cells might be an underestimation of the oligodendrocyte fraction in biocytin networks as GFP fluorescence in these mice starts with the onset of myelination in the second postnatal week (Fuss et al., 2000). Panglial networks in white matter were as well observed at early postnatal ages between p10-25 (Maglione et al., 2010). The early establishment of panglial connections raises the question of their physiological function. A functional role might involve metabolite supply from blood vessels to myelinated axons and K^+ buffering away from sites underneath the myelin sheath. These presumed functions are further supported by recent findings of lactate transfer from oligodendrocytes to axons and vacuolizations underneath the myelin sheath in Cx47 knock-out mice (Menichella et al., 2003; Odermatt et al., 2003; Fünfschilling et al., 2012; Lee et al., 2012).

6.3.2 Heterotypic connexin channels mediate panglial coupling

The GJC involved in panglial coupling in the thalamus and hippocampus were unknown. Connexins are widely expressed throughout the brain and not confined to astrocytes. Oligodendrocytes express Cx29, Cx32 and Cx47. While Cx29 is restricted to the myelin sheath, the other two isoforms do form GJC with neighbouring cells. Cx47 was the most important connexin for oligodendrocyte network formation in white matter (Maglione

et al., 2010). GJC must be formed by heterotypic channels of two different connexins as astrocytes and oligodendrocytes do not express the same set of connexins.
Cell culture studies indicated that the loss of one astrocytic and one oligodendrocytic connexin, either Cx32 and Cx43 or Cx30 and Cx47, should abolish panglial networks. Cx32 can only form channels with Cx30 and Cx43 forms GJC with Cx47 (see also Section 1.4.4). Both knock-out combinations were generated in mice and displayed severe changes including myelin abnormalities, vacuolizations and were partially lethal (Magnotti et al., 2011a; Tress et al., 2012).
Due to the prominent Cx30 expression in the thalamus, the Cx30/47 DKO was chosen to study heterotypic gap junction channels involved in panglial network formation in this study. When injecting the tracer into an astrocyte in these Cx30/47 DKO mice, diffusion into neighbouring astrocytes should still be mediated by Cx43 channels. However, we observed a lack of astrocyte networks (Fig. 5.13B_{1-4}, E_{1-3}; 5.14A, C). Recently, a publication by May et al. (2013) showed that the presence of Cx47 on the cell membrane requires Cx43 expression in astrocytes. This is most likely a mutual effect, implying that lack of Cx47 leads to relocation of Cx43 in astrocytes and would explain the observation of uncoupled cells in Cx30/47 DKO mice. The morphological alterations in the brains of Cx30/47 DKO mice might as well contribute to this effect, because microglia activation and astrogliosis were reported in several brain regions (see Tress et al., 2012). These morphological changes might have altered connexin expression (Giaume et al., 2010) in Cx30/47 DKO mice and thereby influenced GJC in astrocytes. The hypothesis of a mutual effect of Cx43 and Cx47 on their localization was tested by tracer-injection in $Cx30^{(LacZ/LacZ)}$;$Cx47^{(+/EGFP)}$ mice which were heterozygous for the oligodendrocytic connexin. Indeed, panglial networks were restored, confirming a role of Cx47 in Cx43 stabilization in the membrane and a small contribution of Cx43-Cx47 GJCs to panglial coupling in both regions (Fig. 5.13C_{1-4}, F_{1-3}; 5.14A, C). On the contrary, in white matter oligodendrocyte networks displayed normal sizes, but lacked astrocytes in Cx30/47 DKO which is most likely a Cx47 driven effect as the single knock-out of Cx47 displayed smaller networks and lacked astrocytes (Maglione et al., 2010; Tress et al., 2012). In the present study, employing the Cx30/47 DKO mouse line, the proportion of Cx47-EGFP fluorescent oligodendrocytes in biocytin-filled networks (Fig. 5.14C) confirmed the findings of the immunohistochemical study (Fig. 5.7; 5.8) and the PLP-GFP study (Fig. 5.12B). More oligodendrocytes were present in thalamic panglial networks compared to hippocampal tracer-filled networks.
The anatomical structure of panglial networks in grey matter is unknown so far. In PLP-GFP mice, we observed no diffusion preferences in the network because tracer injection in oligodendrocytes or astrocytes always resulted in large GJN. From hippocampal astrocytes it is known that they occupy distinct spatial domains (Bushong et al., 2002). The localization of oligodendrocytes in these domains and networks requires further analysis. In contrast to oligodendrocytes, astrocytes contact blood vessels. Accordingly, the tight link of both glial cells might be a fast transportation route between oligodendrocytes and blood vessels and might play a role in brain homoeostasis.

In the present study, the abundant prevalence of panglial networks was demonstrated for thalamic and hippocampal glial cells. Based on findings in white matter regions and cortex it is tempting to speculate that the formation of panglial networks is a universal feature of glial cells in the brain, though the contribution of astrocytes and oligodendrocytes varies among brain regions and might depend on the density of each cell-type. Mice lacking panglial networks display a strong phenotype and future studies should aim at elucidating the physiological functions of these networks.

6.4 Immunohistochemical analysis reveals a unique population of glial cells

Studying glial cells in the brain requires the reliable identification of different cell-types. Only little is known about thalamic glia and their protein expression profile. In this study, the initial experiments to identify glial cells in biocytin-labelled networks by immunohistochemistry questioned the concept of cell-type specific protein expression in the VB. Here, GS and Olig2 were quantified in the networks and displayed an overlapping expression profile, while in hippocampal networks this effect was not observed (see Section 5.3.1). Proteins used as "classical" cell-type markers in other brain regions were subsequently tested in the thalamus.
Employing transgenic PLP-GFP and Cx43-ECFP knock-in mice, the observation of a potential "classical marker" overlap in thalamic glial networks was further investigated by immunohistochemistry on brain slices. GFAP, a widely used astrocyte marker, was reported to be weakly expressed in the adult thalamus (Frassoni et al., 2000). These findings were confirmed in the present study and were in contrast to the strong, abundant GFAP expression by hippocampal astrocytes (Fig. 5.16A_{1-4}; B_{1-4}). GFAP is an intermediate filament found in astrocytes. PLP-GFP cells were also always devoid of GFAP-labelling (Fig. 5.17C). In conclusion, although GFAP expression is confined to astrocytes, only few cells can be identified and this protein is therefore not a good marker for thalamic astrocytes.
GS was regarded as an astrocyte specific protein in many other studies (Norenberg, 1979; Sonnewald et al., 1997; Coulter and Eid, 2012). GS is an enzyme that metabolises glutamate to glutamine, postulated to be astrocyte specific due to neurotransmitter uptake and detoxification by astrocytes in the tripartite synapse. Unexpectedly, GS was found to be expressed by both oligodendrocytes and astroctyes in the thalamus in contrast to astrocyte restricted expression in the hippocampus (Fig. 5.15A_{1-3}, B_{1-3}). The morphology of GS stained cells differed between brain regions. In the VB, the round GS-labelled cell somata resembled those observed in several studies describing GS expression in oligodendrocytes (D'Amelio et al., 1987; Cammer, 1990), and colocalized with PLP-GFP fluorescence. The role of increased GS expression in thalamic oligodendrocytes remains elusive.

Another widely used marker, S100β, was further investigated in another set of experiments. Due to its previously described expression in NG2 cells (Karram et al., 2008), co-labelling with PLP-GFP and NG2 was investigated. Only a subpopulation of PLP-GFP cells expressed S100β, while most GFP^+ cells were devoid of S100β (Fig. 5.16C_{1-4}, D_{1-3}; 5.17D). It is therefore the most reliable marker to distinguish astrocytes from oligodendrocytes by immunohistochemistry in the thalamus. Additionally, dense S100β staining can be used to macroscopically identify the VB. As shown in an immunohistochemical study by Muneoka et al. (2012) it was possible to identify the ventroposterior nucleus in the thalamus by S100β immunohistochemistry.
In contrast to hippocampal NG2 cells, thalamic NG2 cells mostly lacked S100β expression (Fig. 5.16C_{1-4}, D_{1-4}; 5.17D). This is in line with previous findings by Parri et al. (2010). Additionally, they were devoid of PLP-GFP expression in the thalamus. This might indicate that thalamic NG2 cells in the adult brain do not enter the oligodendrocyte lineage. In white matter regions NG2 cells differentiate into oligodendrocytes, while in grey matter they persist as NG2 cells (Dimou et al., 2008). In contrast, in the hippocampus sparse PLP expression in NG2 cells was described in reporter mice in a previous study (Mallon et al., 2002) and was also observed in the present study. In conclusion, the concept of glial heterogeneity needs to be extended to the fourth type of glia the NG2 cells.
A transcriptome study by Cahoy et al. (2008) described Aldh1L1 as a global astrocyte marker throughout the brain. Accordingly, Aldh1L1 expression was investigated in the thalamus (Fig. 5.16E_{1-4}; 5.17E). Many Aldh1L1 cells with a typical star-like morphology of astrocytes were identified, but half of the Aldh1L1-labelling colocalized with PLP-GFP. These cells displayed the typical round somata of oligodendrocytes. Hence, Aldh1L1 is a possible astrocyte marker, when additionally selecting for cell morphology. Still, further analysis is required to analyse how many astrocytes can be identified by Aldh1L1.
The network analysis individually revealed an overlap of GS and Olig2 in the VB. Cx43-ECFP knock-in mice were employed to reliably identify astrocytes and investigate Olig2 expression. Unexpectedly, half of the thalamic Cx43-ECFP expressing cells expressed Olig2, while in the hippocampus only a small subpopulation expressed Olig2 (Fig. 5.18). The proportion of Olig2 expressing astrocytes might even underestimate the extent of Olig2 expression in astrocytes as 20% of thalamic astrocytes lack Cx43 expression (Fig. 5.3C_4). So far, Olig2 expression in astrocytes was only described in the juvenile brain (Fukuda et al., 2004; Marshall et al., 2005; Cai et al., 2007). In the present study, abundant astrocytic Olig2 expression in the thalamus of the mature brain was observed. This population might represent an "intermediate" cell-type between astrocytes and oligodendrocytes. The functional role of these cells requires further investigation.
Similarly, Aldh1L1 colocalized with Olig2 in cells with and without PLP-GFP fluorescence (Fig. 5.16E_{1-4}). Cells co-labelled for Aldh1L1 and Olig2 likely account for this "intermediate" cell-type. To exclude that the Olig2 expressing astrocytes are immature astrocytes, their gap junction coupling was analysed in Cx43-ECFP mice with

co-staining of Olig2 (Fig. 5.19). Indeed, the "intermediate" cell-type was observed in glial networks and indicates the mature state of these cells.
Immunohistochemical analysis further confirmed the oligodendrocyte-specific PLP-GFP expression. Their round morphology differed from the star-like morphology of astrocytes. GFP^+ cells were devoid of GFAP labelling and never expressed Iba1 or NeuN (Fig. 5.15_{1-3}C, D_{1-3}; $5.16A_{1-4}$-E_{1-4}; 5.17B, C, D). Olig2 staining always colocalized with PLP-GFP in the thalamus (Fig. 5.17E). Additionally, in the hippocampus PLP-GFP cells mostly lacked astrocytic protein expression.
In summary, transgenic and knock-in mice with cell-type specific PLP-GFP and Cx43-ECFP fluorescence can be employed to identify astrocytes and oligodendrocytes. For immunohistochemical analysis S100β is the most reliable marker to distinguish between astrocytes and oligodendrocytes. As it is not an exclusive marker for astrocytes, the morphology of $S100\beta^+$ cells should be analysed as a second criterion. Still, for future immunohistochemical studies the identification of a reliable astrocyte marker will be advantageous.

6.5 Neuron-glia interactions in the thalamus

6.5.1 Metabolite diffusion in panglial networks

Astrocytes have been known for a long time as key players in neuronal synaptic transmission by taking up neurotransmitter from the synaptic cleft, releasing gliotransmitters and controlling local homoeostasis. These functions were summarized in the concept of the tripartite synapse (Araque et al., 1999). The extent of panglial networks in the VB questioned this concept and it might have to be extended to oligodendrocyte participation in brain homoeostasis.
Metabolite supply is regarded to be an astrocytic function in the brain and is summarized in the ANLS concept (see also Fig. 1.4). Astrocytes take up glucose from the blood vessels and by glycolysis produce lactate which is shuffled into neuronal boutons. Increased activity at glutamatergic synapses leads to increased glycolysis in astrocytes. Panglial networks between astrocytes and oligodendrocytes might be a transportation route for metabolites or ions. Indeed, employing the fluorescent glucose analogue 2-NBDG the diffusion of glucose through heterotypic channels from astrocytes to oligodendrocytes was confirmed in the present study. In addition to metabolite transport in astrocytic networks (Rouach et al., 2008), this experiment confirmed the transport of metabolites in panglial networks (Fig. 5.20B). Interestingly, like in the initial biocytin experiments 2-NBDG fluorescence was observed in myelinated fibre tracts (Fig. $5.1B_2$; $5.20A_{1,3}$). A transportation via the extracellular space is unlikely, as 2-NBDG fluorescence was never observed in the extracellular space (Fig. $5.20A_{1-2}$). 2-NBDG can enter gylcolysis like glucose and is rapidly phosphorylated by hexokinases. Phosphorylation of glucose molecules inhibits diffusion through glucose trans-

porters to the extracellular space and glucose and 2-NBDG are trapped inside cells. In the present study, network sizes were smaller employing 2-NBDG compared to biocytin. The fluorescent glucose molecule is larger than biocytin and consists of two ring structures. Its diffusion through GJCs might be sterically limited. Glucose without a fluorescent tag supposedly diffuses further into the network. As described in the ANLS model, astrocytes metabolise glucose and provide lactate to neurons *in vivo*. In addition, they might transfer lactate to neighbouring oligodendrocytes which in turn transport it to myelinated axons. Recent publications reported the oligodendrocytic support of axons with lactate to sustain neuronal activity (Fünfschilling et al., 2012; Lee et al., 2012). The origin of lactate in oligodendrocytes was unclear as oligodendrocytes do not contact blood vessels. Lactate might be derived from the extracellular space, or from astrocytes via panglial GJC as described in the present study.

6.5.2 Neuronal activity requires energy supply

The interactions of glial networks and neurons was further investigated in the present study. As glial networks support several neurons, these effects were analysed on neuronal network scale by recording extracellular field potential recordings. The extent of panglial coupling in the hippocampus was lower compared to the thalamus. It would therefore be advantageous to study glia-neuron interactions in the thalamus. For this reason a method to monitor neuronal activity in the VB was established in the present study. The thalamus receives synaptic input from the lemniscal pathway and the cortico-thalamic pathway. Cortical fibre tracts could be easily identified in DIC optics on acute brain slices and were chosen for stimulation experiments.
A protocol was developed to stimulate the CT pathway on nearly horizontal slices. Field potential responses were small in the VB and therefore trains of five stimuli were applied, while induction of LTP or LTD was avoided. Control recordings for 90 min confirmed the reliability of the designed input parameters for long term recordings (Fig. 5.23). Stimulation of the CT pathway resulted in pre- and postsynaptic responses in the VB as identified by block of synaptic transmission (Fig. 5.22). In contrast to hippocampal field potentials (An et al., 2008), in the thalamus also the presynaptic signal displays a large amplitude which is blocked by TTX application (Fig. 5.22).
Recorded fEPSPs were analysed with a custom made Igor tool. Ten traces were averaged and analysed for the delay and the amplitude of the postsynaptic response. During slow application of receptor blockers NBQX and D-AP5 the amplitude decreased, while the delay increased (Fig. 5.22C). Synaptic transmission was slower and elicited postsynaptic responses in fewer neurons leading to a decrease in amplitude of the fEPSP. After a few minutes, the synaptic transmission was completely blocked. Similar responses were obtained in a study employing coronal slices with a lateral angle when stimulating the CT pathway (Castro-Alamancos and Calcagnotto, 1999).
For studying the effects of panglial networks on neuronal activity, changes in fEPSP in response to extracellular glucose deprivation (GD) were investigated. In a first experi-

mental approach GD was applied after 10 min of recording in ACSF. After 60 min of GD, re-perfusion with ACSF was performed for 20 min, but the fEPSPs could not be restored. Most likely long-time GD leads to neuronal inactivity and cell death which cannot be rescued. In the optic nerve GD cells recovered completely from 45 min of GD, but not from 65 min GD (Ransom and Fern, 1997). In the thalamus the postsynaptic response started to decrease after 16 min of GD. After 21 min the signal decreased to 50% of the normalized maximum amplitude and further decreased over the recording time. In comparison, in the hippocampus the signal decreased to 50% after 30 min of GD (Rouach et al., 2008). Control recordings on another brain slice from the same animals displayed stable fEPSPs in response to the stimulation parameters which confirms a specific effect of GD on fEPSP amplitudes. A previous experimental study tested different glucose concentrations and found optimal responses with 10 mM extracellular glucose. Lower concentrations decreased hippocampal popspike amplitudes, while the paired-pulse-ratio was maintained (An et al., 2008). GD also affects axonal signalling in white matter areas, changes in compound action potentials were only observed after half an hour of GD, followed by a rapid decline in signal (Wender et al., 2000). The delayed changes in white matter compound action potentials compared to the fEPSP changes in VB might indicate a higher energy consumption by synaptic transmission compared to axonal action potential propagation in the optic nerve. hippocampal fEPSP were stable for a longer time during GD compared to thalamic fEPSPs indicating a higher energy consumption in the thalamus. Probably, the thalamus requires high energy supply to sustain both synaptic transmission and axonal signal propagation. Long axons from cortical neurons arrive in the VB and require more local metabolite supply, in contrast to shorter hippocampal Schaffer collaterals. Another possible explanation would be that glycogen storage is increased in the hippocampus compared to the VB.
Astrocytes are the glycogen storage place in the brain (Pellerin and Magistretti, 2012). In the present study the hypothesis of glucose uptake from the blood by astrocytes and the subsequent transfer of energy metabolites in the panglial network was investigated. In conclusion, glucose indeed diffused into panglial networks and neuronal activity in acute slices is sensitive to extracellular GD. In future studies it would be interesting to analyse changes in both, synaptic transmission and axonal signal propagation, during GD. For further analysis of the glial metabolic support mice lacking panglial networks should be employed. It is also of further interest, whether it is possible to rescue the fEPSPs during GD by glucose filling of panglial networks. Understanding panglial metabolite supply will be advantageous to find treatments to rescue energy deprived neuronal tissue in diseases, e.g. ischemia.

6.6 Ionotropic receptor expression in VB astrocytes

Astrocytes have been shown to express ionotropic receptors in several brain regions. Here, a detailed analysis of the AMPA and $GABA_A$ receptor subunit expression profile of astrocytes in the VB was performed. Therefore, functionally characterized and fluorescently identified astrocytes in the VB of juvenile mice were harvested for subsequent RNA analysis.

6.6.1 AMPA receptor expression analysis identifies two astrocyte populations

The RT-PCR results identified two astrocyte populations which could be distinguished by the presence or absence of AMPA receptor subunit expression, revealing astrocyte heterogeneity on receptor expression level. Cells expressing AMPA receptors revealed abundant GluA2 expression, while GluA1 was least expressed. Both splice variants, flip and flop, were found for all four subunits. GluA1 and GluA3 mainly occurred in the flop isoform (Fig. 5.24). The other two receptor subunits were found to a similar proportion as flip or flop. Indeed, astrocytes with and without AMPA receptor currents were also found in the functional receptor study on acutely isolated cells (Höft et al., 2014). In contrast, hippocampal astrocytes lack AMPA receptors, but express glutamate transporters. Instead, another group of glia, hippocampal NG2 cells, were shown to have functional AMPA receptors and abundantly expressed GluA1 and GluA2 subunits (Bergles et al., 2000; Matthias et al., 2003; Seifert et al., 2003; Jabs et al., 2005). Heterogeneous AMPA expression was also reported for striatal astrocytes and NG2 cells (Wang et al., 2008). Thalamic NG2 cells express functional AMPA receptors which were blocked by CNQX (Parri et al., 2010). Radial-glia like cells are neuronal precursors in the SGZ of the dentate gyrus and displayed a heterogeneous AMPA receptor localization on their cell surface. The radial process contained many AMPA receptors, while the cell soma was devoid of AMPA receptors (Renzel et al., 2013). They often expressed the GluA2 subunit, like thalamic astrocytes. In the supraoptic nucleus most astrocytes lacked any glutamate uptake currents and were devoid of glutamate receptors, while a morphologically identified subpopulation expressed glutamate transporters (Matyash and Kettenmann, 2010). In contrast, cerebellar Bergmann glia have functional AMPA receptors with high Ca^{2+} permeabilities lacking the GluA2 subunit (Burnashev et al., 1992; Müller et al., 1992).
VB astrocytes respond to neuronal activity with increased $[Ca^{2+}]_i$ levels, mediated by mGluR5 G-protein coupled receptors, but not AMPA receptors (Parri et al., 2010). These Ca^{2+} elevations in turn lead to gliotransmitter release of glutamate which induces slow inward currents in neurons (Pirttimaki and Parri, 2012). The absence of AMPA receptors mediated $[Ca^{2+}]_i$ (Parri et al., 2010) is in line with the high GluA2 expression level in thalamic astrocytes observed in the present study. AMPA receptors containing the GluA2 subunit are impermeable for Ca^{2+} (Burnashev et al., 1992).

In summary, astrocytic responses to glutamate vary among brain regions, some astrocytes express AMPA receptors, while others express transporters or do not respond at all to glutamate application. The AMPA receptor subunit composition is also highly variable among brain regions and even within a given region, e.g. some thalamic astrocytes lack AMPA receptors.

6.6.2 Astrocytic $GABA_A$ receptor subunit expression

The $GABA_A$ receptor expression profile was assessed by RT-PCR analysis. As observed in other brain regions (Fraser et al., 1995; Israel et al., 2003), all thalamic astrocytes expressed $GABA_A$ receptor subunits (Fig. 5.25). Only in 1 of 9 cells the $\gamma 2$ subunit of the $GABA_A$ receptor was expressed. This subunit is indicative of synaptic localization of the receptor in neurons and in another group of glia, NG2 cells (Essrich et al., 1998; Passlick et al., 2013). Instead, VB astrocytes abundantly expressed the $\gamma 1$ and $\gamma 3$ subunits and also prominently expressed $\beta 1$. In contrast, hippocampal NG2 cells expressed $\beta 3$ more often than $\beta 1$, while all γ subunits were found in most cells (Passlick et al., 2013). Radial-glia like cells which share many properties with astrocytes, also express $GABA_A$ receptors in the adult SGZ. Similarly to thalamic astrocytes, RG-like cells often expressed the $\beta 1$ subunit, but less often the $\gamma 1$ and $\gamma 3$ subunits (Renzel et al., 2013). Astrocytes in the supraoptic nucleus and hippocampus also express $GABA_A$ receptors, the latter often contained the subunits $\alpha 1$, $\alpha 3$ and $\beta 1$ among others (Fraser et al., 1995; Israel et al., 2003).
Functional studies on acutely isolated VB astrocytes always displayed $GABA_A$ receptor currents in response to muscimol (Höft et al., 2014). They respond to GABA with depolarization in the VB and hippocampus (Meier et al., 2008; Höft et al., 2014), and increases in $[Ca^{2+}]_i$ (Meier et al., 2008). Though, $[Ca^{2+}]_i$ responses seem to be mediated mainly by mGluR5 in the VB and were not reduced by a combined block of AMPA, NMDA and $GABA_A$ receptors (Parri et al., 2010). In contrast to neurons, astrocytes respond to GABA with depolarization due to the expression of the NKCC1 cotransporter and the resulting higher $[Cl^-]_i$ concentrations. GABA-signalling on astrocytes might therefore be required to buffer $[Cl^-]_o$ and thereby controls neuronal inhibitory signalling (Losi et al., 2014). Additionally, astrocytes lack the KCl cotransporter KCC2 expressed in mature neurons (Stein et al., 2004). So far, the role of $GABA_A$ receptor activation in astrocytes is not well understood. Additionally, only few studies are available on GABA mediated neuron-astrocyte interactions (Vélez-Fort et al., 2012).
Interestingly, thalamic astrocytes completely lacked the $\alpha 3$ subunit (Fig. 5.25). $\alpha 3$ knock-out mice suffered longer from alcohol induced incoordination (Blednov et al., 2013). Furthermore, this subunit is abundantly expressed by RTN, but not VB neurons (Mozrzymas et al., 2007; Christian and Huguenard, 2013). The $GABA_A$ receptor subunit $\alpha 3$ contains a benzodiazepine-binding site (Christian and Huguenard, 2013). Astrocytes enhance $GABA_A$ receptor mediated currents via endozepine actions in the RTN, but not in the VB (Mozrzymas et al., 2007; Christian and Huguenard, 2013). Astrocytes

negatively modulate $GABA_A$ receptor currents via GABA transporter mediated uptake from the synaptic cleft (Christian and Huguenard, 2013). Physiologically, the absence of this subunit in VB astrocytes, in the present study, might prevent feedback signalling to astrocytes. The expression of $GABA_A$ receptors in RTN astrocytes requires further analysis to confirm this hypotheses.
Benzodiazepines are used to treat neuropsychiatric diseases and seizures. Thalamic dysfunctions are associated with schizophrenia and absence epilepsy (Pinault, 2011; Christian and Huguenard, 2013). Glial cells might play a role in these diseases as increased GS and S100β levels in the thalamus were reported in schizophrenia (Rothermundt et al., 2004; Bruneau et al., 2005). Apparently, benzodiazepine treatment cannot target astrocytes, but these cells modulate neuronal $GABA_A$ receptor signalling in the RTN. For future studies it might be beneficial to identify potential astrocytic targets for new treatments.
GABA-signalling on astrocytes increased GFAP levels and astrocytic branching in the rat forebrain (Runquist and Alonso, 2003). Only few VB astrocytes express GFAP (Frassoni et al., 2000) and it is probably a less important mechanism in the VB.
In summary, VB astrocytes display a heterogeneous AMPA receptor expression profile and abundantly express $GABA_A$ receptors. The impact of this heterogeneous AMPA receptor expression profile on brain function requires further analysis. Astrocytes respond to glutamate with gliotransmitter release and might modulate neuronal activity in the VB. Additionally, the role of GABA receptors on VB astrocytes remains elusive so far, but likely plays an important role in thalamic neuronal circuits which are highly regulated by GABAergic signalling.

7 Summary

Increasing evidence over the past decades revealed the importance of glia in the brain. In this study, astrocytes in the ventrobasal thalamus were characterized in detail for the first time. Glial heterogeneity was investigated by comparing their properties with those of astrocytes in the hippocampus, a brain region in which glial cells have been widely studied.

During development, astrocytes establish gap junction channels with each other. In this study, the networks in the ventrobasal thalamus increased in size until the end of the second postnatal week. Cx30 expression was strongly upregulated during postnatal development and had a predominating role in glial network formation in the mature thalamus. Cx30 and Cx43, but not Cx26, mediated gap junction coupling in the hippocampus and thalamus. Strikingly, some astrocytes were devoid of Cx43. Expression of Cx43 in RG-like cells influences proliferation. The effect of two Cx43 mutations on network sizes were studied to identify the key function, gap junction coupling or adhesion, for proliferation. The function remained elusive. In summary, connexin expression differs among brain regions revealing glial heterogeneity throughout the brain.

Tracer diffusion from astrocytes into the myelin sheath was observed in the ventrobasal thalamus. Such functional gap junction channels between astrocytes and oligodendrocytes were so far unknown. In this study, a panglial network formed by oligodendrocytes and astrocytes was discovered in the hippocampus and the thalamus. Employing Cx30/47 DKO mice, a major impact of Cx30 on panglial network formation was observed in the thalamus. Cx30 and Cx47 do not form functional channels *in vitro*. This leads to the conclusion that panglial coupling is mainly mediated by Cx30:Cx32 channels.

Immunohistochemical analysis in PLP-GFP and Cx43-ECFP mice identified overlapping protein expression of "classical" markers in thalamic astrocytes and oligodendrocytes in contrast to hippocampal glia. S100β was the most reliable marker to distinguish astrocytes and oligodendrocytes in the ventrobasal thalamus. Unexpectedly, an "intermediate" cell-type was identified co-expressing Cx43 and Olig2. It is a mature cell-type which is part of thalamic glial networks and has been described for the first time in this study.

The functional role of panglial networks in metabolite supply to neurons was analysed in the present study. Glucose diffusion from astrocytes to oligodendrocytes was demonstrated in the thalamus employing the fluorescent glucose analogue 2-NBDG in PLP-GFP mice with SR101 labelled astrocytes. For further investigation of glia-neuron interactions, a method to analyse neuronal field potentials in the ventrobasal thalamus

was established and characterized. Extracellular glucose deprivation abolished neuronal postsynaptic field potentials, thereby confirming the neuronal requirement of glial energy supply.
In addition to connexin mediated gap junction channels, the expression of ionotropic AMPA and $GABA_A$ receptors was studied in thalamic astrocytes. In the juvenile thalamus, two astrocyte populations were distinguished by the presence or absence of AMPA receptor expression. The GluA2 subunit was abundantly expressed when AMPA receptors were expressed. All astrocytes expressed $GABA_A$ receptors. They were devoid of the $\alpha 3$ subunit and rarely expressed the $\gamma 2$ subunit required for synaptic $GABA_A$ receptor localization. Instead, all cells expressed the $\gamma 1$ subunit. These data indicate that glial heterogeneity occurs even within a given brain regions.
The present study describes panglial networks in grey matter and their distinct properties among brain regions for the first time. In addition, glial heterogeneity was observed between and within brain regions and enhanced our understanding of glial specializations. In addition, a new "intermediate" cell-type was discovered which is abundantly present in the ventrobasal thalamus.

8 Perspective

The thalamus is the "gate to conciousness" and many studies focused on neurons in this brain region. In the present study, glial cells were extensively characterized in the ventrobasal thalamus and many exciting new properties of glial cells were discovered. Among all results, two major findings challenge our current understanding of glial cells and their function in the brain: Unravelling the role of panglial networks between astrocytes and oligodendrocytes, and the role of the "intermediate" cell-type in the ventrobasal thalamus should be objectives of future studies.

Panglial networks are already established in the second postnatal week and present in both thalamus and hippocampus. Due to the higher number of oligodendrocytes in thalamic glial networks, it will be advantageous to perform functional studies in the ventrobasal thalamus. In this study, a newly established method to assess neuronal activity and neuron-glia interactions in the ventrobasal thalamus was established and can be employed to unravel the function of panglial networks. These networks might play a role in many physiological functions previously attributed to astrocytic networks, e.g. metabolite supply, gliotransmission and K^+ homoeostasis. The experiments performed in the present study suggest a role in metabolite supply to neurons and hence this function should be further investigated. In addition, it might be interesting to analyse the influence of panglial networks on somatosensory input.

Excitingly, the immunohistochemical study identified an "intermediate" cell-type which is abundantly present in the ventrobasal thalamus. The co-expression of previously known "classical" cell-type markers in one cell-type raises the question of their cellular identity and function. Moreover, studying ionotropic receptor expression, two populations of astrocytes were identified by the presence or absence of AMPA receptors. These two populations might account for the "intermediate" cell-type and astrocytes in the ventrobasal thalamus. To answer this question, functional, molecular and immunohistochemical approaches should be combined in future studies. To enhance our understanding of this "intermediate" cell-type, also local specializations of these cells should be considered, as the thalamus is subdivided into several nuclei with highly specific functions. The ventrobasal thalamus contains barreloids which receive signals from the whiskers. Hence, the "intermediate" cell-type might be involved in modulating neuronal activity between barreloids.

9 Appendix

Table 9.1 Cell densities obtained from immunohistochemical analysis in PLP-GFP mice, data are displayed as mean ± SEM cells/mm^3.

Region	**total PLP-GFP**	**only PLP-GFP**	**GFP+GS**	**only GS**
TH	136,911 ± 9,363	7,578 ± 1,978	129,333 ± 8,616	n.a.
HC	22,644 ± 1,573	18,578 ± 1,288	4,067 ± 692	74,175 ± 4,278
Region	**total PLP-GFP**	**only PLP-GFP**	**GFP+NeuN**	
TH	140,867 ± 7,661	140,867 ± 7,661	0	
HC	20,200 ± 1,030	20,200 ± 1,030	0	
Region	**total PLP-GFP**	**only PLP-GFP**	**GFP+GFAP**	**GFP+Iba1**
TH	135,600 ± 8,674	135,600 ± 8,674	0	0
HC	24,267 ± 1,957	24,267 ± 1,957	0	0
Region	**total PLP-GFP**	**only PLP-GFP**	**GFP+S100β**	**GFP+NG2**
TH	158,844 ± 4,092	130,600 ± 2,865	27,933 ± 2,556	289 ± 136
HC	26,447 ± 1,434	16,489 ± 1,184	4,889 ± 785	4,644 ± 408
Region	**S100β+NG2**	**GFP+S100β +NG2**		
TH	22 ± 31	22 ± 31		
HC	622 ± 227	444 ± 116		
Region	**total Aldh1L1**	**only Aldh1L1**	**Aldh1L1+GFP**	**Aldh1L1+Olig2**
TH	65,422 ± 6,242	13,978 ± 3,649	444 ± 522	17,022 ± 4,388
Region	**Aldh1L1+GFP +Olig2**			
TH	33,533 ± 5,111			
Region	**total Cx43-ECFP**	**only Cx43-ECFP**	**Cx43-ECFP+Olig2**	
TH	38,563 ± 1,723	18,293 ± 2,066	20,267 ± 2,917	
HC	52,217 ± 3,215	49,062 ±2,784	3,155 ± 1,107	

Bibliography

Agmon A, Connors BW (1991) Thalamocortical responses of mouse somatosensory (barrel) cortex in vitro. *Neuroscience* 41:365–379.

Agulhon C, Petravicz J, McMullen AB, Sweger EJ, Minton SK, Taves SR, Casper KB, Fiacco TA, McCarthy KD (2008) What is the role of astrocyte calcium in neurophysiology? *Neuron* 59:932–946.

Ahn M, Lee J, Gustafsson A, Enriquez A, Lancaster E, Sul JY, Haydon PG, Paul DL, Huang Y, Abrams CK, Scherer SS (2008) Cx29 and Cx32, two connexins expressed by myelinating glia, do not interact and are functionally distinct. *J Neurosci Res* 86:992–1006.

Allaman I, Bélanger M, Magistretti PJ (2011) Astrocyte-neuron metabolic relationships: for better and for worse. *Trends Neurosci* 34:76–87.

Allen NJ, Barres BA (2009) Neuroscience: Glia - more than just brain glue. *Nature* 457:675–677.

Altevogt BM, Kleopa KA, Postma FR, Scherer SS, Paul DL (2002) Connexin29 is uniquely distributed within myelinating glial cells of the central and peripheral nervous systems. *J Neurosci* 22:6458–6470.

Altevogt BM, Paul DL (2004) Four classes of intercellular channels between glial cells in the CNS. *J Neurosci* 24:4313–4323.

Alvarez-Maubecin V, Garcia-Hernandez F, Williams JT, Van Bockstaele EJ (2000) Functional coupling between neurons and glia. *J Neurosci* 20:4091–4098.

Amaral AI, Meisingset TW, Kotter MR, Sonnewald U (2013) Metabolic aspects of neuron-oligodendrocyte-astrocyte interactions. *Front Endocrinol (Lausanne)* 4:54.

Amaral DG, Witter MP (1989) The three-dimensional organization of the hippocampal formation: a review of anatomical data. *Neuroscience* 31:571–591.

Amat JA, Ishiguro H, Nakamura K, Norton WT (1996) Phenotypic diversity and kinetics of proliferating microglia and astrocytes following cortical stab wounds. *Glia* 16:368–382.

An JH, Su Y, Radman T, Bikson M (2008) Effects of glucose and glutamine concentration in the formulation of the artificial cerebrospinal fluid (ACSF). *Brain Res* 1218:77–86.

Anders S, Minge D, Griemsmann S, Herde MK, Steinhäuser C, Henneberger C (2014) Spatial properties of astrocyte gap junction coupling in the rat hippocampus. *Philos Trans R Soc Lond B Biol Sci* 369:20130600.

Araque A, Parpura V, Sanzgiri RP, Haydon PG (1999) Tripartite synapses: glia, the unacknowledged partner. *Trends Neurosci* 22:208–215.

Barres BA (2008) The mystery and magic of glia: a perspective on their roles in health and disease. *Neuron* 60:430–440.

Barros LF (2013) Metabolic signaling by lactate in the brain. *Trends Neurosci* 36:396–404.

Barros LF, Deitmer JW (2010) Glucose and lactate supply to the synapse. *Brain Res Rev* 63:149–159.

Bear MF, Connors BW, Paradiso MA (2006) *Neuroscience: Exploring the Brain, 3rd Edition* Lippincott Williams and Wilkins, 3rd edition.

Bedner P, Niessen H, Odermatt B, Kretz M, Willecke K, Harz H (2006) Selective permeability of different connexin channels to the second messenger cyclic AMP. *J Biol Chem* 281:6673–6681.

Bedner P, Steinhäuser C, Theis M (2012) Functional redundancy and compensation among members of gap junction protein families? *Biochim Biophys Acta* 1818:1971–1984.

Belluardo N, Mudò G, Trovato-Salinaro A, Le Gurun S, Charollais A, Serre-Beinier V, Amato G, Haefliger JA, Meda P, Condorelli DF (2000) Expression of connexin36 in the adult and developing rat brain. *Brain Res* 865:121–138.

Bennett MVL, Garré JM, Orellana JA, Bukauskas FF, Nedergaard M, Sáez JC (2012) Connexin and pannexin hemichannels in inflammatory responses of glia and neurons. *Brain Res* 1487:3–15.

Bergles DE, Roberts JD, Somogyi P, Jahr CE (2000) Glutamatergic synapses on oligodendrocyte precursor cells in the hippocampus. *Nature* 405:187–191.

Beyer EC, Kistler J, Paul DL, Goodenough DA (1989) Antisera directed against connexin43 peptides react with a 43-kD protein localized to gap junctions in myocardium and other tissues. *J Cell Biol* 108:595–605.

Bezzi P, Gundersen V, Galbete JL, Seifert G, Steinhäuser C, Pilati E, Volterra A (2004) Astrocytes contain a vesicular compartment that is competent for regulated exocytosis of glutamate. *Nat Neurosci* 7:613–620.

Bittman K, Becker DL, Cicirata F, Parnavelas JG (2002) Connexin expression in homotypic and heterotypic cell coupling in the developing cerebral cortex. *J Comp Neurol* 443:201–212.

Blednov YA, Benavidez JM, Black M, Chandra D, Homanics GE, Rudolph U, Harris RA (2013) Linking GABA(A) receptor subunits to alcohol-induced conditioned taste aversion and recovery from acute alcohol intoxication. *Neuropharmacology* 67:46–56.

Blomstrand F, Venance L, Sirén AL, Ezan P, Hanse E, Glowinski J, Ehrenreich H, Giaume C (2004) Endothelins regulate astrocyte gap junctions in rat hippocampal slices. *Eur J Neurosci* 19:1005–1015.

Bosman LWJ, Houweling AR, Owens CB, Tanke N, Shevchouk OT, Rahmati N, Teunissen WHT, Ju C, Gong W, Koekkoek SKE, De Zeeuw CI (2011) Anatomical pathways involved in generating and sensing rhythmic whisker movements. *Front Integr Neurosci* 5:53.

Boulay AC, del Castillo FJ, Giraudet F, Hamard G, Giaume C, Petit C, Avan P, Cohen-Salmon M (2013) Hearing is normal without connexin30. *J Neurosci* 33:430–434.

Bourassa J, Pinault D, Deschênes M (1995) Corticothalamic projections from the cortical barrel field to the somatosensory thalamus in rats: a single-fibre study using biocytin as an anterograde tracer. *Eur J Neurosci* 7:19–30.

Brown AM, Wender R, Ransom BR (2001) Metabolic substrates other than glucose support axon function in central white matter. *J Neurosci Res* 66:839–843.

Brown AM, Ransom BR (2007) Astrocyte glycogen and brain energy metabolism. *Glia* 55:1263–1271.

Bruneau EG, McCullumsmith RE, Haroutunian V, Davis KL, Meador-Woodruff JH (2005) Increased expression of glutaminase and glutamine synthetase mRNA in the thalamus in schizophrenia. *Schizophr Res* 75:27–34.

Burnashev N, Khodorova A, Jonas P, Helm PJ, Wisden W, Monyer H, Seeburg PH, Sakmann B (1992) Calcium-permeable AMPA-kainate receptors in fusiform cerebellar glial cells. *Science* 256:1566–1570.

Bushong EA, Martone ME, Jones YZ, Ellisman MH (2002) Protoplasmic astrocytes in CA1 stratum radiatum occupy separate anatomical domains. *J Neurosci* 22:183–192.

Cahoy JD, Emery B, Kaushal A, Foo LC, Zamanian JL, Christopherson KS, Xing Y, Lubischer JL, Krieg PA, Krupenko SA, Thompson WJ, Barres BA (2008) A transcriptome database for astrocytes, neurons, and oligodendrocytes: a new resource for understanding brain development and function. *J Neurosci* 28:264–278.

Cai J, Chen Y, Cai WH, Hurlock EC, Wu H, Kernie SG, Parada LF, Lu QR (2007) A crucial role for Olig2 in white matter astrocyte development. *Development* 134:1887–1899.

Cammer W (1990) Glutamine synthetase in the central nervous system is not confined to astrocytes. *J Neuroimmunol* 26:173–178.

Castro-Alamancos MA, Calcagnotto ME (1999) Presynaptic long-term potentiation in corticothalamic synapses. *J Neurosci* 19:9090–9097.

Chever O, Lee CY, Rouach N (2014) Astroglial connexin43 hemichannels tune basal excitatory synaptic transmission. *J Neurosci* 34:11228–11232.

Chever O, Pannasch U, Ezan P, Rouach N (2014) Astroglial connexin 43 sustains glutamatergic synaptic efficacy. *Philos Trans R Soc Lond B Biol Sci* 369:20130596.

Christian CA, Huguenard JR (2013) Astrocytes potentiate GABAergic transmission in the thalamic reticular nucleus via endozepine signaling. *Proc Natl Acad Sci U S A* 110:20278–20283.

Chuquet J, Quilichini P, Nimchinsky EA, Buzsáki G (2010) Predominant enhancement of glucose uptake in astrocytes versus neurons during activation of the somatosensory cortex. *J Neurosci* 30:15298–15303.

Cina C, Maass K, Theis M, Willecke K, Bechberger JF, Naus CC (2009) Involvement of the cytoplasmic C-terminal domain of connexin43 in neuronal migration. *J Neurosci* 29:2009–2021.

Cohen-Salmon M, Ott T, Michel V, Hardelin JP, Perfettini I, Eybalin M, Wu T, Marcus DC, Wangemann P, Willecke K, Petit C (2002) Targeted ablation of connexin26 in the inner ear epithelial gap junction network causes hearing impairment and cell death. *Curr Biol* 12:1106–1111.

Connors BW, Long MA (2004) Electrical synapses in the mammalian brain. *Annu Rev Neurosci* 27:393–418.

Cope DW, Di Giovanni G, Fyson SJ, Orbn G, Errington AC, Lorincz ML, Gould TM, Carter DA, Crunelli V (2009) Enhanced tonic GABAA inhibition in typical absence epilepsy. *Nat Med* 15:1392–1398.

Coulter DA, Eid T (2012) Astrocytic regulation of glutamate homeostasis in epilepsy. *Glia* 60:1215–1226.

Crick F, Koch C (2003) A framework for consciousness. *Nat Neurosci* 6:119–126.

Dahl E, Manthey D, Chen Y, Schwarz HJ, Chang YS, Lalley PA, Nicholson BJ, Willecke K (1996) Molecular cloning and functional expression of mouse connexin-30,a gap junction gene highly expressed in adult brain and skin. *J Biol Chem* 271:17903–17910.

D'Amelio FE, Mehler WR, Gibbs MA, Eng LF, Wu JY (1987) Immunocytochemical localization of glutamic acid decarboxylase (GAD) and glutamine synthetase (GS) in the area postrema of the cat. light and electron microscopy. *Brain Res* 410:232–244.

Degen J, Dublin P, Zhang J, Dobrowolski R, Jokwitz M, Karram K, Trotter J, Jabs R, Willecke K, Steinhäuser C, Theis M (2012) Dual reporter approaches for identification of cre efficacy and astrocyte heterogeneity. *FASEB J* 26:4576–4583.

Deng W, Aimone JB, Gage FH (2010) New neurons and new memories: how does adult hippocampal neurogenesis affect learning and memory? *Nat Rev Neurosci* 11:339–350.

Dere E, De Souza-Silva MA, Frisch C, Teubner B, Söhl G, Willecke K, Huston JP (2003) Connexin30-deficient mice show increased emotionality and decreased rearing activity in the open-field along with neurochemical changes. *Eur J Neurosci* 18:629–638.

Dermietzel R, Traub O, Hwang TK, Beyer E, Bennett MV, Spray DC, Willecke K (1989) Differential expression of three gap junction proteins in developing and mature brain tissues. *Proc Natl Acad Sci U S A* 86:10148–10152.

DeSilva TM, Kabakov AY, Goldhoff PE, Volpe JJ, Rosenberg PA (2009) Regulation of glutamate transport in developing rat oligodendrocytes. *J Neurosci* 29:7898–7908.

Dimou L, Simon C, Kirchhoff F, Takebayashi H, Götz M (2008) Progeny of olig2-expressing progenitors in the gray and white matter of the adult mouse cerebral cortex. *J Neurosci* 28:10434–10442.

Dobrowolski R, Sasse P, Schrickel JW, Watkins M, Kim JS, Rackauskas M, Troatz C, Ghanem A, Tiemann K, Degen J, Bukauskas FF, Civitelli R, Lewalter T, Fleischmann BK, Willecke K (2008) The conditional connexin43G138R mouse mutant represents a new model of hereditary oculodentodigital dysplasia in humans. *Hum Mol Genet* 17:539–554.

Doetsch F, Caillé I, Lim DA, García-Verdugo JM, Alvarez-Buylla A (1999) Subventricular zone astrocytes are neural stem cells in the adult mammalian brain. *Cell* 97:703–716.

Doetsch F (2003) The glial identity of neural stem cells. *Nat Neurosci* 6:1127–1134.

Duffy HS, Delmar M, Spray DC (2002) Formation of the gap junction nexus: binding partners for connexins. *J Physiol Paris* 96:243–249.

Elfgang C, Eckert R, Lichtenberg-Fraté H, Butterweck A, Traub O, Klein RA, Hülser DF, Willecke K (1995) Specific permeability and selective formation of gap junction channels in connexin-transfected HeLa cells. *J Cell Biol* 129:805–817.

Elias LAB, Wang DD, Kriegstein AR (2007) Gap junction adhesion is necessary for radial migration in the neocortex. *Nature* 448:901–907.

Enkvist MO, McCarthy KD (1994) Astroglial gap junction communication is increased by treatment with either glutamate or high K+ concentration. *J Neurochem* 62:489–495.

Erzurumlu RS, Murakami Y, Rijli FM (2010) Mapping the face in the somatosensory brainstem. *Nat Rev Neurosci* 11:252–263.

Escartin C, Rouach N (2013) Astroglial networking contributes to neurometabolic coupling. *Front Neuroenergetics* 5:4.

Essrich C, Lorez M, Benson JA, Fritschy JM, Lüscher B (1998) Postsynaptic clustering of major gabaa receptor subtypes requires the gamma 2 subunit and gephyrin. *Nat Neurosci* 1:563–571.

Eugenín EA, Eckardt D, Theis M, Willecke K, Bennett MV, Saez JC (2001) Microglia at brain stab wounds express connexin 43 and in vitro form functional gap junctions after treatment with interferon-gamma and tumor necrosis factor-alpha. *Proc Natl Acad Sci U S A* 98:4190–4195.

Filippov MA, Hormuzdi SG, Fuchs EC, Monyer H (2003a) A reporter allele for investigating connexin 26 gene expression in the mouse brain. *Eur J Neurosci* 18:3183–3192.

Filippov V, Kronenberg G, Pivneva T, Reuter K, Steiner B, Wang LP, Yamaguchi M, Kettenmann H, Kempermann G (2003b) Subpopulation of nestin-expressing progenitor cells in the adult murine hippocampus shows electrophysiological and morphological characteristics of astrocytes. *Mol Cell Neurosci* 23:373–382.

Fraser DD, Duffy S, Angelides KJ, Perez-Velazquez JL, Kettenmann H, MacVicar BA (1995) GABAA/benzodiazepine receptors in acutely isolated hippocampal astrocytes. *J Neurosci* 15:2720–2732.

Frassoni C, Amadeo A, Ortino B, Jaranowska A, Spreafico R (2000) Organization of radial and non-radial glia in the developing rat thalamus. *J Comp Neurol* 428:527–542.

Fukuda S, Kondo T, Takebayashi H, Taga T (2004) Negative regulatory effect of an oligodendrocytic bHLH factor OLIG2 on the astrocytic differentiation pathway. *Cell Death Differ* 11:196–202.

Fünfschilling U, Supplie LM, Mahad D, Boretius S, Saab AS, Edgar J, Brinkmann BG, Kassmann CM, Tzvetanova ID, Möbius W, Diaz F, Meijer D, Suter U, Hamprecht B, Sereda MW, Moraes CT, Frahm J, Goebbels S, Nave KA (2012) Glycolytic oligodendrocytes maintain myelin and long-term axonal integrity. *Nature* 485:517–521.

Fuss B, Mallon B, Phan T, Ohlemeyer C, Kirchhoff F, Nishiyama A, Macklin WB (2000) Purification and analysis of in vivo-differentiated oligodendrocytes expressing the green fluorescent protein. *Dev Biol* 218:259–274.

Gabriel HD, Jung D, Bützler C, Temme A, Traub O, Winterhager E, Willecke K (1998) Transplacental uptake of glucose is decreased in embryonic lethal connexin26-deficient mice. *J Cell Biol* 140:1453–1461.

Giaume C, Fromaget C, el Aoumari A, Cordier J, Glowinski J, Gros D (1991) Gap junctions in cultured astrocytes: single-channel currents and characterization of channel-forming protein. *Neuron* 6:133–143.

Giaume C, Koulakoff A, Roux L, Holcman D, Rouach N (2010) Astroglial networks: a step further in neuroglial and gliovascular interactions. *Nat Rev Neurosci* 11:87–99.

Giaume C, Theis M (2010) Pharmacological and genetic approaches to study connexin-mediated channels in glial cells of the central nervous system. *Brain Res Rev* 63:160–176.

Goldberg GS, Valiunas V, Brink PR (2004) Selective permeability of gap junction channels. *Biochim Biophys Acta* 1662:96–101.

Goodenough DA, Paul DL (2003) Beyond the gap: functions of unpaired connexon channels. *Nat Rev Mol Cell Biol* 4:285–294.

Gosejacob D, Dublin P, Bedner P, Hüttmann K, Zhang J, Tress O, Willecke K, Pfrieger F, Steinhäuser C, Theis M (2011) Role of astroglial connexin30 in hippocampal gap junction coupling. *Glia* 59:511–519.

Grant E, Hoerder-Suabedissen A, Molnár Z (2012) Development of the corticothalamic projections. *Front Neurosci* 6:53.

Griemsmann S, Höft SP, Bedner P, Zhang J, von Staden E, Beinhauer A, Degen J, Dublin P, Cope DW, Richter N, Crunelli V, Jabs R, Willecke K, Theis M, Seifert G, Kettenmann H, Steinhäuser C (2014) Characterization of panglial gap junction networks in the thalamus, neocortex, and hippocampus reveals a unique population of glial cells. *Cereb Cortex* (doi 10.1093/cercor/bhu157).

Grosche J, Matyash V, Möller T, Verkhratsky A, Reichenbach A, Kettenmann H (1999) Microdomains for neuron-glia interaction: parallel fiber signaling to Bergmann glial cells. *Nat Neurosci* 2:139–143.

Guzman SJ, Jonas P (2010) Beyond TARPs: the growing list of auxiliary AMPAR subunits. *Neuron* 66:8–10.

Haberlandt C, Derouiche A, Wyczynski A, Haseleu J, Pohle J, Karram K, Trotter J, Seifert G, Frotscher M, Steinhäuser C, Jabs R (2011) Gray matter NG2 cells display multiple Ca2+-signaling pathways and highly motile processes. *PLoS One* 6:e17575.

Haidarliu S, Ahissar E (2001) Size gradients of barreloids in the rat thalamus. *J Comp Neurol* 429:372–387.

Haydon PG, Carmignoto G (2006) Astrocyte control of synaptic transmission and neurovascular coupling. *Physiol Rev* 86:1009–1031.

Henneberger C, Papouin T, Oliet SHR, Rusakov DA (2010) Long-term potentiation depends on release of D-serine from astrocytes. *Nature* 463:232–236.

Herculano-Houzel S (2014) The glia/neuron ratio: how it varies uniformly across brain structures and species and what that means for brain physiology and evolution. *Glia* 62:1377–1391.

Herculano-Houzel S, Mota B, Lent R (2006) Cellular scaling rules for rodent brains. *Proc Natl Acad Sci U S A* 103:12138–12143.

Hill RA, Grutzendler J (2014) In vivo imaging of oligodendrocytes with sulforhodamine 101. *Nat Methods* 11:1081–1082.

Höft S, Griemsmann S, Seifert G, Steinhäuser C (2014) Heterogeneity in expression of functional ionotropic glutamate and gaba receptors in astrocytes across brain regions: insights from the thalamus. *Philos Trans R Soc Lond B Biol Sci* 369:20130602.

Holthoff K, Witte OW (2000) Directed spatial potassium redistribution in rat neocortex. *Glia* 29:288–292.

Houades V, Koulakoff A, Ezan P, Seif I, Giaume C (2008) Gap junction-mediated astrocytic networks in the mouse barrel cortex. *J Neurosci* 28:5207–5217.

Houades V, Rouach N, Ezan P, Kirchhoff F, Koulakoff A, Giaume C (2006) Shapes of astrocyte networks in the juvenile brain. *Neuron Glia Biol* 2:3–14.

Israel JM, Schipke CG, Ohlemeyer C, Theodosis DT, Kettenmann H (2003) GABAA receptor-expressing astrocytes in the supraoptic nucleus lack glutamate uptake and receptor currents. *Glia* 44:102–110.

Jabs R, Pivneva T, Hüttmann K, Wyczynski A, Nolte C, Kettenmann H, Steinhäuser C (2005) Synaptic transmission onto hippocampal glial cells with hGFAP promoter activity. *J Cell Sci* 118:3791–3803.

Jahn O, Tenzer S, Werner HB (2009) Myelin proteomics: molecular anatomy of an insulating sheath. *Mol Neurobiol* 40:55–72.

Jessen KR, Mirsky R (1985) Glial fibrillary acidic polypeptides in peripheral glia. molecular weight, heterogeneity and distribution. *J Neuroimmunol* 8:377–393.

Kafitz KW, Meier SD, Stephan J, Rose CR (2008) Developmental profile and properties of sulforhodamine 101–labeled glial cells in acute brain slices of rat hippocampus. *J Neurosci Methods* 169:84–92.

Kamasawa N, Sik A, Morita M, Yasumura T, Davidson KGV, Nagy JI, Rash JE (2005) Connexin-47 and connexin-32 in gap junctions of oligodendrocyte somata, myelin sheaths, paranodal loops and Schmidt-Lanterman incisures: implications for ionic homeostasis and potassium siphoning. *Neuroscience* 136:65–86.

Kandel ER, Schwartz JH, Jessell TM, Siegelbaum SA, Hudspeth AJ, editors (2012) *Principles of Neural Science, Fifth Edition (Principles of Neural Science (Kandel))* McGraw-Hill Professional, 5th edition.

Kang J, Jiang L, Goldman SA, Nedergaard M (1998) Astrocyte-mediated potentiation of inhibitory synaptic transmission. *Nat Neurosci* 1:683–692.

Kang J, Kang N, Yu Y, Zhang J, Petersen N, Tian GF, Nedergaard M (2010) Sulforhodamine 101 induces long-term potentiation of intrinsic excitability and synaptic efficacy in hippocampal CA1 pyramidal neurons. *Neuroscience* 169:1601–1609.

Karram K, Goebbels S, Schwab M, Jennissen K, Seifert G, Steinhäuser C, Nave KA, Trotter J (2008) NG2-expressing cells in the nervous system revealed by the NG2-EYFP-knockin mouse. *Genesis* 46:743–757.

Kimelberg HK (2004) The problem of astrocyte identity. *Neurochem Int* 45:191–202.

Klein T, Ling Z, Heimberg H, Madsen OD, Heller RS, Serup P (2003) Nestin is expressed in vascular endothelial cells in the adult human pancreas. *J Histochem Cytochem* 51:697–706.

Krüger O, Plum A, Kim JS, Winterhager E, Maxeiner S, Hallas G, Kirchhoff S, Traub O, Lamers WH, Willecke K (2000) Defective vascular development in connexin 45-deficient mice. *Development* 127:4179–4193.

Kunze A, Congreso MR, Hartmann C, Wallraff-Beck A, Httmann K, Bedner P, Requardt R, Seifert G, Redecker C, Willecke K, Hofmann A, Pfeifer A, Theis M, Steinhäuser C (2009) Connexin expression by radial glia-like cells is required for neurogenesis in the adult dentate gyrus. *Proc Natl Acad Sci U S A* 106:11336–11341.

Kunzelmann P, Schröder W, Traub O, Steinhäuser C, Dermietzel R, Willecke K (1999) Late onset and increasing expression of the gap junction protein connexin30 in adult murine brain and long-term cultured astrocytes. *Glia* 25:111–119.

Laird DW (2006) Life cycle of connexins in health and disease. *Biochem J* 394:527–543.

Lallemand Y, Luria V, Haffner-Krausz R, Lonai P (1998) Maternally expressed PGK-cre transgene as a tool for early and uniform activation of the cre site-specific recombinase. *Transgenic Res* 7:105–112.

Lampe PD, Lau AF (2000) Regulation of gap junctions by phosphorylation of connexins. *Arch Biochem Biophys* 384:205–215.

Landisman CE, Connors BW (2005) Long-term modulation of electrical synapses in the mammalian thalamus. *Science* 310:1809–1813.

Langlet F (2014) Tanycytes, a gateway to the metabolic hypothalamus. *J Neuroendocrinol* 26:753–760.

Laurie DJ, Seeburg PH, Wisden W (1992) The distribution of 13 GABAA receptor subunit mRNAs in the rat brain. II. Olfactory bulb and cerebellum. *J Neurosci* 12:1063–1076.

Lee SC, Cruikshank SJ, Connors BW (2010) Electrical and chemical synapses between relay neurons in developing thalamus. *J Physiol* 588:2403–2415.

Lee SC, Patrick SL, Richardson KA, Connors BW (2014) Two functionally distinct networks of gap junction-coupled inhibitory neurons in the thalamic reticular nucleus. *J Neurosci* 34:13170–13182.

Lee Y, Morrison BM, Li Y, Lengacher S, Farah MH, Hoffman PN, Liu Y, Tsingalia A, Jin L, Zhang PW, Pellerin L, Magistretti PJ, Rothstein JD (2012) Oligodendroglia metabolically support axons and contribute to neurodegeneration. *Nature* 487:443–448.

Li X, Lynn BD, Olson C, Meier C, Davidson KGV, Yasumura T, Rash JE, Nagy JI (2002) Connexin29 expression, immunocytochemistry and freeze-fracture replica immunogold labelling (FRIL) in sciatic nerve. *Eur J Neurosci* 16:795–806.

Li X, Penes M, Odermatt B, Willecke K, Nagy JI (2008) Ablation of Cx47 in transgenic mice leads to the loss of MUPP1, ZONAB and multiple connexins at oligodendrocyte-astrocyte gap junctions. *Eur J Neurosci* 28:1503–1517.

Liebmann M, Stahr A, Guenther M, Witte OW, Frahm C (2013) Astrocytic Cx43 and Cx30 differentially modulate adult neurogenesis in mice. *Neurosci Lett* 545:40–45.

López-Bendito G, Molnár Z (2003) Thalamocortical development: how are we going to get there? *Nat Rev Neurosci* 4:276–289.

Losi G, Mariotti L, Carmignoto G (2014) GABAergic interneuron to astrocyte signalling: a neglected form of cell communication in the brain. *Philos Trans R Soc Lond B Biol Sci* 369:20130609.

Lübkemeier I, Requardt RP, Lin X, Sasse P, Andri R, Schrickel JW, Chkourko H, Bukauskas FF, Kim JS, Frank M, Malan D, Zhang J, Wirth A, Dobrowolski R, Mohler PJ, Offermanns S, Fleischmann BK, Delmar M, Willecke K (2013) Deletion of the last five C-terminal amino acid residues of connexin43 leads to lethal ventricular arrhythmias in mice without affecting coupling via gap junction channels. *Basic Res Cardiol* 108:348.

Lutz SE, Zhao Y, Gulinello M, Lee SC, Raine CS, Brosnan CF (2009) Deletion of astrocyte connexins 43 and 30 leads to a dysmyelinating phenotype and hippocampal CA1 vacuolation. *J Neurosci* 29:7743–7752.

Lynn BD, Tress O, May D, Willecke K, Nagy JI (2011) Ablation of connexin30 in transgenic mice alters expression patterns of connexin26 and connexin32 in glial cells and leptomeninges. *Eur J Neurosci* 34:1783–1793.

Maass K, Ghanem A, Kim JS, Saathoff M, Urschel S, Kirfel G, Grmmer R, Kretz M, Lewalter T, Tiemann K, Winterhager E, Herzog V, Willecke K (2004) Defective epidermal barrier in neonatal mice lacking the C-terminal region of connexin43. *Mol Biol Cell* 15:4597–4608.

Maass K, Shibayama J, Chase SE, Willecke K, Delmar M (2007) C-terminal truncation of connexin43 changes number, size, and localization of cardiac gap junction plaques. *Circ Res* 101:1283–1291.

Maeda S, Nakagawa S, Suga M, Yamashita E, Oshima A, Fujiyoshi Y, Tsukihara T (2009) Structure of the connexin 26 gap junction channel at 3.5 a resolution. *Nature* 458:597–602.

Maglione M, Tress O, Haas B, Karram K, Trotter J, Willecke K, Kettenmann H (2010) Oligodendrocytes in mouse corpus callosum are coupled via gap junction channels formed by connexin47 and connexin32. *Glia* 58:1104–1117.

Magnotti LM, Goodenough DA, Paul DL (2011a) Deletion of oligodendrocyte cx32 and astrocyte cx43 causes white matter vacuolation, astrocyte loss and early mortality. *Glia* 59:1064–1074.

Magnotti LM, Goodenough DA, Paul DL (2011b) Functional heterotypic interactions between astrocyte and oligodendrocyte connexins. *Glia* 59:26–34.

Mallon BS, Shick HE, Kidd GJ, Macklin WB (2002) Proteolipid promoter activity distinguishes two populations of NG2-positive cells throughout neonatal cortical development. *J Neurosci* 22:876–885.

Marshall CAG, Novitch BG, Goldman JE (2005) Olig2 directs astrocyte and oligodendrocyte formation in postnatal subventricular zone cells. *J Neurosci* 25:7289–7298.

Martin SJ, Morris RGM (2002) New life in an old idea: the synaptic plasticity and memory hypothesis revisited. *Hippocampus* 12:609–636.

Martinez-Hernandez A, Bell KP, Norenberg MD (1977) Glutamine synthetase: glial localization in brain. *Science* 195:1356–1358.

Massa PT, Mugnaini E (1982) Cell junctions and intramembrane particles of astrocytes and oligodendrocytes: a freeze-fracture study. *Neuroscience* 7:523–538.

Matthias K, Kirchhoff F, Seifert G, Hüttmann K, Matyash M, Kettenmann H, Steinhäuser C (2003) Segregated expression of AMPA-type glutamate receptors and glutamate transporters defines distinct astrocyte populations in the mouse hippocampus. *J Neurosci* 23:1750–1758.

Matyash V, Kettenmann H (2010) Heterogeneity in astrocyte morphology and physiology. *Brain Res Rev* 63:2–10.

Maxeiner S, Krüger O, Schilling K, Traub O, Urschel S, Willecke K (2003) Spatiotemporal transcription of connexin45 during brain development results in neuronal expression in adult mice. *Neuroscience* 119:689–700.

May D, Tress O, Seifert G, Willecke K (2013) Connexin47 protein phosphorylation and stability in oligodendrocytes depend on expression of connexin43 protein in astrocytes. *J Neurosci* 33:7985–7996.

McKenna MC (2011) Glutamate dehydrogenase in brain mitochondria: do lipid modifications and transient metabolon formation influence enzyme activity? *Neurochem Int* 59:525–533.

Meier SD, Kafitz KW, Rose CR (2008) Developmental profile and mechanisms of GABA-induced calcium signaling in hippocampal astrocytes. *Glia* 56:1127–1137.

Menichella DM, Goodenough DA, Sirkowski E, Scherer SS, Paul DL (2003) Connexins are critical for normal myelination in the CNS. *J Neurosci* 23:5963–5973.

Menichella DM, Majdan M, Awatramani R, Goodenough DA, Sirkowski E, Scherer SS, Paul DL (2006) Genetic and physiological evidence that oligodendrocyte gap junctions contribute to spatial buffering of potassium released during neuronal activity. *J Neurosci* 26:10984–10991.

Mercier F, Hatton GI (2001) Connexin 26 and basic fibroblast growth factor are expressed primarily in the subpial and subependymal layers in adult brain parenchyma: roles in stem cell proliferation and morphological plasticity? *J Comp Neurol* 431:88–104.

Miyake T, Kitamura T (1992) Glutamine synthetase immunoreactivity in two types of mouse brain glial cells. *Brain Res* 586:53–60.

Mohseni P, Sung HK, Murphy AJ, Laliberte CL, Pallari HM, Henkelman M, Georgiou J, Xie G, Quaggin SE, Thorner PS, Eriksson JE, Nagy A (2011) Nestin is not essential for development of the CNS but required for dispersion of acetylcholine receptor clusters at the area of neuromuscular junctions. *J Neurosci* 31:11547–11552.

Montoro RJ, Yuste R (2004) Gap junctions in developing neocortex: a review. *Brain Res Brain Res Rev* 47:216–226.

Morrison BM, Lee Y, Rothstein JD (2013) Oligodendroglia: metabolic supporters of axons. *Trends Cell Biol* 23:644–651.

Mothet JP, Pollegioni L, Ouanounou G, Martineau M, Fossier P, Baux G (2005) Glutamate receptor activation triggers a calcium-dependent and snare protein-dependent release of the gliotransmitter D-serine. *Proc Natl Acad Sci U S A* 102:5606–5611.

Mozrzymas JW, Barberis A, Vicini S (2007) GABAergic currents in RT and VB thalamic nuclei follow kinetic pattern of alpha3- and alpha1-subunit-containing GABAA receptors. *Eur J Neurosci* 26:657–665.

Müller T, Möller T, Berger T, Schnitzer J, Kettenmann H (1992) Calcium entry through kainate receptors and resulting potassium-channel blockade in Bergmann glial cells. *Science* 256:1563–1566.

Muneoka K, Funahashi H, Ogawa T, Whitaker-Azmitia PM, Shioda S (2012) Shared features of S100B immunohistochemistry and cytochrome oxidase histochemistry in the ventroposterior thalamus and lateral habenula in neonatal rats. *Int J Dev Neurosci* 30:499–505.

Nagy JI, Ionescu AV, Lynn BD, Rash JE (2003) Coupling of astrocyte connexins Cx26, Cx30, Cx43 to oligodendrocyte Cx29, Cx32, Cx47: Implications from normal and connexin32 knockout mice. *Glia* 44:205–218.

Nagy JI, Li X, Rempel J, Stelmack G, Patel D, Staines WA, Yasumura T, Rash JE (2001) Connexin26 in adult rodent central nervous system: demonstration at astrocytic gap junctions and colocalization with connexin30 and connexin43. *J Comp Neurol* 441:302–323.

Nagy JI, Lynn BD, Tress O, Willecke K, Rash JE (2011) Connexin26 expression in brain parenchymal cells demonstrated by targeted connexin ablation in transgenic mice. *Eur J Neurosci* 34:263–271.

Nagy JI, Patel D, Ochalski PA, Stelmack GL (1999) Connexin30 in rodent, cat and human brain: selective expression in gray matter astrocytes, co-localization with connexin43 at gap junctions and late developmental appearance. *Neuroscience* 88:447–468.

Nagy JI, Dudek FE, Rash JE (2004) Update on connexins and gap junctions in neurons and glia in the mammalian nervous system. *Brain Res Brain Res Rev* 47:191–215.

Nagy JI, Ionescu AV, Lynn BD, Rash JE (2003) Connexin29 and connexin32 at oligodendrocyte and astrocyte gap junctions and in myelin of the mouse central nervous system. *J Comp Neurol* 464:356–370.

Nagy JI, Rash JE (2003) Astrocyte and oligodendrocyte connexins of the glial syncytium in relation to astrocyte anatomical domains and spatial buffering. *Cell Commun Adhes* 10:401–406.

Nave KA (2010) Myelination and support of axonal integrity by glia. *Nature* 468:244–252.

Nedergaard M, Ransom B, Goldman SA (2003) New roles for astrocytes: redefining the functional architecture of the brain. *Trends Neurosci* 26:523–530.

Neher E, Sakmann B (1976) Single-channel currents recorded from membrane of denervated frog muscle fibres. *Nature* 260:799–802.

Nelles E, Bützler C, Jung D, Temme A, Gabriel HD, Dahl U, Traub O, Stümpel F, Jungermann K, Zielasek J, Toyka KV, Dermietzel R, Willecke K (1996) Defective propagation of signals generated by sympathetic nerve stimulation in the liver of connexin32-deficient mice. *Proc Natl Acad Sci U S A* 93:9565–9570.

Niculescu D, Lohmann C (2013) Gap junctions in developing thalamic and neocortical neuronal networks. *Cereb Cortex* 24:3097–3106.

Niermann H, Amiry-Moghaddam M, Holthoff K, Witte OW, Ottersen OP (2001) A novel role of vasopressin in the brain: modulation of activity-dependent water flux in the neocortex. *J Neurosci* 21:3045–3051.

Nimmerjahn A, Kirchhoff F, Kerr JND, Helmchen F (2004) Sulforhodamine 101 as a specific marker of astroglia in the neocortex in vivo. *Nat Methods* 1:31–37.

Nishiyama A, Komitova M, Suzuki R, Zhu X (2009) Polydendrocytes (NG2 cells): multifunctional cells with lineage plasticity. *Nat Rev Neurosci* 10:9–22.

Nolte C, Matyash M, Pivneva T, Schipke CG, Ohlemeyer C, Hanisch UK, Kirchhoff F, Kettenmann H (2001) GFAP promoter-controlled EGFP-expressing transgenic mice: a tool to visualize astrocytes and astrogliosis in living brain tissue. *Glia* 33:72–86.

Norenberg MD (1979) Distribution of glutamine synthetase in the rat central nervous system. *J Histochem Cytochem* 27:756–762.

Odermatt B, Wellershaus K, Wallraff A, Seifert G, Degen J, Euwens C, Fuss B, Büssow H, Schilling K, Steinhäuser C, Willecke K (2003) Connexin 47 (Cx47)-deficient mice with enhanced green fluorescent protein reporter gene reveal predominant oligodendrocytic expression of Cx47 and display vacuolized myelin in the CNS. *J Neurosci* 23:4549–4559.

Ogata K, Kosaka T (2002) Structural and quantitative analysis of astrocytes in the mouse hippocampus. *Neuroscience* 113:221–233.

Orellana JA, Stehberg J (2014) Hemichannels: new roles in astroglial function. *Front Physiol* 5:193.

Orkand RK, Nicholls JG, Kuffler SW (1966) Effect of nerve impulses on the membrane potential of glial cells in the central nervous system of amphibia. *J Neurophysiol* 29:788–806.

Orthmann-Murphy JL, Abrams CK, Scherer SS (2008) Gap junctions couple astrocytes and oligodendrocytes. *J Mol Neurosci* 35:101–116.

Orthmann-Murphy JL, Enriquez AD, Abrams CK, Scherer SS (2007a) Loss-of-function GJA12/Connexin47 mutations cause Pelizaeus-Merzbacher-like disease. *Mol Cell Neurosci* 34:629–641.

Orthmann-Murphy JL, Freidin M, Fischer E, Scherer SS, Abrams CK (2007b) Two distinct heterotypic channels mediate gap junction coupling between astrocyte and oligodendrocyte connexins. *J Neurosci* 27:13949–13957.

Pannasch U, Derangeon M, Chever O, Rouach N (2012) Astroglial gap junctions shape neuronal network activity. *Commun Integr Biol* 5:248–254.

Pannasch U, Freche D, Dallérac G, Ghézali G, Escartin C, Ezan P, Cohen-Salmon M, Benchenane K, Abudara V, Dufour A, Lübke JHR, Déglon N, Knott G, Holcman D, Rouach N (2014) Connexin 30 sets synaptic strength by controlling astroglial synapse invasion. *Nat Neurosci* 17:549–558.

Pannasch U, Rouach N (2013) Emerging role for astroglial networks in information processing: from synapse to behavior. *Trends Neurosci* 36:405–417.

Pannasch U, Vargová L, Reingruber J, Ezan P, Holcman D, Giaume C, Syková E, Rouach N (2011) Astroglial networks scale synaptic activity and plasticity. *Proc Natl Acad Sci U S A* 108:8467–8472.

Paolicelli RC, Bolasco G, Pagani F, Maggi L, Scianni M, Panzanelli P, Giustetto M, Ferreira TA, Guiducci E, Dumas L, Ragozzino D, Gross CT (2011) Synaptic pruning by microglia is necessary for normal brain development. *Science* 333:1456–1458.

Parri HR, Crunelli V (2001) Pacemaker calcium oscillations in thalamic astrocytes in situ. *Neuroreport* 12:3897–3900.

Parri HR, Gould TM, Crunelli V (2001) Spontaneous astrocytic Ca2+ oscillations in situ drive NMDAR-mediated neuronal excitation. *Nat Neurosci* 4:803–812.

Parri HR, Crunelli V (2002) Astrocytes, spontaneity, and the developing thalamus. *J Physiol Paris* 96:221–230.

Parri HR, Gould TM, Crunelli V (2010) Sensory and cortical activation of distinct glial cell subtypes in the somatosensory thalamus of young rats. *Eur J Neurosci* 32:29–40.

Passlick S, Grauer M, Schäfer C, Jabs R, Seifert G, Steinhäuser C (2013) Expression of the 2-subunit distinguishes synaptic and extrasynaptic GABA(A) receptors in NG2 cells of the hippocampus. *J Neurosci* 33:12030–12040.

Passlick S, Trotter J, Seifert G, Steinhäuser C, Jabs R (2014) The NG2 protein is not required for glutamatergic neuron-ng2 cell synaptic signaling. *Cereb Cortex* (doi 10.1093/cercor/bhu171).

Pellerin L, Magistretti PJ (1994) Glutamate uptake into astrocytes stimulates aerobic glycolysis: a mechanism coupling neuronal activity to glucose utilization. *Proc Natl Acad Sci U S A* 91:10625–10629.

Pellerin L, Magistretti PJ (2012) Sweet sixteen for ANLS. *J Cereb Blood Flow Metab* 32:1152–1166.

Perea G, Navarrete M, Araque A (2009) Tripartite synapses: astrocytes process and control synaptic information. *Trends Neurosci* 32:421–431.

Pereda AE (2014) Electrical synapses and their functional interactions with chemical synapses. *Nat Rev Neurosci* 15:250–263.

Pinault D (2011) Dysfunctional thalamus-related networks in schizophrenia. *Schizophr Bull* 37:238–243.

Pirttimaki TM, Parri HR (2012) Glutamatergic input-output properties of thalamic astrocytes. *Neuroscience* 205:18–28.

Porter JT, McCarthy KD (1997) Astrocytic neurotransmitter receptors in situ and in vivo. *Prog Neurobiol* 51:439–455.

Ralston r H (1969) The synaptic organization of lemniscal projections to the ventrobasal thalamus of the cat. *Brain Res* 14:99–115.

Rampon C, Jiang CH, Dong H, Tang YP, Lockhart DJ, Schultz PG, Tsien JZ, Hu Y (2000) Effects of environmental enrichment on gene expression in the brain. *Proc Natl Acad Sci U S A* 97:12880–12884.

Ransom BR, Fern R (1997) Does astrocytic glycogen benefit axon function and survival in CNS white matter during glucose deprivation? *Glia* 21:134–141.

Rash JE (2010) Molecular disruptions of the panglial syncytium block potassium siphoning and axonal saltatory conduction: pertinence to neuromyelitis optica and other demyelinating diseases of the central nervous system. *Neuroscience* 168:982–1008.

Rash JE, Yasumura T, Davidson KG, Furman CS, Dudek FE, Nagy JI (2001) Identification of cells expressing Cx43, Cx30, Cx26, Cx32 and Cx36 in gap junctions of rat brain and spinal cord. *Cell Commun Adhes* 8:315–320.

Rash JE, Yasumura T, Dudek FE (1998) Ultrastructure, histological distribution, and freeze-fracture immunocytochemistry of gap junctions in rat brain and spinal cord. *Cell Biol Int* 22:731–749.

Rash JE, Yasumura T, Dudek FE, Nagy JI (2001) Cell-specific expression of connexins and evidence of restricted gap junctional coupling between glial cells and between neurons. *J Neurosci* 21:1983–2000.

Reaume AG, de Sousa PA, Kulkarni S, Langille BL, Zhu D, Davies TC, Juneja SC, Kidder GM, Rossant J (1995) Cardiac malformation in neonatal mice lacking connexin43. *Science* 267:1831–1834.

Renzel R, Sadek AR, Chang CH, Gray WP, Seifert G, Steinhäuser C (2013) Polarized distribution of AMPA, but not GABAA , receptors in radial glia-like cells of the adult dentate gyrus. *Glia* 61:1146–1154.

Requardt RP, Kaczmarczyk L, Dublin P, Wallraff-Beck A, Mikeska T, Degen J, Waha A, Steinhäuser C, Willecke K, Theis M (2009) Quality control of astrocyte-directed cre transgenic mice: the benefits of a direct link between loss of gene expression and reporter activation. *Glia* 57:680–692.

Richter N, Wendt S, Georgieva PB, Hambardzumyan D, Nolte C, Kettenmann H (2014) Glioma-associated microglia and macrophages/monocytes display distinct electrophysiological properties and do not communicate via gap junctions. *Neurosci Lett* 583C:130–135.

Rock RB, Gekker G, Hu S, Sheng WS, Cheeran M, Lokensgard JR, Peterson PK (2004) Role of microglia in central nervous system infections. *Clin Microbiol Rev* 17:942–964.

Rothermundt M, Falkai P, Ponath G, Abel S, Brkle H, Diedrich M, Hetzel G, Peters M, Siegmund A, Pedersen A, Maier W, Schramm J, Suslow T, Ohrmann P, Arolt V (2004) Glial cell dysfunction in schizophrenia indicated by increased S100B in the CSF. *Mol Psychiatry* 9:897–899.

Rouach N, Avignone E, Même W, Koulakoff A, Venance L, Blomstrand F, Giaume C (2002) Gap junctions and connexin expression in the normal and pathological central nervous system. *Biol Cell* 94:457–475.

Rouach N, Koulakoff A, Abudara V, Willecke K, Giaume C (2008) Astroglial metabolic networks sustain hippocampal synaptic transmission. *Science* 322:1551–1555.

Roux L, Benchenane K, Rothstein JD, Bonvento G, Giaume C (2011) Plasticity of astroglial networks in olfactory glomeruli. *Proc Natl Acad Sci U S A* 108:18442–18446.

Rozental R, Giaume C, Spray DC (2000) Gap junctions in the nervous system. *Brain Res Brain Res Rev* 32:11–15.

Runquist M, Alonso G (2003) Gabaergic signaling mediates the morphological organization of astrocytes in the adult rat forebrain. *Glia* 41:137–151.

Saab AS, Neumeyer A, Jahn HM, Cupido A, imek AAM, Boele HJ, Scheller A, Le Meur K, Gtz M, Monyer H, Sprengel R, Rubio ME, Deitmer JW, De Zeeuw CI, Kirchhoff F (2012) Bergmann glial AMPA receptors are required for fine motor coordination. *Science* 337:749–753.

Sahlender DA, Savtchouk I, Volterra A (2014) What do we know about gliotransmitter release from astrocytes? *Philos Trans R Soc Lond B Biol Sci* 369:20130592.

Sargiannidou I, Vavlitou N, Aristodemou S, Hadjisavvas A, Kyriacou K, Scherer SS, Kleopa KA (2009) Connexin32 mutations cause loss of function in schwann cells and oligodendrocytes leading to PNS and CNS myelination defects. *J Neurosci* 29:4736–4749.

Scherer SS, Deschênes SM, Xu YT, Grinspan JB, Fischbeck KH, Paul DL (1995) Connexin32 is a myelin-related protein in the PNS and CNS. *J Neurosci* 15:8281–8294.

Scherer SS, Xu YT, Nelles E, Fischbeck K, Willecke K, Bone LJ (1998) Connexin32-null mice develop demyelinating peripheral neuropathy. *Glia* 24:8–20.

Schmechel DE, Rakic P (1979) A Golgi study of radial glial cells in developing monkey telencephalon: morphogenesis and transformation into astrocytes. *Anat Embryol (Berl)* 156:115–152.

Schnell C, Hagos Y, Hülsmann S (2012) Active sulforhodamine 101 uptake into hippocampal astrocytes. *PLoS One* 7:e49398.

Schnell C, Shahmoradi A, Wichert SP, Mayerl S, Hagos Y, Heuer H, Rossner MJ, Hülsmann S (2013) The multispecific thyroid hormone transporter OATP1C1 mediates cell-specific sulforhodamine 101-labeling of hippocampal astrocytes. *Brain Struct Funct* (doi 10.1007/s00429-013-0645-0).

Schools GP, Zhou M, Kimelberg HK (2006) Development of gap junctions in hippocampal astrocytes: evidence that whole cell electrophysiological phenotype is an intrinsic property of the individual cell. *J Neurophysiol* 96:1383–1392.

Seifert G, Steinhäuser C (1995) Glial cells in the mouse hippocampus express AMPA receptors with an intermediate Ca2+ permeability. *Eur J Neurosci* 7:1872–1881.

Seifert G, Hüttmann K, Binder DK, Hartmann C, Wyczynski A, Neusch C, Steinhäuser C (2009) Analysis of astroglial K+ channel expression in the developing hippocampus reveals a predominant role of the Kir4.1 subunit. *J Neurosci* 29:7474–7488.

Seifert G, Weber M, Schramm J, Steinhäuser C (2003) Changes in splice variant expression and subunit assembly of AMPA receptors during maturation of hippocampal astrocytes. *Mol Cell Neurosci* 22:248–258.

Seri B, Garca-Verdugo JM, McEwen BS, Alvarez-Buylla A (2001) Astrocytes give rise to new neurons in the adult mammalian hippocampus. *J Neurosci* 21:7153–7160.

Sherman SM, Guillery RW (2002) The role of the thalamus in the flow of information to the cortex. *Philos Trans R Soc Lond B Biol Sci* 357:1695–1708.

Sierra A, Abiega O, Shahraz A, Neumann H (2013) Janus-faced microglia: beneficial and detrimental consequences of microglial phagocytosis. *Front Cell Neurosci* 7:6.

Söhl G, Eiberger J, Jung YT, Kozak CA, Willecke K (2001) The mouse gap junction gene connexin29 is highly expressed in sciatic nerve and regulated during brain development. *Biol Chem* 382:973–978.

Söhl G, Maxeiner S, Willecke K (2005) Expression and functions of neuronal gap junctions. *Nat Rev Neurosci* 6:191–200.

Söhl G, Willecke K (2003) An update on connexin genes and their nomenclature in mouse and man. *Cell Commun Adhes* 10:173–180.

Solan JL, Lampe PD (2014) Specific Cx43 phosphorylation events regulate gap junction turnover in vivo. *FEBS Lett* 588:1423–1429.

Sonnewald U, Westergaard N, Schousboe A (1997) Glutamate transport and metabolism in astrocytes. *Glia* 21:56–63.

Spassky N, Merkle FT, Flames N, Tramontin AD, Garca-Verdugo JM, Alvarez-Buylla A (2005) Adult ependymal cells are postmitotic and are derived from radial glial cells during embryogenesis. *J Neurosci* 25:10–18.

Stallcup WB (1981) The NG2 antigen, a putative lineage marker: immunofluorescent localization in primary cultures of rat brain. *Dev Biol* 83:154–165.

Stegmüller J, Werner H, Nave KA, Trotter J (2003) The proteoglycan NG2 is complexed with alpha-amino-3-hydroxy-5-methyl-4-isoxazolepropionic acid (AMPA) receptors by the PDZ glutamate receptor interaction protein (GRIP) in glial progenitor cells. implications for glial-neuronal signaling. *J Biol Chem* 278:3590–3598.

Stein V, Hermans-Borgmeyer I, Jentsch TJ, Hübner CA (2004) Expression of the KCl cotransporter KCC2 parallels neuronal maturation and the emergence of low intracellular chloride. *J Comp Neurol* 468:57–64.

Steinhäuser C, Jabs R, Kettenmann H (1994) Properties of GABA and glutamate responses in identified glial cells of the mouse hippocampal slice. *Hippocampus* 4:19–35.

Strohschein S, Hüttmann K, Gabriel S, Binder DK, Heinemann U, Steinhäuser C (2011) Impact of aquaporin-4 channels on K+ buffering and gap junction coupling in the hippocampus. *Glia* 59:973–980.

Suzuki A, Stern SA, Bozdagi O, Huntley GW, Walker RH, Magistretti PJ, Alberini CM (2011) Astrocyte-neuron lactate transport is required for long-term memory formation. *Cell* 144:810–823.

Takasaki C, Yamasaki M, Uchigashima M, Konno K, Yanagawa Y, Watanabe M (2010) Cytochemical and cytological properties of perineuronal oligodendrocytes in the mouse cortex. *Eur J Neurosci* 32:1326–1336.

Taketo M, Schroeder AC, Mobraaten LE, Gunning KB, Hanten G, Fox RR, Roderick TH, Stewart CL, Lilly F, Hansen CT (1991) FVB/N: an inbred mouse strain preferable for transgenic analyses. *Proc Natl Acad Sci U S A* 88:2065–2069.

Tekkök SB, Brown AM, Westenbroek R, Pellerin L, Ransom BR (2005) Transfer of glycogen-derived lactate from astrocytes to axons via specific monocarboxylate transporters supports mouse optic nerve activity. *J Neurosci Res* 81:644–652.

Teubner B, Odermatt B, Guldenagel M, Sohl G, Degen J, Bukauskas F, Kronengold J, Verselis VK, Jung YT, Kozak CA, Schilling K, Willecke K (2001) Functional expression of the new gap junction gene connexin47 transcribed in mouse brain and spinal cord neurons. *J Neurosci* 21:1117–1126.

Teubner B, Michel V, Pesch J, Lautermann J, Cohen-Salmon M, Söhl G, Jahnke K, Winterhager E, Herberhold C, Hardelin JP, Petit C, Willecke K (2003) Connexin30 (Gjb6)-deficiency causes severe hearing impairment and lack of endocochlear potential. *Hum Mol Genet* 12:13–21.

Theis M, Mas C, Döring B, Krger O, Herrera P, Meda P, Willecke K (2001) General and conditional replacement of connexin43-coding DNA by a lacz reporter gene for cell-autonomous analysis of expression. *Cell Commun Adhes* 8:383–386.

Theis M, Giaume C (2012) Connexin-based intercellular communication and astrocyte heterogeneity. *Brain Res* 1487:88–98.

Theis M, Jauch R, Zhuo L, Speidel D, Wallraff A, Döring B, Frisch C, Söhl G, Teubner B, Euwens C, Huston J, Steinhuser C, Messing A, Heinemann U, Willecke K (2003) Accelerated hippocampal spreading depression and enhanced locomotory activity in mice with astrocyte-directed inactivation of connexin43. *J Neurosci* 23:766–776.

Theis M, Shl G, Eiberger J, Willecke K (2005) Emerging complexities in identity and function of glial connexins. *Trends Neurosci* 28:188–195.

Trapp BD, Nishiyama A, Cheng D, Macklin W (1997) Differentiation and death of premyelinating oligodendrocytes in developing rodent brain. *J Cell Biol* 137:459–468.

Tress O, Maglione M, May D, Pivneva T, Richter N, Seyfarth J, Binder S, Zlomuzica A, Seifert G, Theis M, Dere E, Kettenmann H, Willecke K (2012) Panglial gap junctional communication is essential for maintenance of myelin in the CNS. *J Neurosci* 32:7499–7518.

Tress O, Maglione M, Zlomuzica A, May D, Dicke N, Degen J, Dere E, Kettenmann H, Hartmann D, Willecke K (2011) Pathologic and phenotypic alterations in a mouse expressing a connexin47 missense mutation that causes Pelizaeus-Merzbacher-like disease in humans. *PLoS Genet* 7:e1002146.

Tronche F, Kellendonk C, Kretz O, Gass P, Anlag K, Orban PC, Bock R, Klein R, Schütz G (1999) Disruption of the glucocorticoid receptor gene in the nervous system results in reduced anxiety. *Nat Genet* 23:99–103.

Trotter J, Karram K, Nishiyama A (2010) NG2 cells: Properties, progeny and origin. *Brain Res Rev* 63:72–82.

van den Berg CJ, Garfinkel D (1971) A stimulation study of brain compartments. metabolism of glutamate and related substances in mouse brain. *Biochem J* 123:211–218.

Van Der Loos H (1976) Barreloids in mouse somatosensory thalamus. *Neurosci Lett* 2:1–6.

Vélez-Fort M, Audinat E, Angulo MC (2012) Central role of GABA in neuron-glia interactions. *Neuroscientist* 18:237–250.

Verity AN, Campagnoni AT (1988) Regional expression of myelin protein genes in the developing mouse brain: in situ hybridization studies. *J Neurosci Res* 21:238–248.

Virchow R (1846) Über das granulierte Ansehen der Wandungen der Gehirnventrikel. *Allg. Z. Psychiatr.* 3:242–250.

Wallraff A, Köhling R, Heinemann U, Theis M, Willecke K, Steinhäuser C (2006) The impact of astrocytic gap junctional coupling on potassium buffering in the hippocampus. *J Neurosci* 26:5438–5447.

Wallraff A, Odermatt B, Willecke K, Steinhäuser C (2004) Distinct types of astroglial cells in the hippocampus differ in gap junction coupling. *Glia* 48:36–43.

Wang DD, Bordey A (2008) The astrocyte odyssey. *Prog Neurobiol* 86:342–367.

Wang LP, Cheung G, Kronenberg G, Gertz K, Ji S, Kempermann G, Endres M, Kettenmann H (2008) Mild brain ischemia induces unique physiological properties in striatal astrocytes. *Glia* 56:925–934.

Wasseff SK, Scherer SS (2011) Cx32 and Cx47 mediate oligodendrocyte:astrocyte and oligodendrocyte:oligodendrocyte gap junction coupling. *Neurobiol Dis* 42:506–513.

Wasseff SK, Scherer SS (2014) Activated microglia do not form functional gap junctions in vivo. *J Neuroimmunol* 269:90–93.

Wender R, Brown AM, Fern R, Swanson RA, Farrell K, Ransom BR (2000) Astrocytic glycogen influences axon function and survival during glucose deprivation in central white matter. *J Neurosci* 20:6804–6810.

Willecke K, Eiberger J, Degen J, Eckardt D, Romualdi A, Güldenagel M, Deutsch U, Söhl G (2002) Structural and functional diversity of connexin genes in the mouse and human genome. *Biol Chem* 383:725–737.

Wisden W, Laurie DJ, Monyer H, Seeburg PH (1992) The distribution of 13 GABAA receptor subunit mRNAs in the rat brain. I. Telencephalon, diencephalon, mesencephalon. *J Neurosci* 12:1040–1062.

Yamamoto T, Ochalski A, Hertzberg EL, Nagy JI (1990) On the organization of astrocytic gap junctions in rat brain as suggested by LM and EM immunohistochemistry of connexin43 expression. *J Comp Neurol* 302:853–883.

Yum SW, Zhang J, Valiunas V, Kanaporis G, Brink PR, White TW, Scherer SS (2007) Human connexin26 and connexin30 form functional heteromeric and heterotypic channels. *Am J Physiol Cell Physiol* 293:C1032–C1048.

Zantua JB, Wasserstrom SP, Arends JJ, Jacquin MF, Woolsey TA (1996) Postnatal development of mouse "whisker" thalamus: ventroposterior medial nucleus (VPM), barreloids, and their thalamocortical relay neurons. *Somatosens Mot Res* 13:307–322.

Zhang J (2013) Astroglial connexins in adult neurogenesis: Mechanistic insight from mutant mice Ph.D. diss., University of Bonn.

Zhang J, Dublin P, Griemsmann S, Klein A, Brehm R, Bedner P, Fleischmann BK, Steinhäuser C, Theis M (2013) Germ-line recombination activity of the widely used hGFAP-cre and nestin-cre transgenes. *PLoS One* 8:e82818.

Zhou M, Kimelberg HK (2001) Freshly isolated hippocampal CA1 astrocytes comprise two populations differing in glutamate transporter and ampa receptor expression. *J Neurosci* 21:7901–7908.

Zhuo L, Theis M, Alvarez-Maya I, Brenner M, Willecke K, Messing A (2001) hGFAP-cre transgenic mice for manipulation of glial and neuronal function in vivo. *Genesis* 31:85–94.

Zimmerman L, Parr B, Lendahl U, Cunningham M, McKay R, Gavin B, Mann J, Vassileva G, McMahon A (1994) Independent regulatory elements in the nestin gene direct transgene expression to neural stem cells or muscle precursors. *Neuron* 12:11–24.

List of Figures

List of Tables